TGAL-86-7

(12)

AD-A182 722

# PROPAGATION AND EXCITATION OF Lg, Sn, AND P-Pn WAVES FROM EASTERN UNITED STATES EARTHQUAKES BY REGRESSION ANALYSIS OF RSTN DATA

J.H. Goncz, W.C. Dean, Z.A. Der, A.C. Lees,
K.L. McLaughlin, T.W. McElfresh, and M.E. Marshall

# SEISMIC ATTENUATION STUDIES AT U.K. ARRAYS

D. Wilmer Rivers

Teledyne Geotech Alexandria Laboratories
314 Montgomery Street
Alexandria, Virginia 22314-1581



May 1987

FINAL TECHNICAL REPORT: October 1984 - October 1986
ARPA ORDER NO: 5331
PROJECT TITLE: U.K. Array, RSTN High Frequency Research
CONTRACT: MDA903-85-C-0086

Approved for Public Release; Distribution Unlimited.

Prepared for:
DEFENSE ADVANCED RESEARCH PROJECTS AGENCY
1400 Wilson Boulevard
Arlington, VA 22209

Monitored By:
DEPARTMENT OF THE ARMY
Defense Supply Service
Room 1D 245, The Pentagon
Washington, D.C. 20310

UNCLASSIFIED
SECURITY CLASSIFICATION OF THIS PAGE

ADA182722

# REPORT DOCUMENTATION PAGE

Form Approved
OMB No 0704-0188
Exp Date: Jun 30, 1986

| | |
|---|---|
| 1a REPORT SECURITY CLASSIFICATION<br>Unclassified | 1b RESTRICTIVE MARKINGS |
| 2a SECURITY CLASSIFICATION AUTHORITY | 3 DISTRIBUTION / AVAILABILITY OF REPORT<br>Approved for Public Release; Distribution Unlimited. |
| 2b DECLASSIFICATION / DOWNGRADING SCHEDULE | |
| 4 PERFORMING ORGANIZATION REPORT NUMBER(S)<br>TGAL-86-7 | 5 MONITORING ORGANIZATION REPORT NUMBER(S) |
| 6a NAME OF PERFORMING ORGANIZATION<br>Teledyne Geotech<br>Alexandria Laboratories<br>6b OFFICE SYMBOL (If applicable) | 7a NAME OF MONITORING ORGANIZATION<br>Department of the Army<br>DSSW |
| 6c ADDRESS (City, State, and ZIP Code)<br>314 Montgomery Street<br>Alexandria, VA 22314-1581 | 7b ADDRESS (City, State, and ZIP Code)<br>Room 1D 245, Pentagon<br>Washington, D.C. 20310 |
| 8a NAME OF FUNDING / SPONSORING ORGANIZATION<br>DARPA<br>8b OFFICE SYMBOL (If applicable)<br>GSD | 9 PROCUREMENT INSTRUMENT IDENTIFICATION NUMBER<br>MDA-903-85-C-0086 |
| 8c ADDRESS (City, State, and ZIP Code)<br>1400 Wilson Blvd.<br>Arlington, VA 22209 | 10 SOURCE OF FUNDING NUMBERS<br>PROGRAM ELEMENT NO. / PROJECT NO. / TASK NO. / WORK UNIT ACCESSION NO. |

11 TITLE (Include Security Classification)
1) Propagation and Excitation of Lg, Sn, and P-Pn Waves from Eastern United States Earthquakes by Regression Analysis of RSTN Data; 2) Seismic Attenuation Studies at U.K. Arrays

12 PERSONAL AUTHOR(S)
J.H. Goncz, W.C. Dean, Z.A. Der, A.C. Lees, K.L. McLaughlin, T.W. McElfresh, M.E. Marshall

| 13a TYPE OF REPORT | 13b TIME COVERED | 14 DATE OF REPORT (Year, Month, Day) | 15 PAGE COUNT |
|---|---|---|---|
| Final Technical | FROM 10/84 TO 10/86 | May 1987 | 133 |

16 SUPPLEMENTARY NOTATION

| 17 COSATI CODES | | | 18 SUBJECT TERMS (Continue on reverse if necessary and identify by block number) |
|---|---|---|---|
| FIELD | GROUP | SUB-GROUP | seismic waves, regional phases, attenuation, RSTN stations, IDAS program |
| | | | |
| | | | |

19 ABSTRACT (Continue on reverse if necessary and identify by block number)

(12. Continued)

and D.W. Rivers


Propagation and Excitation of *Lg*, *Sn*, and *P–Pn* Waves from Eastern United States Earthquakes by Regression Analysis of RSTN Data

1.) By applying regression analysis to amplitudes of the regional phases *Pn*, *Sn* and *Lg* in various frequency ranges we have derived the attenuation rates, extrapolated source spectra, and relative site responses for these phases in Eastern North America using RSTN data. Observed regional phase amplitudes are modeled with three parameters according to the regression model:


→ next Page

(19. Continued)

| 20 DISTRIBUTION / AVAILABILITY OF ABSTRACT | 21 ABSTRACT SECURITY CLASSIFICATION | |
|---|---|---|
| ☐ UNCLASSIFIED/UNLIMITED ☐ SAME AS RPT. ☐ DTIC USERS | Unclassified | |
| 22a NAME OF RESPONSIBLE INDIVIDUAL<br>Dr. Robert R. Blandford | 22b TELEPHONE (Include Area Code)<br>(202) 697-6506 | 22c OFFICE SYMBOL<br>GSD |

DD FORM 1473, 84 MAR

83 APR edition may be used until exhausted
All other editions are obsolete

SECURITY CLASSIFICATION OF THIS PAGE
UNCLASSIFIED

(19. Continued)

$$\log A_{ij}(f_k) - \log G(\Delta_{ij}) = E_j(f_k) + \log S_i(f_k) - 0.4343\,(\gamma(f_k)\,\Delta_{ij})$$

where $i$ is the site index, $j$ is the event index, and $\Delta_{ij}$ is the event-station distance in degrees. $A$, the amplitude, and $G$, the dispersion/geometrical-spreading factor, are known or assumed quantities for the phase. Model parameters to be estimated are $E(f_k)$, the source strength, $S(f_k)$, the station bias, and $\gamma(f_k)$, the anelastic attenuation coefficient.

Resulting estimates for $Q(f) = \pi f/\gamma U$, where $U$ is group velocity for the specified phase are:

$$Q_{Pn}(f) = 640\,f^{0.50}$$
$$Q_{Sn}(f) = 825\,f^{0.80}$$
$$Q_{Lg}(f) = 1000\,f^{0.35}$$

assuming a combined dispersion and geometrical spreading factor of $\sim\Delta^{-5/6}$, appropriate to the amplitude decay of an Airy phase. Since the combined dispersion/geometrical spreading factor can be traded off against Q(f) and the level of the source excitation, a computer program that relates Q to various spreading factors is also given in this report. Since $Q(f)$ apparently increases with frequency more rapidly for *Pn* and *Sn* than it does for *Lg*, path attenuation produces a seismogram in which *Lg* appears as a low frequency signal, while *Pn* and *Sn* appear as high frequency signals. This effect, which becomes more pronounced with increasing distance, is a path attenuation effect and is apparently not due to source excitation.

The estimated source excitation levels for all three phases exhibit high-frequency falloff rates between $f^{-2}$ and $f^{-3}$ and have approximately the same shape. The average day and night noise levels of the RSTN stations were also measured as part of this study. The seismic noise displacement amplitude falls off roughly as $f^{-2}$ over the frequency band from 1 to 20 Hz. A diurnal variation in the noise levels is observed at all of the RSTN sites, with the daytime noise averaging from 1.5 to 3 times higher than the nighttime noise.

The final part of this study involved estimation of regional phase detection thresholds at the RSTN stations. We find for distances less than 16°, that *Lg* has the lowest detection threshold, followed by *Sn*, *Pg*, and *Pn*. The frequency at which each phase has its minimum threshold decreases rapidly with distance, most dramatically for *Lg*. At 3°, all four phases have their lowest thresholds in the 4-8 Hz range; this shifts to 1-4 Hz by 16°. These results are consistent with the observations of the behavior of regional phases from the bandpass-filtered seismograms. Minimum 50% detection thresholds for *Lg* range from magnitude 1.9 at 3° to magnitude 3 at 16°. The standard deviation of these estimates is 0.3 to 0.4 m.u., and the addition of 2 m.u. is required to bring the detection thresholds to the 98% level.

## Seismic Attenuation Studies at U.K. Arrays

The productivity of any future U.S. researchers using Blacknest data and of the Blacknest staff themselves will be significantly enhanced if the interactive graphics capability of the Sun workstation were used for the analysis of seismic array data. It was therefore decided that the objective of this task would be to devise data base display and analysis software that could be used on the Sun workstation at Blacknest. In particular, software would be installed that would make the Blacknest data accessible by programs already written to handle data archived at the Center for Seismic Studies in Arlington, Virginia. This would make the U.K. data readily available to future U.S. researchers, and it would lay the necessary groundwork for any international data exchange experiment that, unlike the GSETT, would involve the exchange of waveforms as well as of parameter data. Also, the Blacknest staff would be instructed in the use of the new software, so that they could add to it and, over a period of

(19. Continued)

time, adapt their data analysis from the batch mode processing on the mainframe computer to interactive processing on the Sun workstation.

Although the software development project involved performing a variety of tasks such as writing and maintaining utility programs and copying selected software from the Center, there were two programs that were developed which are the most important for researchers who wish to process U.K. seismic array data on the Sun workstation. The first of these programs is RDBNST, which de-archives the array data that are stored in a dozen different formats in the Blacknest tape library and converts them to the ".w" format used at the Center. RDBNST is much more "user friendly" than its predecessor, and this is a necessary feature for the program to be used by Blacknest personnel who are inexperienced with UNIX and who are unfamiliar with the Center's data base structure. When coupled with the seismogram display capabilities that were developed for the Sun, the RDBNST program should make it easy for the staff at Blacknest to satisfy requests from the U.S. for data from specific events. This was tested successfully when data were provided to the Center for 2 specific spans of 2 hours duration, for each one of the 4 U.K. seismic arrays, in response to a request from DARPA.

New software was also written for the purpose of examining seismic array data such as those which are archived at Blacknest. In order that this software be easily modified by Blacknest staff, most of the code was written in FORTRAN 77. The new program is based on the "SunCore" graphics system rather than on "SunWindows", unlike other currently available waveform analysis packages. This program that was developed at Blacknest for displaying and making measurements on multi-channel data is known as the Interactive Display of Array Seismograms (IDAS) program. It has been ported from the Sun workstation at Blacknest to workstations at the Center, so researchers there can examine the U.K. array data also. Copies of IDAS have been provided to other contractors in the U.S., namely Science Applications International, ENSCO, and Science Horizons. Copies have also been sent to the Australian National University and to the Ruhr - Universitat Bochum Institut fur Geophysik in Germany. Documentation of the program has furthermore been provided to other international participants in the GSETT. IDAS has been used for the analysis of data not only from the 4 arrays operated by the U.K. but also for the analysis of data recorded at NORESS and at Grafenberg.



## SUMMARY

Propagation and Excitation of *Lg*, *Sn*, and *P–Pn* Waves from Eastern United States Earthquakes by Regression Analysis of RSTN Data

By applying regression analysis to amplitudes of the regional phases *Pn*, *Sn* and *Lg* in various frequency ranges we have derived the attenuation rates, extrapolated source spectra, and relative site responses for these phases in Eastern North America using RSTN data. Observed regional phase amplitudes are modeled with three parameters according to the regression model:

$$\log A_{ij}(f_k) - \log G(\Delta_{ij}) = E_j(f_k) + \log S_i(f_k) - 0.4343\,(\gamma(f_k)\,\Delta_{ij})$$

where $i$ is the site index, $j$ is the event index, and $\Delta_{ij}$ is the event-station distance in degrees. $A$, the amplitude, and $G$, the dispersion/geometrical-spreading factor, are known or assumed quantities for the phase. Model parameters to be estimated are $E(f_k)$, the source strength, $S(f_k)$, the station bias, and $\gamma(f_k)$, the anelastic attenuation coefficient.

Resulting estimates for $Q(f) = \pi f/\gamma U$, where $U$ is group velocity for the specified phase are:

$$Q_{Pn}(f) = 640\, f^{0.50}$$
$$Q_{Sn}(f) = 825\, f^{0.80}$$
$$Q_{Lg}(f) = 1000\, f^{0.35}$$

assuming a combined dispersion and geometrical spreading factor of $-\Delta^{-5/6}$, appropriate to the amplitude decay of an Airy phase. Since the combined dispersion/geometrical spreading factor can be traded off against Q(f) and the level of the source excitation, a computer program that relates Q to various spreading factors is also given in this report. Since $Q(f)$ apparently increases with frequency more rapidly for *Pn* and *Sn* than it does for *Lg*, path attenuation produces a seismogram in which *Lg* appears as a low frequency signal, while *Pn* and *Sn* appear as high frequency signals. This effect, which becomes more pronounced with increasing distance, is a path attenuation effect and is apparently not due to source excitation.

The estimated source excitation levels for all three phases exhibit high-frequency falloff rates between $f^{-2}$ and $f^{-3}$ and have approximately the same shape. The average day and night noise levels of the RSTN stations were also measured as part of this study. The seismic noise displacement amplitude falls off roughly as $f^{-2}$ over the frequency band from 1 to 20 Hz. A diurnal variation in the noise leve's is observed at all of the RSTN sites, with the daytime noise averaging from 1.5 to 3 times higher than the nighttime noise.

The final part of this study involved estimation of regional phase detection thresholds at the RSTN stations. We find for distances less than 16°, that *Lg* has the lowest detection threshold, followed by *Sn*, *Pg*, and *Pn*. The frequency at which each phase has its minimum threshold decreases rapidly with distance, most dramatically for *Lg*. At 3°, all four phases have their lowest thresholds in the 4-8 Hz range; this shifts to 1-4 Hz by 16°. These results are consistent with the observations of the behavior of regional phases from the bandpass-filtered seismograms. Minimum 50% detection thresholds for *Lg* range from magnitude 1.9 at 3° to magnitude 3 at 16°. The standard deviation of these estimates is 0.3 to 0.4 m.u., and the addition of 2 m.u. is required to bring the detection thresholds to the 98% level.

The productivity of any future U.S. researchers using Blacknest data and of the Blacknest staff themselves will be significantly enhanced if the interactive graphics capability of the Sun workstation were used for the analysis of seismic array data. It was therefore decided that the objective of this task would be to devise data base display and analysis software that could be used on the Sun workstation at Blacknest. In particular, software would be installed that would make the Blacknest data accessible by programs already written to handle data archived at the Center for Seismic Studies in Arlington, Virginia. This would make the U.K. data readily available to future U.S. researchers, and it would lay the necessary groundwork for any international data exchange experiment that, unlike the GSETT, would involve the exchange of waveforms as well as of parameter data. Also, the Blacknest staff would be instructed in the use of the new software, so that they could add to it and, over a period of time, adapt their data analysis from the batch mode processing on the mainframe computer to interactive processing on the Sun workstation.

Although the software development project involved performing a variety of tasks such as writing and maintaining utility programs and copying selected software from the Center, there were two programs that were developed which are the most important for researchers who wish to process U.K. seismic array data on the Sun workstation. The first of these programs is RDBNST, which de-archives the array data that are stored in a dozen different formats in the Blacknest tape library and converts them to the ".w" format used at the Center. RDBNST is much more "user friendly" than its predecessor, and this is a necessary feature for the program to be used by Blacknest personnel who are inexperienced with UNIX and who are unfamiliar with the Center's data base structure. When coupled with the seismogram display capabilities that were developed for the Sun, the RDBNST program should make it easy for the staff at Blacknest to satisfy requests from the U.S. for data from specific events. This was tested successfully when data were provided to the Center for 2 specific spans of 2 hours duration, for each one of the 4 U.K. seismic arrays, in response to a request from DARPA.

New software was also written for the purpose of examining seismic array data such as those which are archived at Blacknest. In order that this software be easily modified by Blacknest staff, most of the code was written in FORTRAN 77. The new program is based on the "SunCore" graphics system rather than on "SunWindows", unlike other currently available waveform analysis packages. This program that was developed at Blacknest for displaying and making measurements on multi-channel data is known as the Interactive Display of Array Seismograms (IDAS) program. It has been ported from the Sun workstation at Blacknest to workstations at the Center, so researchers there can examine the U.K. array data also. Copies of IDAS have been provided to other contractors in the U.S., namely Science Applications International, ENSCO, and Science Horizons. Copies have also been sent to the Australian National University and to the Ruhr - Universitat Bochum Institut fur Geophysik in Germany. Documentation of the program has furthermore been provided to other international participants in the GSETT. IDAS has been used for the analysis of data not only from the 4 arrays operated by the U.K. but also for the analysis of data recorded at NORESS and at Grafenberg.

TABLE OF CONTENTS

# LIST OF FIGURES

# LIST OF TABLES

(THIS PAGE INTENTIONALLY LEFT BLANK)

# PROPAGATION AND EXCITATION OF Lg, Sn, AND P–Pn WAVES FROM EASTERN UNITED STATES EARTHQUAKES BY REGRESSION ANALYSIS OF RSTN DATA

by

John H. Goncz, William C. Dean, Zoltan A. Der,

Alison C. Lees, Keith L. McLaughlin,

Thomas W. McElfresh, and Margaret E. Marshall

(THIS PAGE INTENTIONALLY LEFT BLANK)

## SUMMARY

By applying regression analysis to amplitudes of the regional phases *Pn*, *Sn* and *Lg* in various frequency ranges we have derived the attenuation rates and extrapolated source spectra for these phases in Eastern North America using RSTN data, mostly from earthquakes. Vertical component seismograms extending in time from before the *P* arrival to after the *Lg* arrival were band-pass filtered and the maximum zero-to-peak signal amplitudes within predicted *Pn*, *Sn* and *Lg* arrival time windows were picked. The nine band-pass filters utilized had center frequencies $f_k$ that span the frequency range from 0.4 Hz to 20 Hz evenly on the log-frequency scale. The outputs of these filters were used to determine the *Q* factors of the regional phases analyzed as functions of frequency.

Observed regional phase amplitudes are modeled with three parameters according to the regression model:

$$\log A_{ij}(f_k) - \log G(\Delta_{ij}) = E_j(f_k) + \log S_i(f_k) - 0.4343\,(\gamma(f_k)\,\Delta_{ij})$$

where $i$ is the site index, $j$ is the event index and $\Delta_{ij}$ is the event-station distance in degrees. The left hand side contains known or assumed quantities; $A$ is the amplitude and $G$ is the dispersion/geometrical-spreading factor appropriate for the phase. For arrivals for which this factor is not well known we assumed various plausible factors to limit the values of $\gamma$ and $Q(f)=\frac{\pi f}{\gamma U}$ as well as the estimates of the source strength defined below. Model parameters to be estimated are on the right hand side of the equation; $E(f_k)$ is the source strength, $S(f_k)$ is the station bias and $\gamma(f_k)$ is the anelastic attenuation coefficient.

For an event to be used in the regression analyses we required that there must be at least two sites that receive the same signal phase for a given event. The RSTN network is well suited for this kind of analysis because during its operational life it has provided a data set that

contains a broad range in source sizes (mb = 1.7 to 6.2) and a broad range in epicentral distances ( $\Delta$ = 0.6 to 33 deg). Together, these broad ranges in the independent variables tend to reduce the uncertainties of the estimated model parameters.

Earthquake magnitudes do not appear in the regression analysis because source strengths were estimated at each frequency $E(f_k)$ independently. These $E(f_k)$'s can be regressed upon network magnitudes and the resulting straight line relations used to construct source excitation spectra from magnitudes 2 to 6.

Approximate expressions for $Q(f) = \pi f/\gamma U$, where $U$ is group velocity for the specified phase are:

$$Q_{Pn}(f) = 640\, f^{0.50}$$

$$Q_{Sn}(f) = 825\, f^{0.80}$$

$$Q_{Lg}(f) = 1000\, f^{0.35}$$

All these were obtained for a combined dispersion and geometrical spreading factor of $\sim\Delta^{-5/6}$, appropriate to the amplitude decay of an Airy phase. Since the combined dispersion/geometrical spreading factor can be traded off against Q(f), and our data cannot resolve this nonuniqueness, a simple computer program that relates Q to various spreading factors is also given in this report assuming various group velocities and fitted in specified epicentral distance ranges. The reader can compare, using this program, various values of Q reported in the literature which were obtained by using various spreading factors.

The estimated source excitation levels for all three phases exhibit high-frequency falloff rates between $f^{-2}$ and $f^{-3}$ and have approximately the same shape. Generally, in the 200-1200 km distance range, the *Lg* amplitude spectral level is roughly one order of magnitude larger than the *Pn* and *Sn* amplitude spectra for the same event at 1 Hz.

Because, apparently, $Q(f)$ increases with frequency more rapidly for *Pn* and *Sn* than it does for *Lg*, path attenuation produces a seismogram in which *Lg* appears as a low frequency signal, while *Pn* and *Sn* appear as high frequency signals. This effect, which becomes more pronounced with increasing distance, is a path attenuation effect and is apparently not due to source excitation.

The average day and night noise levels of the RSTN stations were also measured as part of this study. The seismic noise displacement amplitude falls off roughly as $f^{-2}$ over the frequency band from 1 to 20 Hz. A diurnal variation in the noise levels is observed at all of the RSTN sites, with the daytime noise averaging 1.5 times higher than the nighttime noise at RSSD, the quietest site, and up to 3 times higher for some frequencies at RSCP and RSON. The site with the largest seasonal variation is RSNT which is quietest in the winter when the Great Slave Lake is frozen. The RSTN noise levels are comparable to the noise levels measured in Fennoscandia and are very similar to results from other studies of the same stations.

The final part of this study involved estimation of regional phase detection thresholds at the RSTN stations. We find for distances less than 16°, that *Lg* has the lowest detection threshold, followed by *Sn*, *Pg*, and *Pn*. The results for *Pg* are marginal because *Pg* is not often a prominent arrival on our mostly eastern North America paths. The frequency at which each phase has its minimum threshold decreases rapidly with distance, most dramatically for *Lg*. At 3°, all four phases have their lowest thresholds in the 4-8 Hz range; this shifts to 1-4 Hz by 16°. These results are consistent with the observations of the behavior of regional phases from the bandpass-filtered seismograms. Minimum 50% detection thresholds for *Lg* range from magnitude 1.9 at 3° to magnitude 3 at 16°. The standard deviation of these estimates is 0.3 to 0.4 m.u., and the addition of 2 m.u. is required to bring the detection thresholds to the 98% level.

# INTRODUCTION

Understanding the propagation and excitation characteristics of regional seismic arrivals (*Pn*, *Pg*, *Sn* and *Lg*) is of importance for detection, discrimination, and yield estimation of nuclear explosions, and this knowledge is especially important for the siting of stations to be used to monitor a Comprehensive Test Ban Treaty (CTBT) or a Threshold Test Ban Treaty (TTBT). This study focuses on two aspects of these problems, attenuation of regional phases and detection thresholds for regional phases. These investigations are done using regional arrivals recorded at the RSTN stations from events in eastern and central North America.

The importance of research along these lines is stressed in a recent review paper by Evernden *et al* (1986) which discusses the implications of regional propagation characteristics of various crustal phases with regards to detectability and discrimination capability for decoupled nuclear explosions by a hypothetical internal network in the USSR. As pointed out by Evernden *et al*, in order to have confidence in our capabilities to detect and discriminate regional events, as would be required by a CTBT, it is important to have a better understanding of the frequency dependence of attenuation, local site noise structures, the characteristics and physics of high frequency signal propagation, and the source characteristics of small explosions and earthquakes.

One goal of this study is to determine the frequency-dependent attenuation characteristics of various seismic phases (*Pn*, *Pg*, *Sn* and *Lg*) from local and regional events. Simultaneously, we utilize the data to estimate the source excitation spectra of the regional phases *Pn*, *Pg*, *Sn* and *Lg* from earthquakes as functions of frequency. Throughout this study we utilized RSTN data exclusively. In order to use RSTN sites for the measurement of the propagation characteristics of regional events and to evaluate the RSTN sites with regards to detection capability, we apply a statistical regression model of the signal amplitudes measured which contains rela-

tively few parameters to be estimated. Since we can only measure the signals at the output (the seismogram), the model includes the attenuation properties of the earth as well as the spectral characteristics of the sources and sites. The result is a measure of the apparent spatial attenuation; we do not distinguish between anelastic and scattering attenuation. Station bias is estimated only for the RSTN sites relative to each other, not compared to some other seismic network. Thus these station terms are constrained to sum to zero at each frequency for the RSTN network.

There have been a number of studies of the attenuation properties of regional phases, particularly Lg, in various regions of the world (e.g. Nuttli 1973 in Eastern US; Mitchell 1975 in North America; Bollinger 1979 in Southeastern US; Nuttli 1980 in Iran; Nicolas *et al* 1982 in France; Hasegawa 1985 in Eastern Canada; Gupta and Burnetti 1980 in Eurasian shield regions, Campillo *et al* 1985 in France, Chun *et al* 1987 in Canada). In most of these studies the attenuation effects have been estimated by *a priori* assuming the authors' preferred forms of the geometrical spreading-dispersion effect and fitting Q(f). The model appropriate to the anelastic attenuation contribution to the amplitude-distance relation is an exponential decay of the individual frequency components with distance. Most studies which use time domain amplitudes model the combined dispersion and geometrical spreading with terms which go approximately as the $-5/6$ or $-1$ power of distance for *Lg* (see Ewing *et al* 1957, Nuttli 1973) depending whether the Airy phase or other parts of the dispersed wave trains are assumed to be measured. It is less certain what exponential geometrical-dispersion spreading decay factors are the most appropriate to *Pn*, *Pg*, and *Sn* since the physics of the propagation of these phases is not yet understood. The geometrical spreading factor (composed of cylindrical spreading and dispersion) cannot be determined uniquely by regression analyses of data since the $\Delta^{-n}$ and $\exp(-fT/Q(f))$ functions trade off against each other. Although the mathematical forms of these factors are different they cannot be separated by regression analyses because of the great

scatter in all regional amplitude data sets. Moreover, we often have to fit the data in limited distance ranges.

In any case, by assuming a geometrical spreading factor and fitting a Q(f) we essentially obtain an empirical fit to the observed amplitude-distance function, and extrapolating the amplitudes backwards to the source we obtain an estimate of the source spectrum regardless of what geometrical spreading factor was assumed. The various choices for the geometrical spreading factor make a significant difference mostly in the ratios of the absolute amplitudes of the various phases very near to the source. It appears that since Q(f) dominates the spectra at high frequencies the choice of geometrical spreading factors, as long as they are reasonable, is not critical.

Another plausible approach to choosing the most appropriate geometrical spreading factor is to run synthetic seismograms for the most likely models of the local crustal structure (Bouchon 1982, Campillo *et al* 1984) with an infinite $Q$ and to measure the decay rate of the phase amplitudes and regard these as due only to geometrical spreading. By fitting a function of the form $\Delta^{-n}$ to these one can then attribute the residual amplitude decay in the observed data to the exponential attenuation factor. Using this approach Campillo *et al* (1984) predicted, for a crustal model of France, that the geometrical spreading effect for *Pg* should be $\Delta^{-1.5}$. This would imply that for *P*, the $Q$ should be infinite or very large near 1-2 Hz for a similar crustal structure assumed for the eastern North America, since the observed amplitude decay is also $\Delta^{-1.5}$ (Warren et al 1978) as evidenced by the Early Rise data.

Unfortunately, when this approach is used, it not possible to verify that the crustal models chosen represent the structure of the region studied well enough for such analyses. Moreover, many published synthetic seismograms are quite different from the observed ones. We were unable to find in the literature synthetic seismograms with prominent, high frequency Sn

phases similar to those seen in actual seismograms and shown later in this report. Moreover, most techniques for computing synthetic seismograms tend to deteriorate in accuracy with increasing frequency, and there have been no satisfactory means devised yet to model the significant scattered energy in the seismograms present at high frequencies. In addition, the geometrical spreading factor may also be frequency dependent since the low and high frequency energy in the various phases may not be controlled by the same waveguide.

Unlike the network used by Campillo *et al* (1985), the RSTN sites are few in number and fairly distant from each other (10 to 16 degrees separate the neighboring RSTN stations). Hence in this study the distance variation must come from many sources in different locations recorded at a few stations. This implies that we are forced to assume that all of the sources and all of the paths have the same properties within our chosen area of study in order to keep the number of unknowns in our regression analyses reasonable. Thus, our results give statistically averaged propagation and detection characteristics over eastern North America, not exact predictions for any given event over any specified path. This way we shall obtain a fairly representative average picture of the propagation characteristics of regional phases over stable regions.

The second main goal of this study is to estimate the detection magnitude thresholds at the RSTN network of regional phases propagating primarily through eastern North America (ENA). We estimate 50% detection thresholds for *Pn*, *Pg*, *Sn*, and *Lg* for a suite of frequencies from 1-16 Hz at various distances by measuring relative amplitude levels of noise and each of the seismic phases. For regional distances of 3 to 16°, smaller events are best detected at the higher frequencies.

The basic plan of this report is as follows: the first part discusses the propagation attenuation model used for the regressions. Then we present estimates of $Q(f)$ for various regional

phases, followed by estimates of the source spectra and scaling laws for each. In the following section we review and compare results of other studies in both stable and tectonic environments with ours. This is followed by the analyses of background noise at each RSTN station. Following this we present estimates of the detection thresholds for each regional arrival as functions of frequency and distance. Our results are again compared to those of other studies. The emphasis in this study is on the *Lg* phase since it usually has the maximum amplitude of the regional phases and is anticipated to have the lowest detection thresholds at many frequencies.

## PROPAGATION-ATTENUATION MODEL

The time domain amplitude decay for dispersed surface waves is given by Ewing *et al* (1957) and Nuttli (1973) as

$$A \sim A_0 \, \Delta^{-1/3} (\sin \Delta)^{-1/2} \, e^{-\gamma \Delta} , \tag{1}$$

where $\Delta$ is the epicentral distance, measured in degrees, and $\gamma$ is the coefficient of anelastic attenuation. For regional distances, the combined dispersion (for an Airy phase) and geometrical spreading, $\Delta^{-1/3}$ and $(\sin \Delta^{-1/2})$, respectively, is $\sim\Delta^{-5/6}$ for small $\Delta$.

The parameter $\gamma$ is related to the quality factor Q by

$$\gamma = \frac{\pi f}{U \, Q(f)} , \tag{2}$$

where $U$ is the group velocity and $f$ is the frequency of the wave, equal to the reciprocal of its period.

If we consider a given phase from an earthquake source, the output amplitude of the seismic signal recorded at a seismometer $\Delta$ degrees from the source can be written as

$$A_{ij}(f) = E_j(f) \, S_i(f) \, \Delta_{ij}^{-1/3} (\sin \Delta_{ij})^{-1/2} e^{-\gamma \Delta_{ij}} \tag{3}$$

where $A_{ij}$ is the amplitude received at the ith station from the jth event in a set of seismograms,

$E_j$ is the event effect of the jth event, essentially a measure of the event magnitude, and $S_i$ is the station bias of the ith RSTN site relative to the average of all RSTN sites.

Equation (3), describing a regression model of the regional signal propagation, is written for a single frequency, but it also holds for a narrow band of frequencies in the seismic signal passband. Thus, we can solve the problem for the relevant parameters at any frequency in the signal passband and so derive estimates of the spectra of the source effect E, the station effect S, and $Q$.

We are also assuming that the radiation pattern of all events is, on the average, azimuthally isotropic. This may be justified on the basis of synthetic simulation studies for the phase *Lg* (Alexander and Von Seggern, 1983, personal communication) that indicated that the total radiation pattern for Lg was close to isotropic for a wide variety of source mechanisms. It appears that since *Lg* arrivals are made up of many modes, even if the radiation pattern for individual modes is strongly directional, the superposition of many such modes must be much less asymmetric. However, we must note that a recent study by Kim *et al* (1985) asserts that visible asymmetries exist in the radiation pattern of a Swedish earthquake. In any case, when estimating attenuation rates from many earthquakes such asymmetries will simply increase the "noise level" of the least squares fitting procedure without affecting the results as long as the radiation patterns in the events used are sufficiently different.

It is not clear what form the combined geometrical spreading and dispersion should take for regional arrivals other than *Lg*. Since these may also be thought of as made up of numerous normal modes (Harvey 1981) we may try the same forms as used for Lg. Alternatively, we may adopt the values measured from synthetic seismograms of these phases computed by assuming no losses in anelastic attenuation (Harvey 1981, Bouchon 1982, Kennett and Clarke 1983a,b). As we shall see later, quite different spreading factors may yield similar

Q estimates at high frequencies where attenuation is the dominant factor in determining the wave amplitudes.

Finally, we assume that there is no variation in signal with variation in source depth. All the events in this study are shallow, less than 30 km deep and most are less than 20 km deep. Certainly the very deep events which might be poor generators of *Lg* (Noponen and Burnetti 1980) are missing.

Some of these assumptions can be modified or removed by adding complexity to the model. Such would be the case if different $Q$ values were assigned to different geographic areas and the $Q$ for each source to receiver path adjusted to allow for the distance traversed through each of these areas. For this report however, only the simpler model defined by the above assumptions is used.

By taking logarithms of the terms in equation (1) of our model we get

$$\log_{10} A_{ij} = \log_{10} E_j + \log_{10} S_i - \frac{1}{3} \log_{10} \Delta_{ij} - \frac{1}{2} \log_{10}(\sin \Delta_{ij}) - 0.4343\, \gamma\, \Delta_{ij} + \varepsilon_{ij} . \quad (4)$$

The logarithms are to the base 10 so the event effect and station effect terms are proportional to the normal magnitude scales (for $m_b$, $M_s$, etc) used in seismology. The $\varepsilon_{ij}$ is an error term.

Rewriting Equation (4) putting all the known terms on the right hand side and keeping all the terms to be estimated on the left, we have

$$\log_{10} E_j + \log_{10} S_i - 0.4343\, \gamma\, \Delta_{ij} = \log_{10} A_{ij} + (\frac{1}{3}) \log_{10} (\Delta_{ij}) + (\frac{1}{2}) \log_{10} (\sin \Delta_{ij}) . \quad (5)$$

The matrix form of this equation becomes

$$\mathbf{G\ m = d} \quad (6)$$

where **d** is the data vector which includes the *Lg* amplitude measurements along with the Airy phase dispersion and geometric spreading terms, 1/3 log Δ and 1/2 log sin Δ, respectively, and

where m is the model, a vector of the event effects ($E$), the station effects ($S$), and the $\gamma$ term we are trying to estimate. G is the coefficient matrix, mostly of 1's and 0's describing the presence or absence of each model vector term for the particular station-event pair representing a single equation. The least squares solution of (6) is:

$$\mathbf{m} = (\mathbf{G}^T \mathbf{G})^{-1} \mathbf{G}^T \mathbf{d} . \quad (7)$$

## DATA ANALYSIS

### Selection of Events

Lists of events were compiled from several earthquake bulletins for this study, including the PDE lists from the USGS National Earthquake Information Network (NEIS), the Central Mississippi Valley Earthquake Bulletin (St. Louis University), the Seismic Network of Utah (University of Utah), the Southeastern US Seismic Network (Virginia Polytechnic Institute), the Northeastern US Seismic Network (Weston Observatory, Boston University), the Lamont-Doherty Network (Columbia University), and the Tennessee Earthquake Information Center (Memphis State University). Most of the local networks recorded events of small magnitude, too small to be seen at more than one RSTN site. Consequently, the predominant number of events are from the PDE lists of NEIS.

Figure 1 shows the geographical distribution of the epicenters and the RSTN stations. Figure 2 shows the paths from the epicenters to the RSTN sites for the *Lg* detections at 1 Hz. The complete list of events used in this study is given in Table 1.

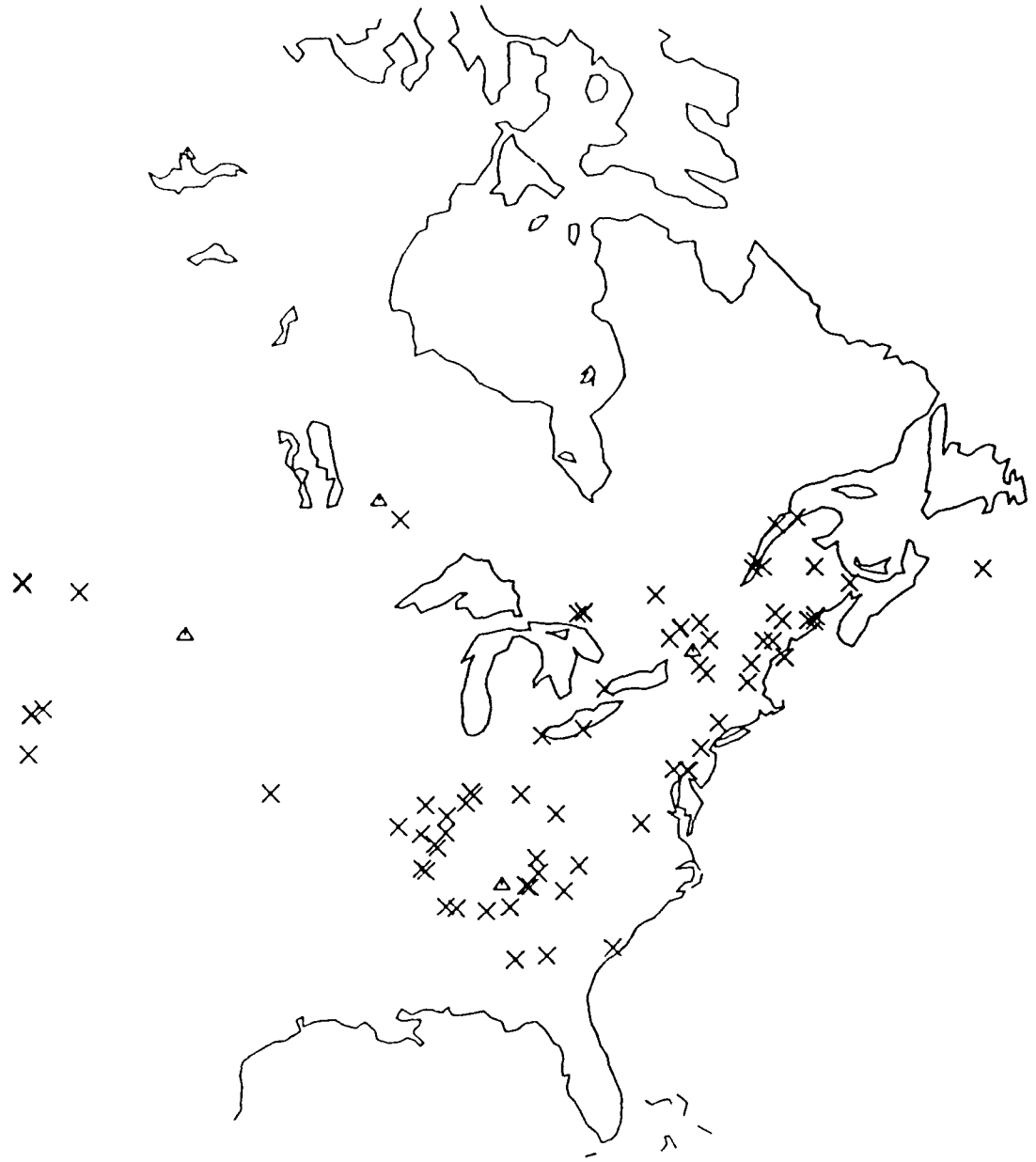

**Figure 1.** Geographical distribution of RSTN stations (triangles) and epicenters (crosses) used in this study.

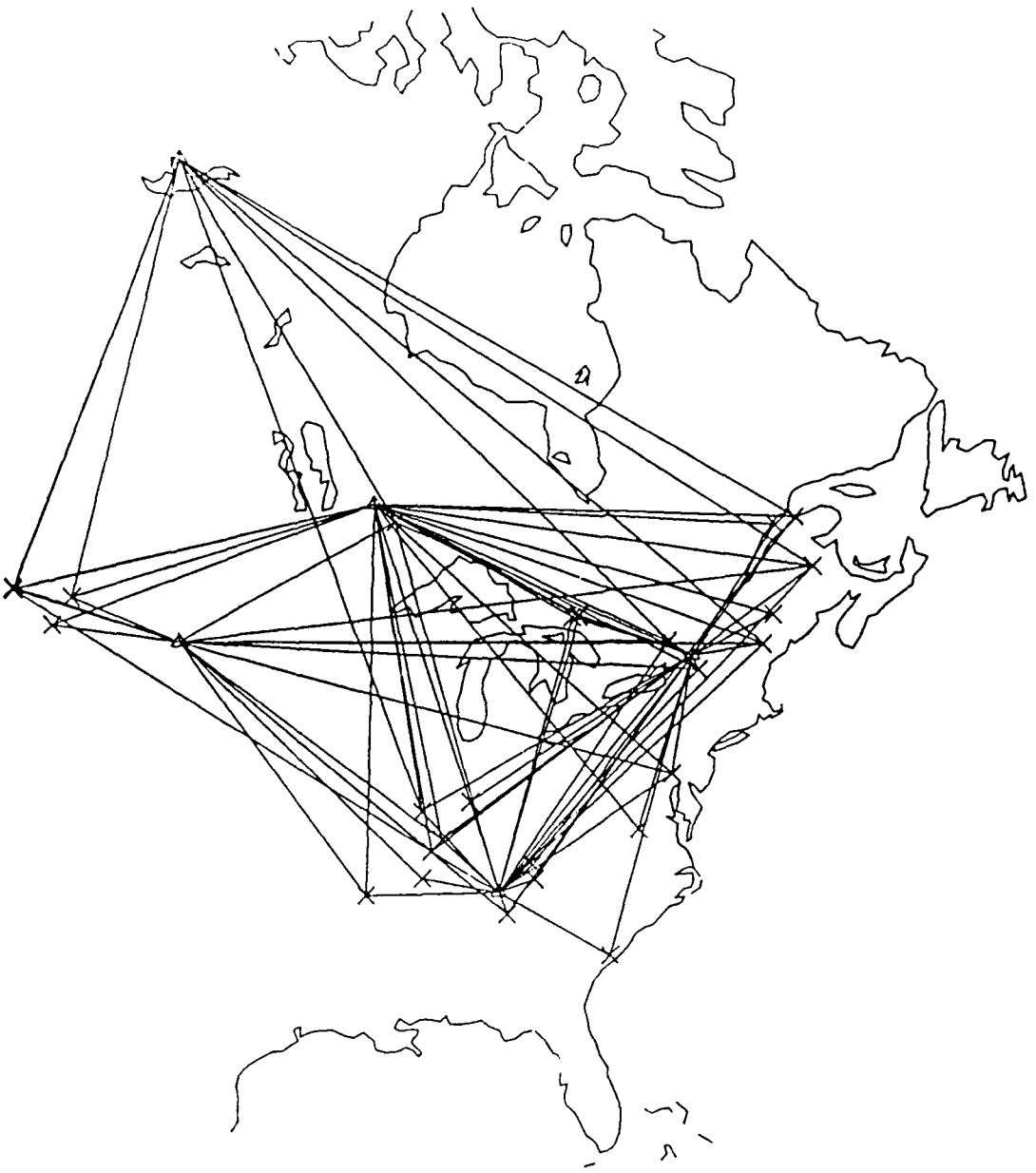

**Figure 2.** Epicenter-to-station paths used for studying *Lg* at 1 Hz. The path coverage is representative of that used for each of the regional phases for each frequency band.

# TABLE 1

Earthquakes Used in RSTN High Frequency Study

| DATE (yr/doy) | ORIGTIME (GMT) | LAT (degN) | LON (degW) | DEPTH (km) | ml (mb) | EVENT (name) |
|---|---|---|---|---|---|---|
| 1983010 | 04:03:18.3 | 39.67 | -110.65 | 7.9 | 2.4 | 3U010a |
| 1983012 | 02:49:41.1 | 39.28 | -84.60 | 0.0 | 1.9 | 3M012a |
| 1983012 | 17:46:22.9 | 39.33 | -111.10 | 1.3 | 2.0 | 3U012a |
| 1983013 | 23:49:16.9 | 39.28 | -111.15 | 5.0 | 2.2 | 3U013a |
| 1983017 | 19:35:51.0 | 49.11 | -66.98 | 18.0 | 4.1 | 3B017 |
| 1983017 | 19:35:51.0 | 49.11 | -66.98 | 18.0 | 4.5 | 3P017 |
| 1983019 | 02:30:41.6 | 35.28 | -92.16 | 4.0 | 3.9 | 3S019 |
| 1983019 | 10:40:35.5 | 39.32 | -111.12 | 9.2 | 2.1 | 3U019a |
| 1983021 | 01:34:58.8 | 39.31 | -111.19 | 9.4 | 2.3 | 3U021a |
| 1983022 | 07:46:57.9 | 41.87 | -81.19 | 5.0 | 2.7 | 3P022 |
| 1983022 | 11:44:49.1 | 39.95 | -111.95 | 4.0 | 2.8 | 3P022a |
| 1983023 | 07:46:59.3 | 41.86 | -81.16 | 0.0 | 3.0 | 3M023a |
| 1983026 | 14:07:44.8 | 32.73 | -83.38 | 5.0 | 3.5 | 3P026 |
| 1983026 | 14:07:44.8 | 32.73 | -83.38 | 5.0 | 3.5 | 3V026b |
| 1983027 | 22:09:35.0 | 36.05 | -83.62 | 15.0 | 2.6 | 3P027 |
| 1983027 | 23:37:11.8 | 37.78 | -110.67 | 7.0 | 3.3 | 3U027a |
| 1983036 | 13:08:19.0 | 34.73 | -88.31 | 3.0 | 3.2 | 3S036 |
| 1983037 | 20:25:15.5 | 44.57 | -110.64 | 5.0 | 4.7 | 3P037 |
| 1983039 | 10:54:54.9 | 43.3 | -111.19 | 7.0 | 4.4 | 3P039 |
| 1983040 | 16:10:23.5 | 38.60 | -97.75 | 0.0 | 1.7 | 3K040a |
| 1983042 | 15:46:56.0 | 48.99 | -68.30 | 18.0 | 3.6 | 3B042 |
| 1983050 | 05:45:45.1 | 40.65 | -74.77 | 6.0 | 2.5 | 3P050 |
| 1983054 | 08:09:14.2 | 37.08 | -88.87 | 20.0 | 3.0 | 3P054 |
| 1983054 | 08:51:27.0 | 36.19 | -89.60 | 9.0 | 3.6 | 3P054a |
| 1983057 | 19:59:35.4 | 41.55 | -73.66 | 7.0 | 2.9 | 3P057 |
| 1983072 | 13:03:11.6 | 43.70 | -71.33 | 2.0 | 2.9 | 3P072 |
| 1983073 | 20:41:40.0 | 44.85 | -57.00 | 18.0 | 4.0 | 3P073 |
| 1983083 | 14:27:20.4 | 42.96 | -71.71 | 1.0 | 2.9 | 3P083 |
| 1983084 | 02:47:11.1 | 35.34 | -82.46 | 9.0 | 3.2 | 3P084 |
| 1983102 | 20:13:05.0 | 43.69 | -69.41 | 18.0 | 2.7 | 3P102 |
| 1983133 | 17:26:02.0 | 47.00 | -66.60 | 5.0 | 3.6 | 3P133 |
| 1983133 | 23:40:57.0 | 47.00 | -66.60 | 5.0 | 4.1 | 3P133a |
| 1983135 | 05:16:21.6 | 38.77 | -89.57 | 9.0 | 4.3 | 3P135 |
| 1983136 | 02:01:57.0 | 47.70 | -69.93 | 10.0 | 4.0 | 3P136 |
| 1983147 | 23:03:35.1 | 45.54 | -69.46 | 10.0 | 3.2 | 3P147 |
| 1983149 | 05:45:49.8 | 44.50 | -70.41 | 2.0 | 3.9 | 3P149 |
| 1983153 | 06:30:23.0 | 47.45 | -70.22 | 10.0 | 3.4 | 3P153 |
| 1983155 | 05:00:23.0 | 47.46 | -69.65 | 10.0 | 3.0 | 3P155 |
| 1983161 | 04:22:39.0 | 47.00 | -66.60 | 5.0 | 3.3 | 3P161 |
| 1983162 | 13:47:58.0 | 47.00 | -66.60 | 5.0 | 3.4 | 3P162 |
| 1983180 | 02:06:14.1 | 43.73 | -69.46 | 16.0 | 2.4 | 3P180 |
| 1983189 | 19:29:05.9 | 35.54 | -84.15 | 11.0 | 3.3 | 3P189 |
| 1983224 | 14:08:47.6 | 44.97 | -67.68 | 12.0 | 3.6 | 3P224 |
| 1983224 | 14:08:47.6 | 44.97 | -67.68 | 12.0 | 3.6 | 3B224 |
| 1983229 | 14:03:15.0 | 38.47 | -82.77 | 12.0 | 3.5 | 3P229 |
| 1983240 | 10:44:03.9 | 34.66 | -87.77 | 7.0 | 2.6 | 3P240 |
| 1983240 | 22:45:06.5 | 36.70 | -83.84 | 5.0 | 3.1 | 3P240a |
| 1983277 | 17:18:40.0 | 43.44 | -79.79 | 2.0 | 3.1 | 3P277 |

| | | | | | | |
|---|---|---|---|---|---|---|
| 1983280 | 10:18:46.1 | 43.94 | -74.26 | 13.0 | 5.1 | 3P280 |
| 1983280 | 10:39:38.5 | 43.95 | -74.26 | 8.0 | 3.5 | 3P280a |
| 1983280 | 10:59:03.8 | 43.95 | -74.26 | 8.0 | 2.9 | 3P280b |
| 1983284 | 04:10:55.0 | 45.21 | -75.77 | 15.0 | 4.2 | 3P284 |
| 1983285 | 02:17:06.3 | 43.95 | -74.26 | 8.0 | 2.8 | 3P285 |
| 1983289 | 03:00:47.0 | 45.62 | -75.05 | 11.0 | 3.1 | 3P289 |
| 1983301 | 14:06:06.6 | 44.06 | -113.86 | 10.0 | 6.2 | 3P301 |
| 1983301 | 19:51:24.4 | 44.07 | -113.91 | 7.0 | 5.4 | 3P301a |
| 1983303 | 01:24:51.2 | 44.08 | -113.97 | 13.0 | 4.3 | 3P303 |
| 1983303 | 17:02:53.3 | 44.44 | -69.88 | 10.0 | 2.9 | 3B303 |
| 1983305 | 10:16:52.0 | 45.68 | -73.90 | 18.0 | 3.5 | 3P305 |
| 1983310 | 09:02:19.8 | 32.94 | -80.16 | 10.0 | 3.1 | 3P310b |
| 1983310 | 09:04:14.6 | 32.93 | -80.15 | 11.0 | 2.2 | 3P310a |
| 1983310 | 21:04:44.8 | 44.15 | -113.97 | 12.0 | 4.3 | 3P310 |
| 1983321 | 19:55:06.5 | 39.83 | -75.66 | 5.0 | 2.2 | 3P321 |
| 1983338 | 10:48:33.7 | 45.19 | -69.14 | 1.0 | 3.4 | 3P338 |
| 1983342 | 12:23:05.3 | 45.08 | -67.21 | 10.0 | 3.2 | 3P342 |
| 1983346 | 05:15:09.5 | 39.83 | -75.66 | 5.0 | 2.0 | 3P346 |
| 1983362 | 12:24:21.0 | 47.01 | -76.33 | 18.0 | 3.4 | 3P362 |
| 1983365 | 06:31:12.1 | 32.60 | -84.90 | 5.0 | 2.6 | 3P365 |
| 1983365 | 17:17:27.2 | 32.57 | -84.92 | 5.0 | 2.6 | 3P365a |
| 1984012 | 02:48:15.7 | 37.59 | -89.75 | 2.0 | 3.0 | 4P012 |
| 1984014 | 09:08:34.5 | 45.05 | -67.18 | 8.0 | 3.4 | 4P014 |
| 1984014 | 09:09:33.1 | 45.05 | -67.18 | 8.0 | 3.6 | 4P014a |
| 1984014 | 20:14:31.2 | 41.65 | -83.43 | 5.0 | 2.5 | 4P014b |
| 1984017 | 19:04:46.0 | 45.56 | -75.12 | 19.0 | 3.1 | 4P017 |
| 1984019 | 05:26:09.2 | 44.88 | -67.34 | 11.0 | 3.8 | 4P019 |
| 1984019 | 23:03:34.0 | 39.79 | -75.52 | 5.0 | 2.4 | 4P019a |
| 1984042 | 11:26:41.0 | 50.23 | -92.24 | 18.0 | 3.9 | 4P042 |
| 1984044 | 22:42:45.3 | 37.21 | -89.02 | 2.0 | 3.3 | 4P044 |
| 1984045 | 20:54:31.0 | 36.12 | -83.73 | 8.0 | 3.7 | 4P045 |
| 1984045 | 22:56:10.4 | 37.21 | -89.00 | 2.0 | 3.6 | 4P045a |
| 1984055 | 03:17:14.0 | 47.00 | -66.60 | 5.0 | 3.7 | 4P055 |
| 1984108 | 04:44:43.8 | 38.38 | -88.44 | 20.0 | 3.4 | 4P108 |
| 1984110 | 04:54:58.3 | 39.92 | -76.32 | 5.0 | 3.0 | 4P110 |
| 1984114 | 01:36:00.1 | 39.92 | -76.36 | 5.0 | 4.1 | 4P114 |
| 1984164 | 18:26:48.2 | 38.92 | -87.46 | 3.0 | 3.4 | 4P164 |
| 1984172 | 14:12:27.0 | 46.58 | -80.80 | 1.0 | 3.4 | 4P172 |
| 1984172 | 16:10:22.0 | 46.63 | -80.78 | 1.0 | 3.5 | 4P172a |
| 1984172 | 16:18:17.0 | 46.53 | -80.80 | 1.0 | 3.3 | 4P172b |
| 1984178 | 15:15:19.9 | 36.10 | -89.39 | 12.0 | 3.3 | 4P178 |
| 1984181 | 07:58:29.3 | 37.70 | -88.47 | 2.0 | 4.1 | 4P181 |
| 1984188 | 17:24:52.0 | 46.53 | -81.17 | 1.0 | 4.0 | 4P188 |
| 1984210 | 23:39:27.3 | 39.22 | -87.07 | 10.0 | 4.0 | 4P210 |
| 1984212 | 07:33:46.5 | 37.83 | -90.92 | 7.0 | 3.0 | 4P212 |
| 1984222 | 02:42:35.2 | 34.56 | -86.31 | 5.0 | 3.0 | 4P222 |
| 1984230 | 18:05:46.8 | 37.87 | -78.32 | 8.0 | 4.2 | 4P230 |
| 1984233 | 10:58:16.6 | 44.91 | -73.48 | 12.0 | 3.2 | 4P233 |
| 1984242 | 06:50:56.4 | 39.37 | -87.22 | 10.0 | 3.2 | 4P242 |
| 1984243 | 16:26:28.5 | 35.56 | -84.34 | 14.0 | 3.2 | 4P243 |
| 1984243 | 16:41:52.2 | 35.61 | -84.37 | 15.0 | 2.4 | 4P243a |
| 1984267 | 08:56:31.0 | 46.00 | -64.80 | 18.0 | 3.9 | 4P267 |
| 1984283 | 11:54:26.2 | 34.72 | -85.16 | 5.0 | 4.0 | 4P283 |
| 1984296 | 18:58:41.9 | 36.36 | -81.67 | 8.0 | 3.1 | 4P296 |
| 1984297 | 06:26:21.5 | 43.59 | -73.94 | 1.0 | 3.2 | 4P297 |

In this study we used a naming convention for events to facilitate searching and editing event files and analysis results. Since the RSTN data did not become available until 1982 and after, the event name includes the last number of the year, a letter indicating which bulletin listed the event, and the three digits indicating the day of the year. Thus event 4P150 was an event on day 150 of 1984 listed by the NEIS PDE bulletin. A second event on this same day is referred to as 4P150a; a third event would be 4P150b, and so on. The bulletin codes are listed in Table 2.

TABLE 2

Bulletin Codes for Event Names

| Letter Code | Bulletin |
|---|---|
| B | Northeastern US Seismic Network Bulletin, Boston College, Weston Observatory |
| D | Lamont-Doherty Network Bulletin, Columbia University National Earthquake Information Service |
| K | Kansas-Nebraska Regional Network Bulletin, University of Kansas |
| M | Ohio-Indiana Regional Network Bulletin, University of Michigan |
| P | Preliminary Determination of Epicenters, National Earthquake Information Service, US Dept. of Interior, Geologic Survey |
| S | Central Mississippi Valley Earthquake Bulletin, St. Louis University |
| T | Tennessee Earthquake Information Center Bulletin, Memphis State University |
| U | Utah Seismic Network Bulletin, University of Utah |
| V | Southeastern US Seismic Network Bulletin, Virginia Polytechnic Institute & State University |

## Signal and Noise Spectra

The amplitude versus frequency data needed for the regression analysis can be obtained from either spectra or from bandpass filtered time domain data. Typical *Lg* spectra and accompanying noise spectra sampled prior to the onset of the *Pn* phase are shown in the Figure 3 for an event at the five RSTN stations. The spectral windows were 25.6 seconds long and were tapered with a Parzen time window. The spectra have been corrected for instrument

displacement response and smoothed with a 16 point running average. The signal spectra are plotted with pluses (+) and noise spectra plotted with zeros (o). The best S/N ratio of *Lg* for this event is typically at around 2-4 Hz, and the S/N ratio decreases considerably below 1 Hz due to low frequency microseismic noise.

## Narrow Band Filtering

While spectra such as those shown in Figure 3 can be used to obtain the amplitude versus frequency data, we have chosen to use bandpass filtered seismograms instead. The approach used is essentially identical to that of Mechler *et al* (1980), and it has the advantage of giving a clear picture of the behavior of the regional arrivals in both the frequency and time domains. The relative amplitudes of the various arrivals vary from band to band, some are not apparent in some frequency bands, and the decrease in amplitudes with distance also varies with frequency.

The entire regional seismogram for an event at an RSTN site includes some noise before the initial *P* plus the *Pn*, *Pg*, *Sn* and *Lg* phases. This trace is used as the input to each of nine Butterworth band-pass filters. The center frequencies of these filters were equally spaced on the log(frequency) scale and they all had a 24 db/octave falloff at the flanks. The choice for this filtering method was based on the requirement that all filter outputs would exhibit relatively low ringing, so that the codas of the phases could be recognized. Had we chosen bandpass filters equally spaced on the frequency scale the phases would have run into each other at high frequencies because of the long ringing time of the filters. The frequency ratio corresponding to the spacing of the filter center frequencies was 1.54:1.

The outputs of the nine narrow passband filters were rectified and smoothed using a running average of 20 points applied twice (which amounts to a triangular weighting (smoothing) function over 1 second duration) to produce an envelope tracing of the filtered seismogram.

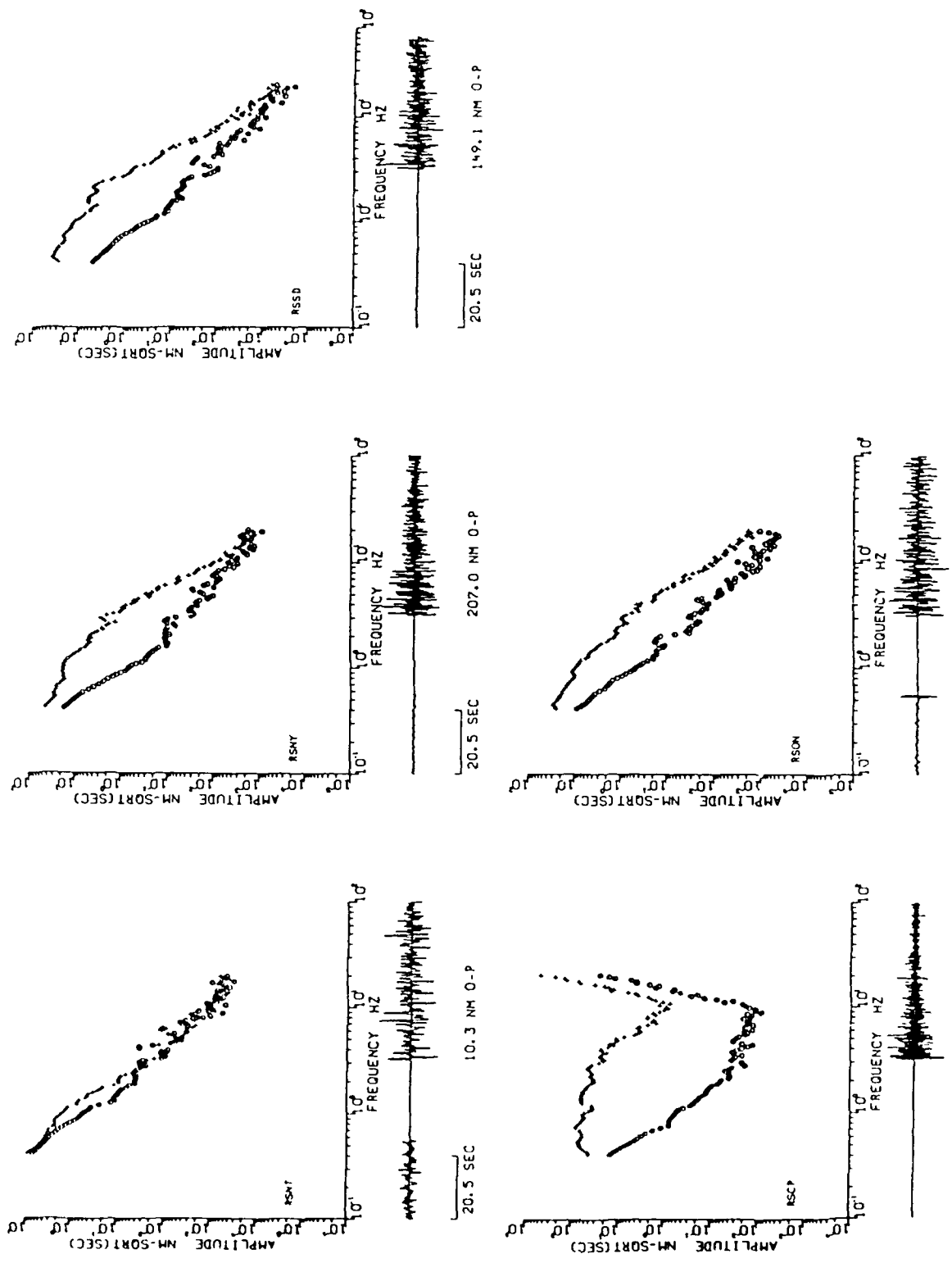


**Figure 3.** Examples of $L_g$ signal (crossed) and noise (open circles) spectra at the five RSTN stations for an $m_b$ 4.3 earthquake, event 3P135. Below each pair of spectra are the original noise (left) and signal (right) traces, plotted on the same scale. The noise window is from before the *P* arrival.

Finally, the signal amplitude for a particular phase such as *Lg* is the maximum amplitude of the filtered envelope trace in the expected arrival time window for the phase. The frequency assigned to that reading is determined by counting the average number of zero crossings per second for all of the filtered seismograms (prior to rectifying) in the data set (over 100 earthquakes) through that narrow bandpass filter. In all cases, the frequency is below the center of the filter passband since both the signal and the noise displacement spectra decay with increasing frequency and the dominant frequency of the band-pass filtered signal usually is not quite the same as the central frequency of the band-pass filter although in most cases they are not too different from it. These measured frequencies were used in the regression analysis.

Examples of the envelope seismograms are shown in Figures 4a-4e. In each case, the top trace is the envelope of the unfiltered data. The following nine traces are the outputs of the nine passband filters from lowest to highest frequency.

Figures 4a to 4d show seismograms associated with shield type propagation. At low frequencies *Lg* dominates, but as the frequency increases *Pn* becomes prominent (Figure 4a). At larger distances, *Lg* disappears as the frequency increases, and *Pn* and *Sn* dominate. Seismograms of similar nature have also been observed in eastern Canada (Shin 1985, Shin and Herrmann 1987) and at NORESS over paths of "shield" type (Kvaerna and Ringdal 1986).

Figure 4e shows typical features for events located in the tectonically active western part of North America as recorded at RSSD. In contrast to the previous examples, such events show a clear *Pg* phase and an *Lg* that is seen to high frequencies. No *Sn* is visible. The *Pn* phase sometimes emerges at high frequencies with low amplitudes although it is not visible at low frequencies.

Most of the features of our results are similar to those obtained by Mechler *et al* (1980). Mechler *et al* studied regional wave propagation across France using bandpass filtered seismo-

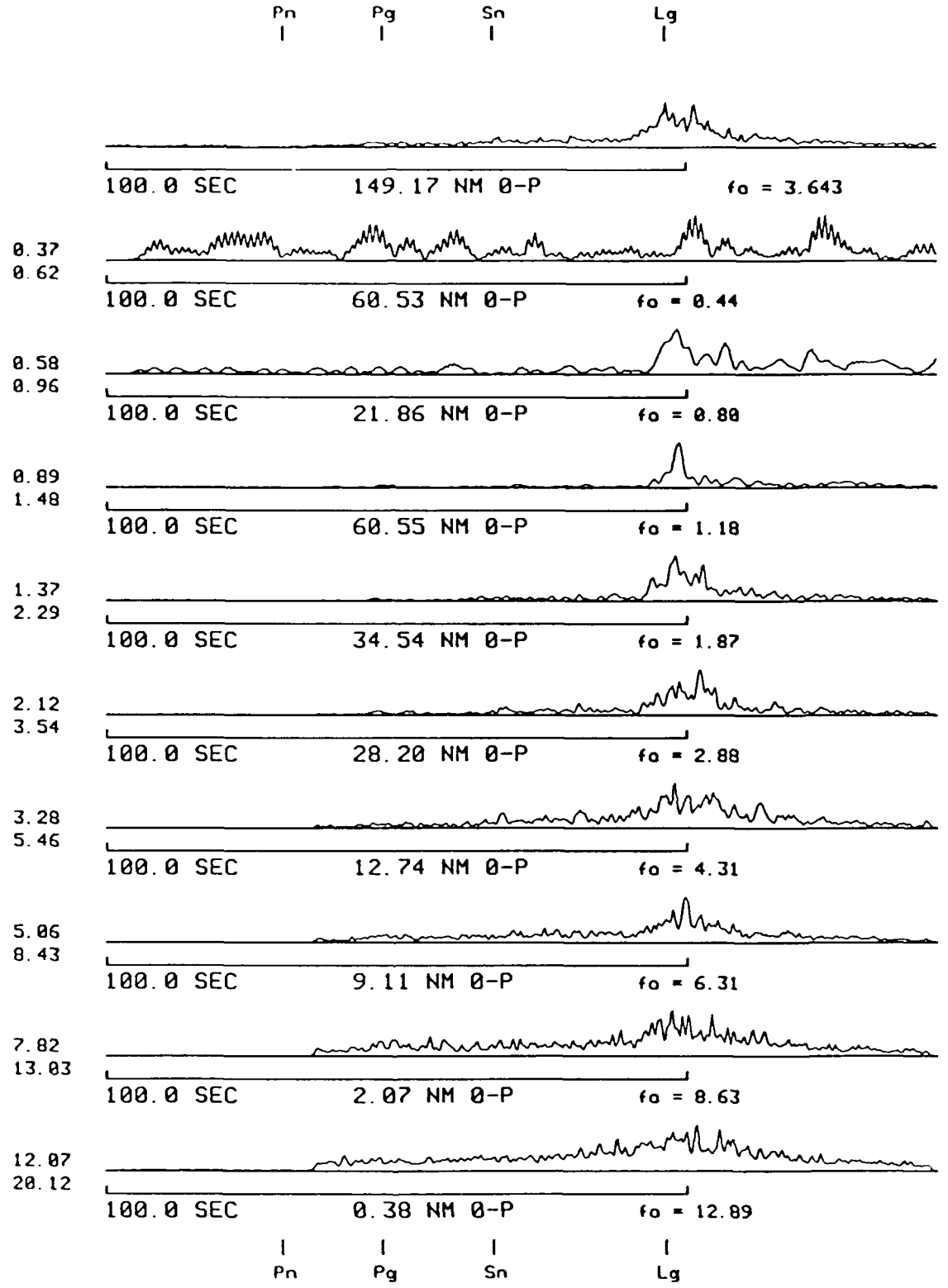


**Figure 4a.** Broadband envelope seismograms (top) followed by narrow band envelope seismograms. The corners of the frequency band are to the left of each seismogram. The maximum amplitude and the average frequency (from counting zero-crossings prior to rectification) are below each trace. Estimates of arrival times of the regional phases *Pn*, *Pg*, *Sn*, and *Lg* are marked above and below each suite of traces. Seismograms for an $m_b$ 3.2 earthquake, event 3P147, recorded at RSNY at the epicentral distance of 3.7 degrees. Only *Pn* and *Lg* phases are discernible.

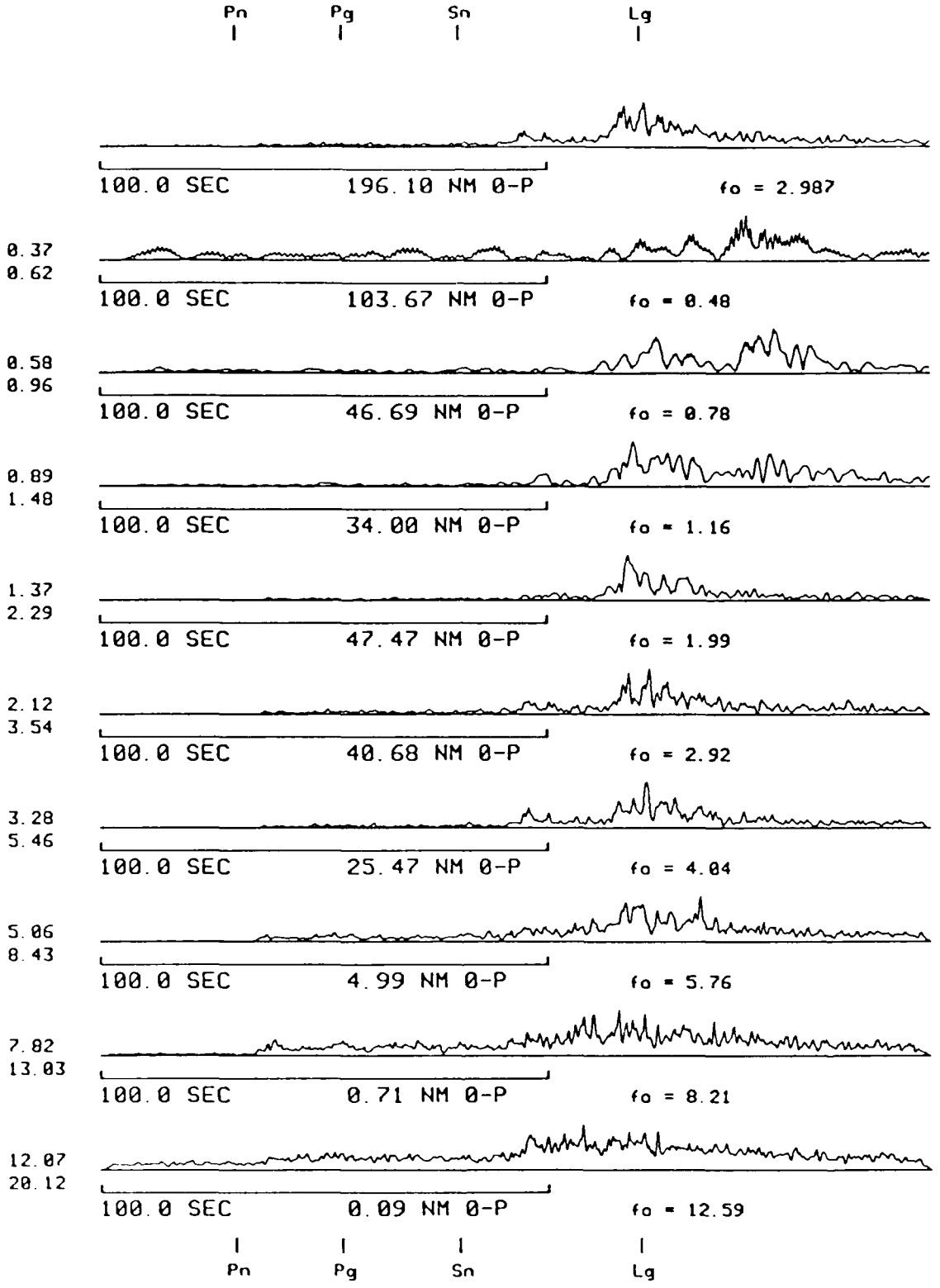


Figure 4b. Like Figure 4a except seismograms for an $m_b$ 4.0 earthquake, event 4P188, recorded at RSNY at the epicentral distance of 5.1 degrees. The phases *Pn*, *Sn* and *Lg* are discernible. *Lg* is the largest phase at low frequencies. The *Sn* phase becomes dominant at the highest frequencies, while *Lg* disappears into the coda of *Sn*.

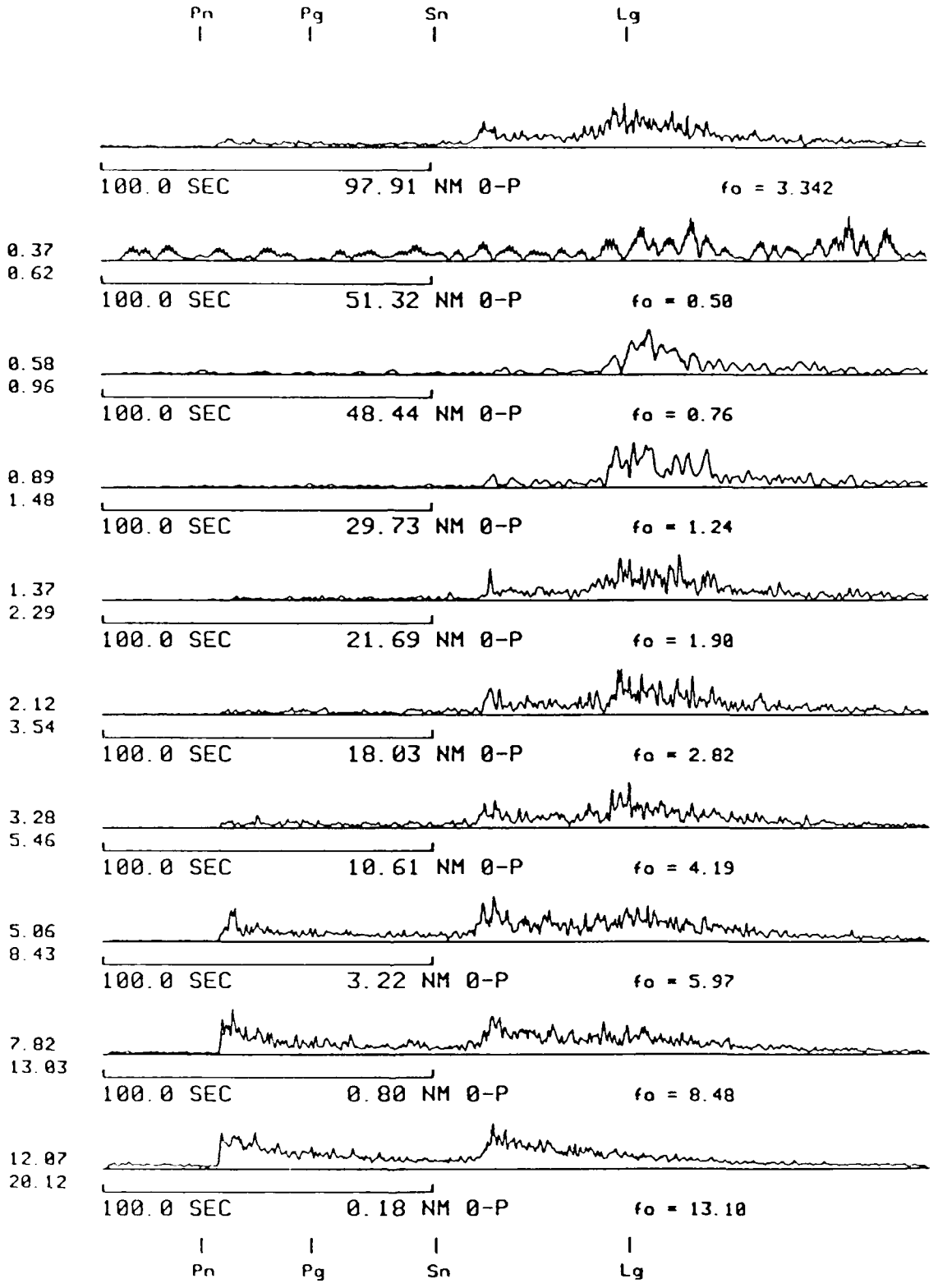


Figure 4c. Like Figure 4a except seismograms for an $m_b$ 4.1 earthquake, event 4P230, recorded at RSNY at the epicentral distance of 6.9 degrees. As in Figure 4b, *Lg* dominates at low frequencies, while *Pn* is very small in comparison. At the highest frequencies *Pn* and *Sn* dominate with much higher S/N ratios than at lower frequencies.

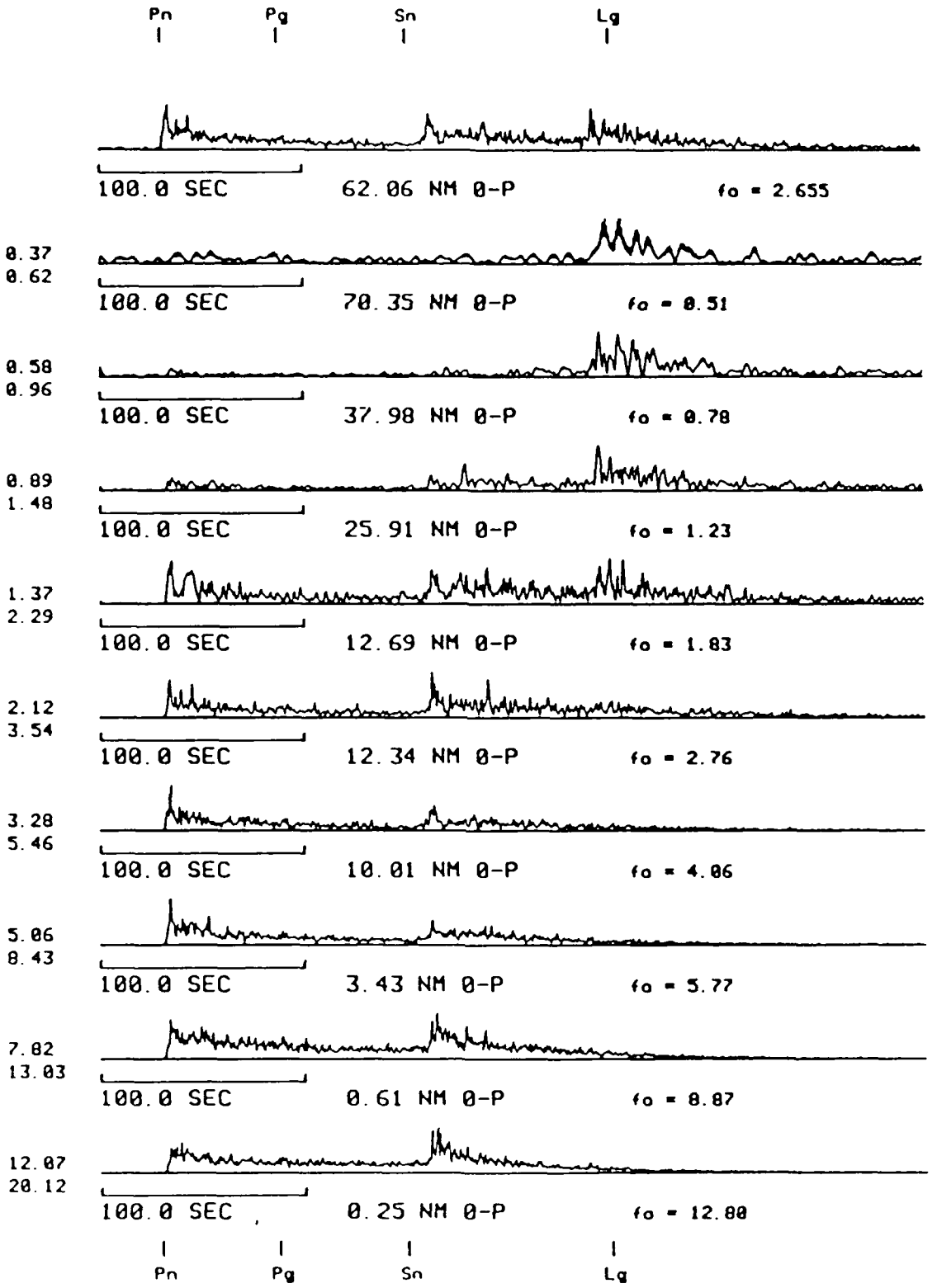


Figure 4d. Like Figure 4a except seismograms for an $m_b$ 4.3 magnitude earthquake, event 3P135, recorded at RSON at the epicentral distance of 12.4 degrees. The relative behavior of the three phases *Pn*, *Sn* and *Lg* is similar to that in Figures 4b and 4c.

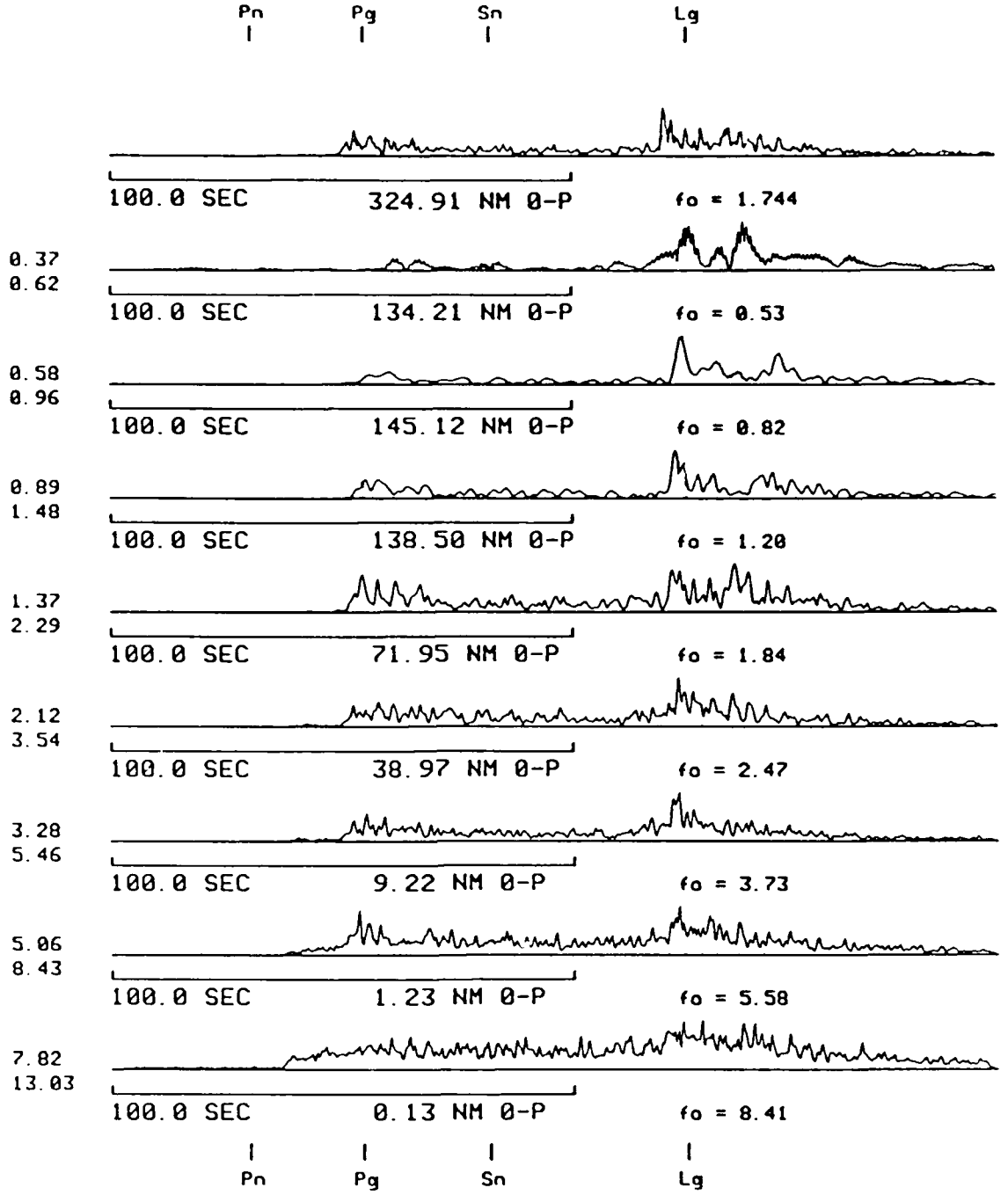


**Figure 4e.** Like Figure 4a except seismograms for an $m_b$ 4.4 magnitude earthquake, 3P039, recorded at RSSD at the epicentral distance of 5.3 degrees. The relative behavior of *Pn*, *Sn* and *Lg* is quite dissimilar to the previous examples, *Sn* is not visible, *Lg* persists to quite high frequencies, and there is a prominent *Pg* phase besides the small *Pn*. The highest S/N is at lower frequencies. The path crossed some tectonically active regions in the western United States.

grams and found that *Pn* and *Sn* have their maximum energy at higher frequencies than do *Pg* and *Lg*. The main difference between the results of Mechler *et al* and this study is that in our data the Pg arrivals are less pronounced and are often absent. This is probably due to the different nature of the propagation paths in the two studies. Most of our paths are in the shield-like eastern North America and show little or no *Pg* while our paths from events in the tectonically active regions of the western North America tend to show a clear *Pg*, and more *Lg* and less *Pn* and *Sn* than the eastern paths. Mechler *et al*'s paths are across France which has more recently been more active tectonically than has eastern North America. The difference in the relative amounts of *Pn* and *Pg* observed on different propagation paths may be due to the different crustal and upper mantle velocity structures.

The frequency dependences of the attenuation and of the excitation of the various crustal arrivals will have to be explained eventually with some appropriate models of the crustal waveguide. Given the fact that most theoretical algorithms for doing theoretical simulations of regional arrivals become less efficient and are expensive to run as frequency increases while the valid data extend to very high frequencies, this poses a major challenge to theoreticians. Moreover, it seems certain that the amplitude decay of crustal phases is mostly caused by scattering and not anelastic attenuation, which requires the development of theoretical models of scattering appropriate to the crust and uppermost mantle. The examples above demonstrate that there is quite a variety in the appearances of the seismograms for various paths and that the regional phases *Pn*, *Pg*, *Sn* and *Lg* appear and disappear in the various frequency bands depending on the nature of the propagation paths. Thus in any scheme devised for an automatic recognition of the regional phases one needs a knowledge base that incorporates all the regionally varying characteristics of regional arrivals (Kennett and Mykkeltveit 1984; Kennett *et al* 1985; Mykkeltveit and Kvaerna 1986).

## Signal Selection

As stated previously, the signal amplitudes used in the regression analyses are the peak values of the filtered envelope traces in the expected arrival time window of the particular phase. These values are read by the computer from the envelope traces themselves rather than read by an analyst from the plotted waveforms. Obvious noise readings were deleted manually later in a quality control phase. This way, not all traces are read for all frequencies for all RSTN sites for each event.

In order to avoid the use of marginal and noisy data we decided that to be included in our data set, an *Lg* signal must be detectable at any site on the unfiltered, raw seismogram. Although this limits the data sets mostly to larger signals, we also eliminate many marginal events with poor S/N ratios while retaining a sufficient number of events for reliable analyses of the data. In estimating thresholds of detection from such a set of larger events we had to determine the sizes of events that would have a S/N ratio of unity (50% threshold) by extrapolating the data to smaller events.

For each raw, unfiltered seismogram where an *Lg* was detected, we scanned the narrow passband envelope traces to determine, by eye, in which of the frequency passbands the *Lg* phase was seen. Only these signal amplitudes at these frequencies were entered into the regression analysis.

The net result of this selection process is that 227 station-event pairs of *Lg* signals were included in the analysis. Table 3 shows the distribution of event magnitudes included in this study for which at least one RSTN site detected an *Lg* phase.

TABLE 3
DISTRIBUTION OF EVENT MAGNITUDES USED IN *Lg* ANALYSES

| magnitude ($m_b$ or $m_l$) | number no. | magnitude ($m_b$ or $m_l$) | number no. |
|---|---|---|---|
| 1.7 | 1 | 3.4 | 8 |
| 1.9 | 1 | 3.5 | 6 |
| 2.0 | 2 | 3.6 | 7 |
| 2.1 | 1 | 3.7 | 2 |
| 2.2 | 3 | 3.8 | 1 |
| 2.3 | 1 | 3.9 | 4 |
| 2.4 | 4 | 4.0 | 5 |
| 2.5 | 2 | 4.1 | 4 |
| 2.6 | 4 | 4.2 | 2 |
| 2.7 | 2 | 4.3 | 3 |
| 2.8 | 2 | 4.4 | 1 |
| 2.9 | 5 | 4.5 | 1 |
| 3.0 | 7 | 5.1 | 1 |
| 3.1 | 6 | 5.4 | 1 |
| 3.2 | 8 | 6.2 | 1 |
| 3.3 | 6 | ... | . |

## *RESULTS*

In this section, we discuss the results of the joint regression analyses performed for attenuation, source, and receiver terms. First, $Q$, source spectra, and station terms are presented for *Lg*, and then the results for *Pn* and *Sn*. Our results are compared with those from other studies for both shield and tectonic regions. We also present average noise spectra at the five RSTN stations for both day and night conditions.

### Q vs. Frequency for Lg

The results of the regression of 227 Lg signal measurements from 114 earthquakes recorded at the five RSTN sites are shown in Table 4. The Table shows the predominant frequency of each of the nine narrow passband filters as measured by the rate of zero crossings together with the regression estimate of $\gamma$ and its standard deviation. The combined geometri-

cal spreading and dispersion was taken at $\Delta^{-5/6}$ per Equation (1). $Q$ is determined immediately from the estimate of $\gamma$ using Equation (2).

TABLE 4
FREQUENCY VERSUS ATTENUATION FOR *Lg*

| Freq Band No. | Dominant Frequency (Hz) | Number of Signals | $\gamma$ (deg$^{-1}$) | $\hat{s}(\gamma)$ (deg$^{-1}$) | Q | $\hat{s}(Q)$ | RMS of Amplitude Residuals |
|---|---|---|---|---|---|---|---|
| 1 | 0.5 | 48 | 0.062 | 0.019 | 774 | 235 | 0.16 |
| 2 | 0.7 | 69 | 0.079 | 0.010 | 939 | 117 | 0.13 |
| 3 | 1.1 | 121 | 0.104 | 0.010 | 1103 | 101 | 0.17 |
| 4 | 1.8 | 121 | 0.162 | 0.009 | 1109 | 62 | 0.16 |
| 5 | 2.8 | 95 | 0.174 | 0.018 | 1585 | 163 | 0.23 |
| 6 | 4.1 | 65 | 0.278 | 0.018 | 1482 | 98 | 0.17 |
| 7 | 5.9 | 32 | 0.292 | 0.040 | 2025 | 278 | 0.25 |
| 8 | 9.1 | 18 | 0.442 | 0.054 | 2055 | 252 | 0.10 |
| 9 | 13.7 | 18 | 0.500 | 0.123 | 2730 | 670 | 0.23 |

Figure 5 shows a log-log plot of $\gamma$ versus frequency. Figure 6 shows a similar plot for $Q$ versus frequency on a log-log scale. The straight-line fit to this estimate of $Q$ is

$$Q = 1000f^{0.35} . \quad (8)$$

It has been suggested that at frequencies above 7 or 10 Hz in the Appalachians and eastern Canada, *Lg* experiences significant contamination from *Sn* coda (Shin 1985, Chun *et al* 1987, Shin and Herrmann 1987). This is suggested by the way that *Lg* disappears into the *Sn* coda at higher frequencies on bandpassed seismograms such as those for eastern North America events in Figures 4a to 4c. To reduce the chances for such errors, we have also computed $Q_{Lg}$ only using frequencies up to 5.9 Hz and 9.1 Hz, respectively. In both cases, the $Q_{Lg}$ agrees with Equation (8). This is probably because at each frequency only *Lg* observations that had been confirmed by an analyst examing the bandpass filtered seismograms were included in the analysis. Thus, many fewer *Lg* observations were used at the higher frequencies than at frequencies around 1-3 Hz where *Lg* dominates (see column 3 of Table 4).

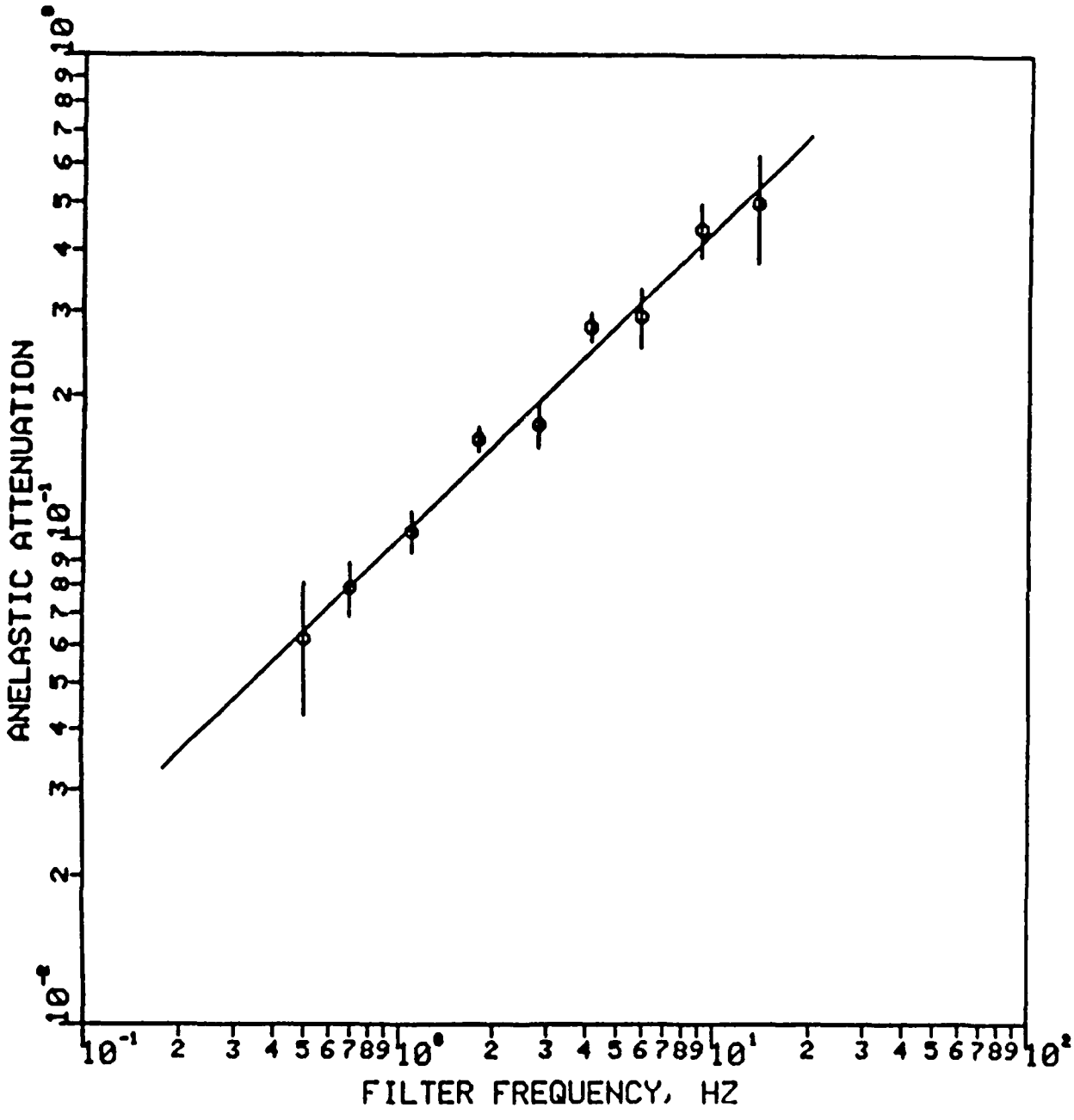


Figure 5. Log-log plot of *Lg* attenuation coefficient γ versus frequency. The estimated standard deviation is indicated by bars.

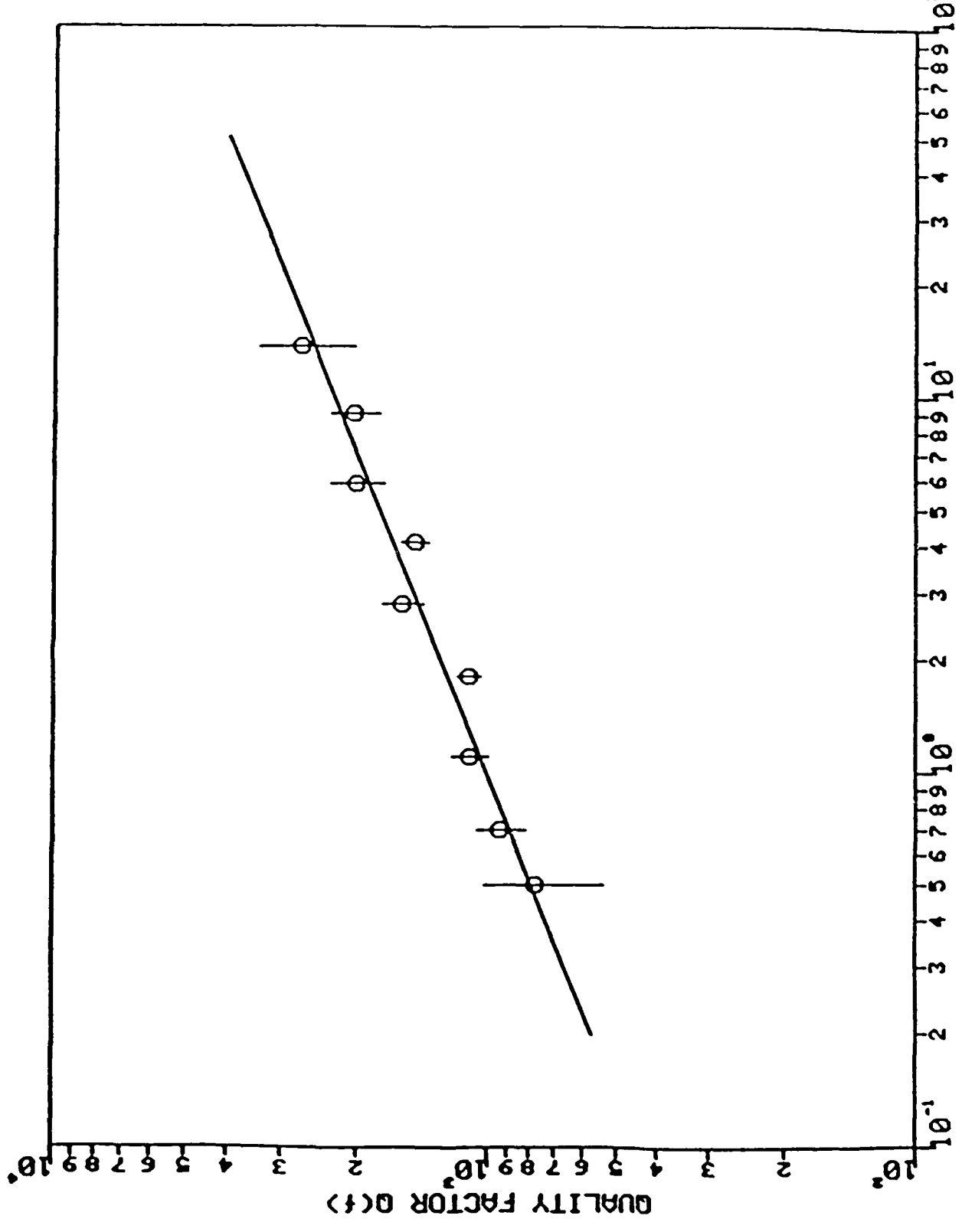


**Figure 6.** Log-log plot of $Q$ versus frequency for $L_R$. The bars indicate one standard deviation of the $Q$ estimates.

## Station Effects

In the regression analysis the station bias to *Lg* signals for RSTN sites is measured relative to each other. This means that the sum of all RSTN station bias measures is unity at all frequencies. The bias as a function of frequency for all five RSTN's is shown in Figure 7. Since the RSCP site cuts off sharply for frequencies beyond 8 Hz, no attempt was made to include its bias with those from the other sites beyond 8 Hz. We had no data from RSNT above 3.5 Hz.

The station effect (y-axis) is a logarithmic measure like the magnitude scale. RSSD is the site with the largest negative bias, especially at the higher frequencies. The other sites are near zero or with positive bias to compensate for RSSD. The bias for all RSTN sites at frequencies less than 3 Hz is slight. These results are not inconsistent with the site terms found by Gupta and McLaughlin (1987b). Gupta and McLaughlin find that the RSSD site term has a downward trend at frequencies above 3 Hz, while the RSON and RSNY site terms are flatter than the RSSD site term. We do not expect too many similarities between our results and those of Gupta and McLaughlin because Gupta and McLaughlin's data set included many more stations than ours, and the site terms are not absolute but are relative to each other. The lower high frequency amplitudes at RSSD might be because some Lg arrivals with low high frequency content were included in our data. These probably come from mixed tectonic-stable paths covering part of western North America. Gupta and McLaughlin (1987a) have also found from a similar study which included many LRSM stations that large site amplitudes correlate well with soft site geology while small site amplitudes correlate well with hard rock site geology.

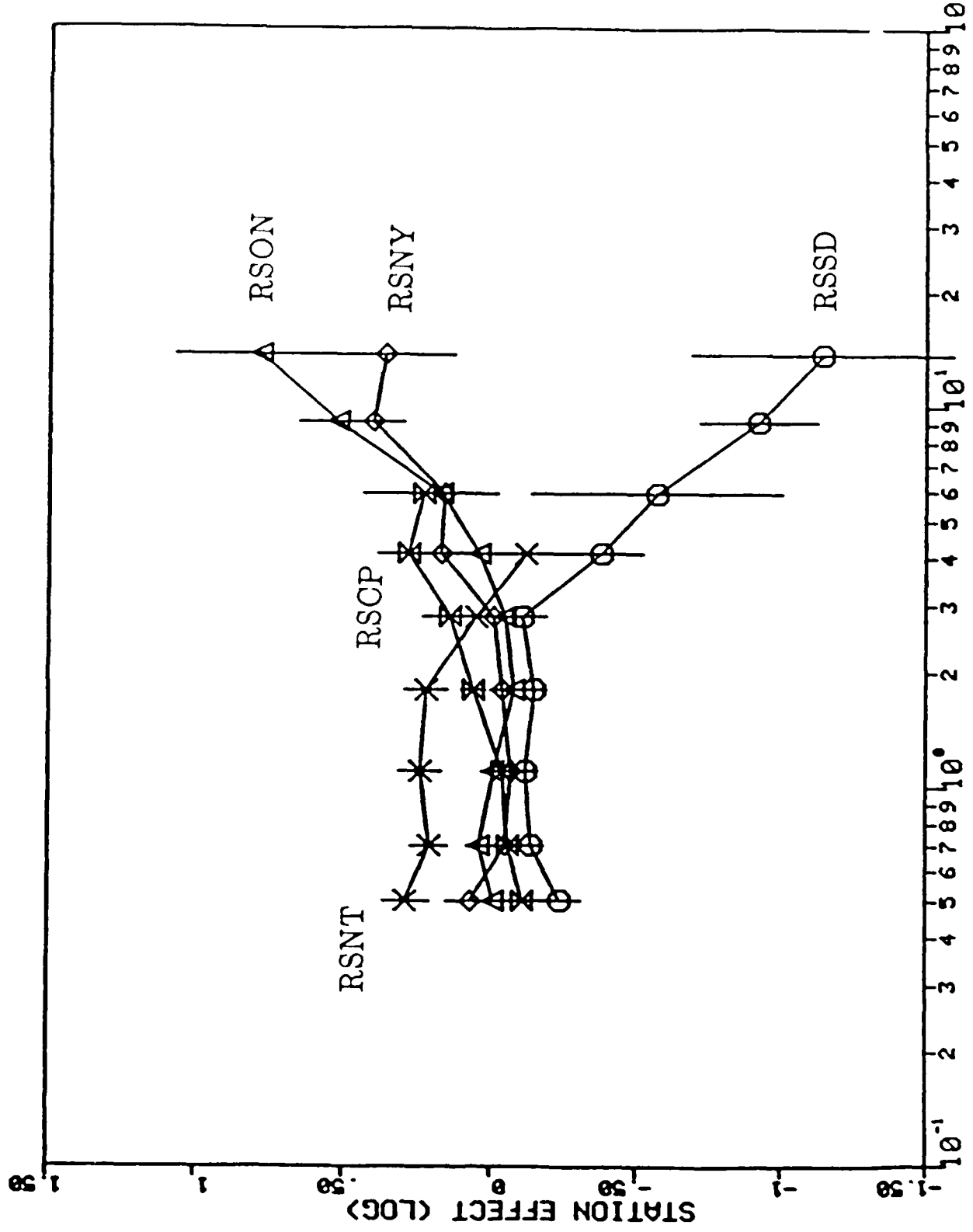


Figure 7. Station effect versus frequency for $L_g$ for the five RSTN stations.

## Source Spectra for Lg

The regression analysis yields an event effect which is a measure of the *Lg* excitation and the size of the event. Figure 8 shows the Lg event effect estimates versus network magnitude with a linear least squares fit for each of the nine frequency bands. We use local magnitude when it is available and substitute $m_b$ for the other events. The numbers on the Figure correspond to the frequency band from which the data was obtained; i.e. 3 is for the third frequency band which has a dominant frequency of 1.1 Hz (see first two columns of Table 4). We can read this set of curves at a particular magnitude to produce a spectral estimate of the event effect for eastern US earthquakes of that magnitude. By repeating this process for a suite of magnitudes we can generate a family of source spectral responses as shown on Figure 9. These source spectral responses represent *average* source functions for events in the eastern and central US at a distance of 11.39° from the source ($\Delta^{-1/3} = (sin\ \Delta)^{-1/2}$).

The source spectra estimated from *Lg* signals show ill-defined corner frequencies for the lower magnitudes ( $m_b$ = 2, 3, & 4) which shift to lower frequencies with increasing magnitude as most proposed scaling laws predict. The frequency coverage (0.5 to 13.7 Hz) is not low enough to show the corner frequency for the larger magnitudes. There is not enough data available for the larger magnitudes around $m_b$ 5 and 6 for the details of these two curves to be significant. The decay of the source spectral estimates above the corner frequency appears to be $f^{-2}$ to $f^{-3}$ at the high frequency end of the spectra.

## Q vs Frequency for Pn and Sn

We have followed the approach used above to estimate the attenuation and source excitation characteristics for both *P–Pn* and *Sn* signals. We lump the *Pn* and *P* waves together in this analysis. Since we are mostly interested in the detectability of phases at various distances we need not make any distinction between the two types of arrivals. It seems likely, though,

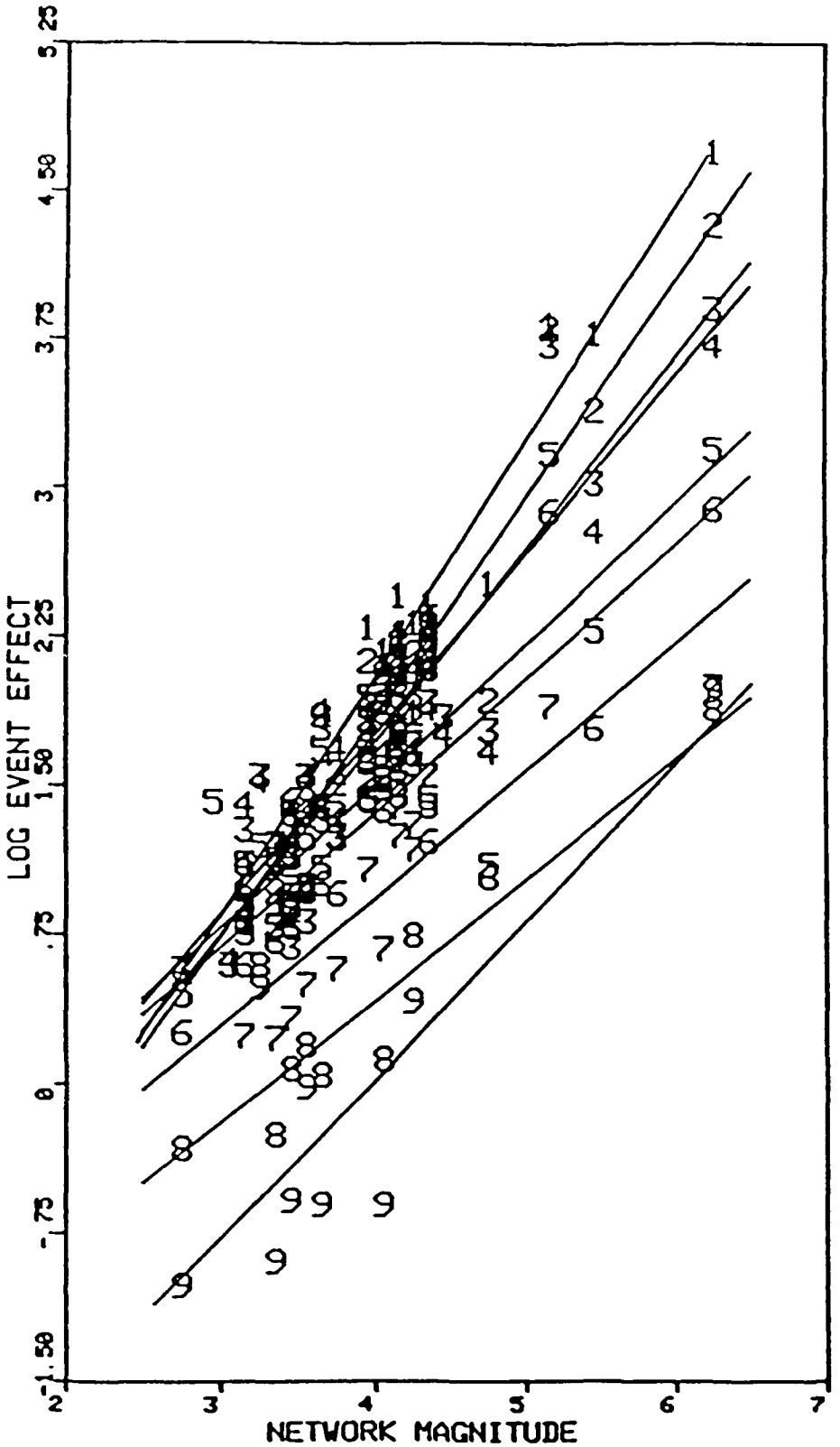


Figure 8. Regressions of *Lg* event effect versus magnitude for each of the various frequency bands. The numbers 1, 2, ..., 9 correspond to the number of each frequency band (column 1 of Table 4); the corresponding frequencies are in column 2 of Table 4.

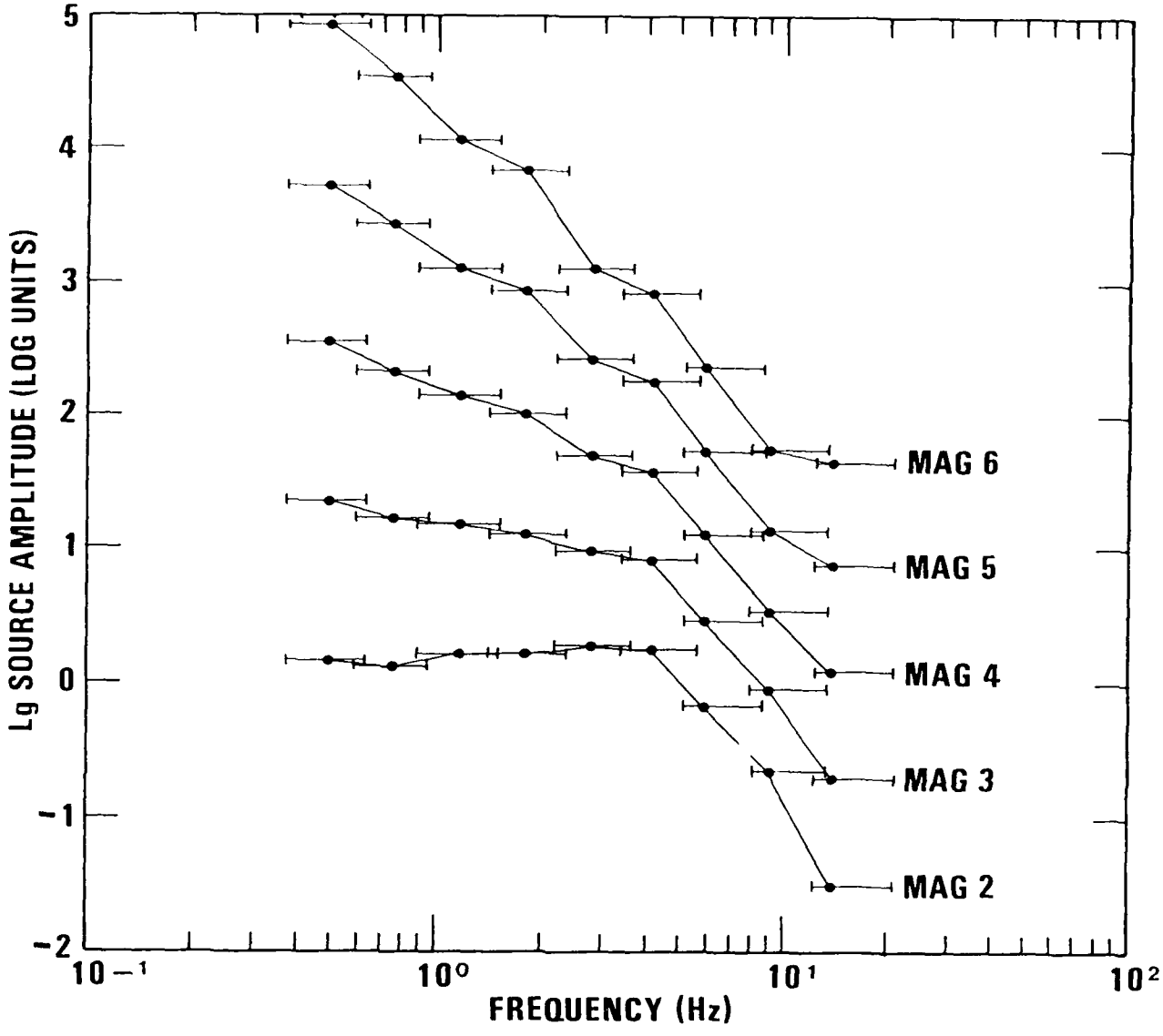


Figure 9. Average *Lg* source spectra for Canadian and eastern US earthquakes estimated from the event effects of the regression analysis in Figure 8.

that what we observe at very high frequencies is *Pn*, while at lower frequencies and large distance direct *P*, traveling through the upper mantle, may dominate. The frequency dependencies of $Q$ for the *P* phases may thus be artifacts due to the changing nature of the arrivals with frequency. Again, this makes no difference as far as detectability studies are concerned.

We have used the same events as those used in the *Lg* study. Again only short period vertical seismograms were processed. Since both *Sn* and *Pn* signals normally are smaller than the *Lg* signals, fewer of the seismograms in this database provided *Sn* and *Pn* detections than was the case with *Lg*. Consequently, there are fewer station-event pairs in the *Pn* and *Sn* analyses than there are in the *Lg* analysis.

There were 64 signal measurements from 31 earthquakes for *Sn* and 62 signal measurements from 27 earthquakes for *Pn*. Table 5 shows the regression results for *Pn* with the geometrical spreading factor inversely proportional to distance.

TABLE 5

FREQUENCY VERSUS ATTENUATION FOR *Pn* with $1 / \Delta$

| Freq Band No. | Dominant Frequency (Hz) | Number of Signals | $\gamma$ ($deg^{-1}$) | $\hat{s}(\gamma)$ ($deg^{-1}$) | Q | $\hat{s}(Q)$ | RMS of Amplitude Residuals |
|---|---|---|---|---|---|---|---|
| 1 | 0.5 | ‡ | ‡ | ‡ | ‡ | ‡ | ‡ |
| 2 | 0.7 | ‡ | ‡ | ‡ | ‡ | ‡ | ‡ |
| 3 | 1.1 | 23 | 0.068 | 0.038 | 738 | 418 | 0.14 |
| 4 | 1.8 | 38 | 0.078 | 0.026 | 1007 | 341 | 0.17 |
| 5 | 2.8 | 46 | 0.102 | 0.023 | 1187 | 267 | 0.17 |
| 6 | 4.1 | 52 | 0.133 | 0.025 | 1351 | 250 | 0.17 |
| 7 | 5.9 | 45 | 0.155 | 0.033 | 1665 | 357 | 0.18 |
| 8 | 9.1 | 28 | 0.189 | 0.067 | 2109 | 743 | 0.14 |
| 9 | 13.7 | ‡ | ‡ | ‡ | ‡ | ‡ | ‡ |

‡ insufficient data

Table 6 shows the regression results for *Sn*. For *Sn* the combined geometrical spreading and dispersion factor was inversely proportional to distance to the 5/6 power, just as was the case for *Lg*.

TABLE 6
FREQUENCY VERSUS ATTENUATION FOR *Sn*

| Freq Band No. | Dominant Frequency (Hz) | Number of Signals | $\gamma$ ($deg^{-1}$) | $\hat{s}(\gamma)$ ($deg^{-1}$) | Q | $\hat{s}(Q)$ | RMS of Amplitude Residuals |
|---|---|---|---|---|---|---|---|
| 1 | 0.5 | ‡ | ‡ | ‡ | ‡ | ‡ | ‡ |
| 2 | 0.7 | 14 | 0.039 | 0.076 | 1488 | 2928 | 0.10 |
| 3 | 1.1 | 25 | 0.086 | 0.015 | 1032 | 178 | 0.05 |
| 4 | 1.8 | 45 | 0.105 | 0.019 | 1332 | 237 | 0.10 |
| 5 | 2.8 | 48 | 0.123 | 0.017 | 1744 | 247 | 0.10 |
| 6 | 4.1 | 41 | 0.149 | 0.024 | 2139 | 348 | 0.12 |
| 7 | 5.9 | 42 | 0.161 | 0.029 | 2862 | 507 | 0.13 |
| 8 | 9.1 | 31 | 0.13 | 0.049 | 5435 | 2031 | 0.19 |
| 9 | 13.7 | ‡ | ‡ | ‡ | ‡ | ‡ | ‡ |

‡ insufficient data

Figure 10 gives these results for $Q$ versus frequency with the same geometrical spreading factor, $\Delta^{-5/6}$, for *Pn* and *Sn* as the one used for *Lg*. The least squares fit for $Q$ versus frequency for the different phases are:

$$\text{for } Lg,\ Q(f) = 1000f^{0.35}$$

$$\text{for } Sn,\ Q(f) = 825f^{0.80}$$

$$\text{for } Pn,\ Q(f) = 640f^{0.50}$$

The various formulas shown for different geometrical spreading-dispersion relationships all give about the same amplitude decrease rates with distance in the 200-1200 km distance range where most of the data were fitted. Since the $\Delta^{-5/6}$ geometrical spreading-dispersion factor may not be appropriate to *Sn* and *Pn*, in Table 7 we list the Q(f) formulas for some other candidate exponential distance factors:

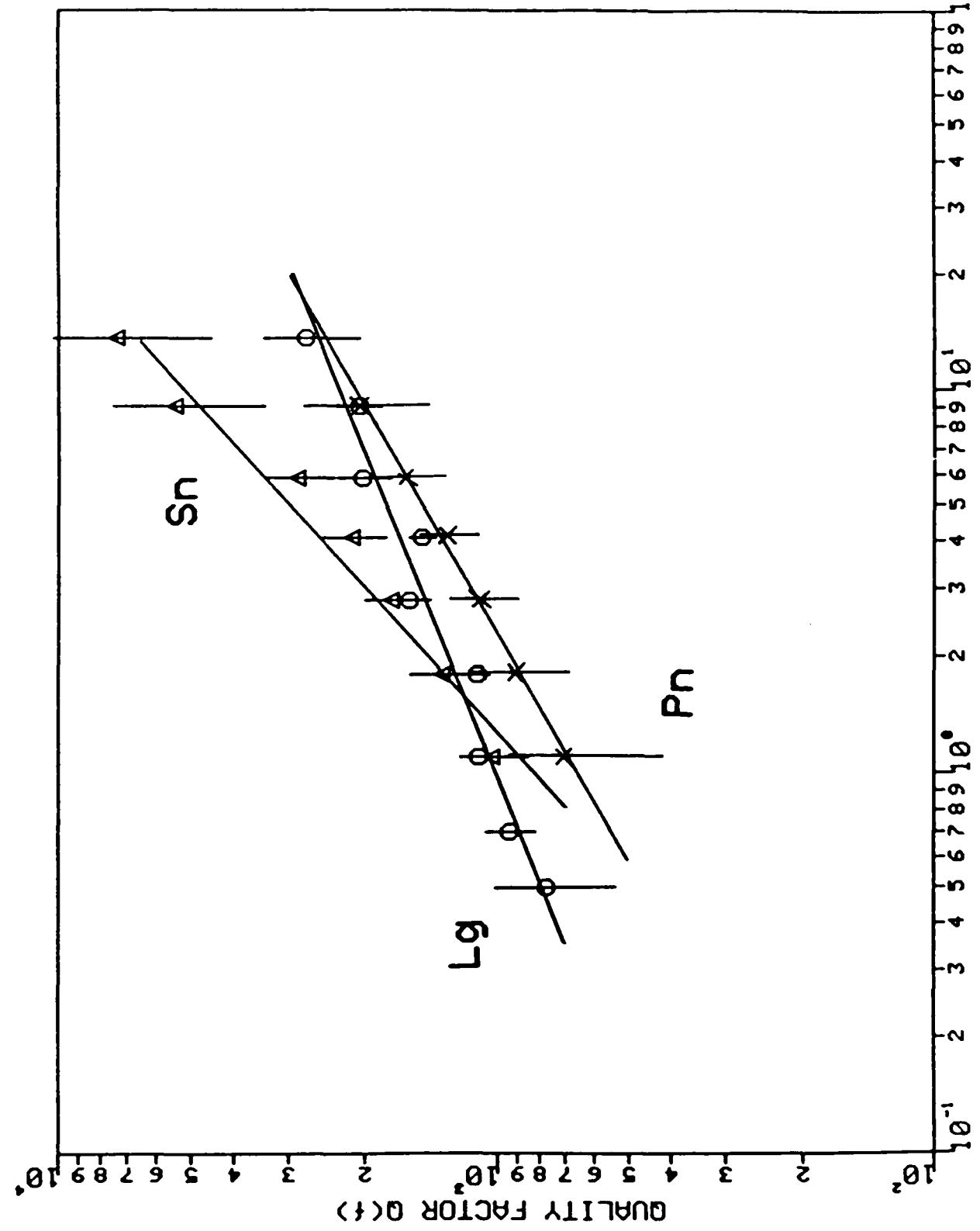


Figure 10. $Q$ versus frequency for $Pn$, $Sn$, and $Lg$. A combined geometrical spreading and dispersion term of $\Delta^{-5/6}$ was assumed for all phases.

| TABLE 7 | | | | |
|---|---|---|---|---|
| Q for Different Assumed Geometrical Spreading + Dispersion Values | | | | |
| Phase | Assumed Geometrical Spreading + Dispersion | | | |
| | $\Delta^{-1/2}$ | $\Delta^{-5/6}$ | $\Delta^{-1}$ | $\Delta^{-1.5}$ |
| *Pn* | $480\,f^{0.60}$ | $640\,f^{0.50}$ | $770\,f^{0.45}$ | $1840\,f^{0.10}$ |
| *Sn* | $610\,f^{0.85}$ | $825\,f^{0.80}$ | $1000\,f^{0.75}$ | $2660\,f^{0.10}$ |
| *Lg* | | $1000\,f^{0.35}$ | | |

If the reader wishes to compare these results with those appropriate to some other spreading-dispersion factor, in Table 8 we give a listing of a computer program that can be used to relate Q(f) values obtained by two different $\Delta^{-n}$ factors as fitted in various distance ranges. Later in this report we shall compare findings of various researchers with regards to Q(f) for the various crustal arrivals by the use of this program. The fact that we have used $\Delta^{-5/6}$ as a standard of comparison does not mean that we believe that this factor is the right one for all crustal arrivals.

## TABLE 8

### FORTRAN77 Program *newq*

```
      program newq

c     This program allows an examination of the range of plausible tradeoffs
c     between Q and the combined geometrical spreading/dispersion expressed as Δ^-n
c
c     Given the Q, Q1, at some frequency, f, for a given distance range,
c     imin to imax (in km), assuming an exponent of distance, n1, for the
c     combined geometrical spreading and dispersion,
c     calculates the Q, Q2, at f, for a different exponent of distance, n2,
c     assuming the model below:
c
c     given Q1, n1, n2, U, and f, finds Q2 for a given distance range
c
c           A ~ A0 Δ^-n e^-γΔ ,   where γ = πf/UQ

      real n1,n2
      real ds(30),x(30),y(30)
      character*80 dum

      data pi/3.14159265/

c     'ENTER EXPONENTS n1 AND n2:'
      read(5,*) dum
      read(5,*) n1,n2
c     'ENTER Q1:'
```

```
      read(5,*) dum
      read(5,*) q1
c     'ENTER GROUP VELOCITY:'
      read(5,*) dum
      read(5,*) u
c     'ENTER FREQUENCY (Hz):'
      read(5,*) dum
      read(5,*) freq
c     'ENTER MIN AND MAX DISTANCES (km), AND DISTANCE SIZE STEP:'
c     "distance size step" must be an integral multiple of the difference between
c     the min & max distances
      read(5,*) dum
      read(5,*) imin,imax,istep
      ndist=((imax-imin)/istep)+1

      gamma1=pi*freq/u/q1

c     Linearize the equation Δ^-n1 e^-γ1Δ , = Δ^-n2 e^-γ2Δ ,
c     by taking the log of both sides.
c
c     Then do a least squares fit of the linearized equation over the given distance range,
c     constraining the midpoint of the new fit to equal the midpoint of the old fit.
c     (This constraint is necessary since there is a third term, the source, being
c     traded off in addition to the Q and geometrical spreading/dispersion terms.)
c
      do 20 i=1,ndist
            ds(i)=float(imin)+float((i-1)*istep)
            x(i)=ds(i)
            y(i)=(n1-n2)*log(ds(i))
   20 continue
      xa=0.0
      ya=0.0
      pts=float(ndist)
      do 30 i=1,ndist
            xa=xa+x(i)
            ya=ya+y(i)
   30 continue
      aa=0.0
      bb=0.0
      xa=xa/pts
      ya=ya/pts
      do 40 i=1,ndist
            aa=aa+(x(i)-xa)*(y(i)-ya)
            bb=bb+(x(i)-xa)**2.
   40 continue
      b=aa/bb
      a=ya*b*xa
      gamma2=gamma1+b
      q2=pi*freq/u/gamma2
      print *,freq,q2

c     After repeating this procedure for a suite of frequencies, one can calculate Q(f) from
c     the resulting table of Q versus f

      end
```

A constraint on which model for the attenuation of *Pn* is the most applicable is provided by the Early Rise data described by Warren *et al* (1978). They succeeded to fit the amplitude

decay of *Pn* phases with a $\Delta^{-1.5}$ near 1 Hz in the distance range of 50-1200 km. This would favor models of very high Q coupled with a geometrical spreading factor near $\Delta^{-1.5}$. For all of the phases analyzed $Q$ increases with frequency. However, for none of them does $Q$ increase with frequency to the first power which it must to give the same propagation efficiency at high frequencies (20 to 40 Hz) as at 1 Hz. From these data it does appear that $Q(f)$ for *Sn* is significantly higher than that for *Pn* at all frequencies.

## Source Spectra for Pn and Sn

The estimates of the source excitation functions for *Pn* and *Sn* are derived in the same way as those for *Lg*. Figures 11 and 12 show the source spectral estimates for *Pn* ( $\Delta^{-1}$), and *Sn* respectively. The source spectra for *Pn* have the same shape regardless of the geometrical spreading factor assumed since that factor is only a function of distance, not of frequency. Incidentally, we have found no significant differences in the shapes of source spectral estimates when we used geometrical spreading factors other than $\Delta^{-5/6}$, only their absolute levels were different.

The *Pn* and *Sn* amplitude spectra have generally the same shape as the *Lg* spectra, though the *Pn* and *Sn* amplitude spectral levels are roughly one order of magnitude less than the *Lg* amplitude spectral levels for an event of the same magnitude. Like the *Lg* source spectra, the *Pn* and *Sn* source spectra have ill defined corner frequencies, partially because these source spectra are averages over many events with possibly varying stress drops. The high frequency fall-off rates for *Sn* are $\sim f^{-2}$ to $f^{-3}$. For *Pn*, the fall-off rates appear lower (though we probably do not have have enough frequencies in our data to properly resolve the corner frequencies of the smaller magnitude events).

We see no evidence for significantly different fall-off rates between *P* and *S* phases such as suggested by Evernden *et al* (1986) who found a *P* high frequency fall-off of $f^{-3}$ and a *S*

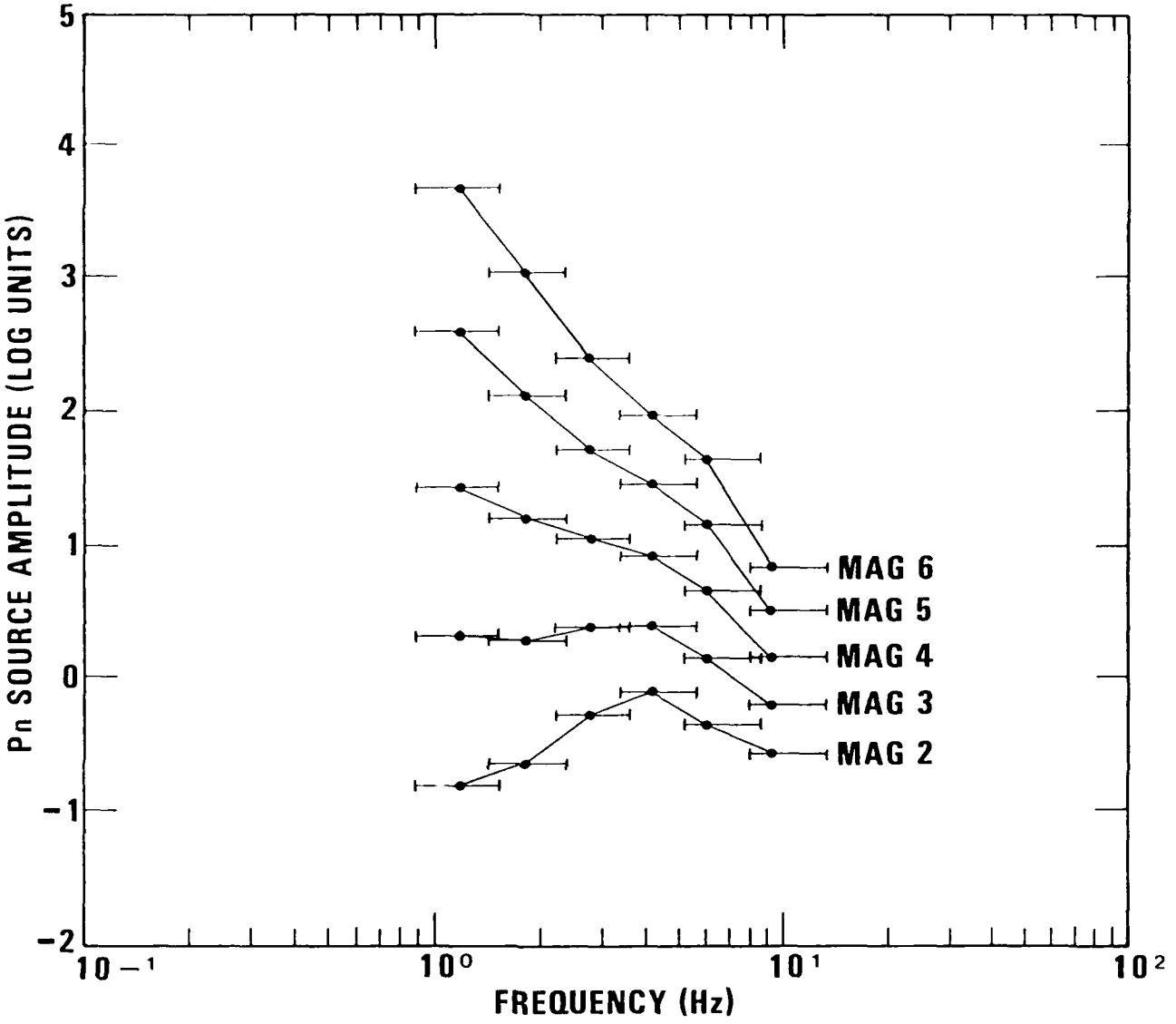


Figure 11. Source excitation functions estimated from *Pn* signals assuming combined geometrical spreading and dispersion of $\Delta^{-1}$.

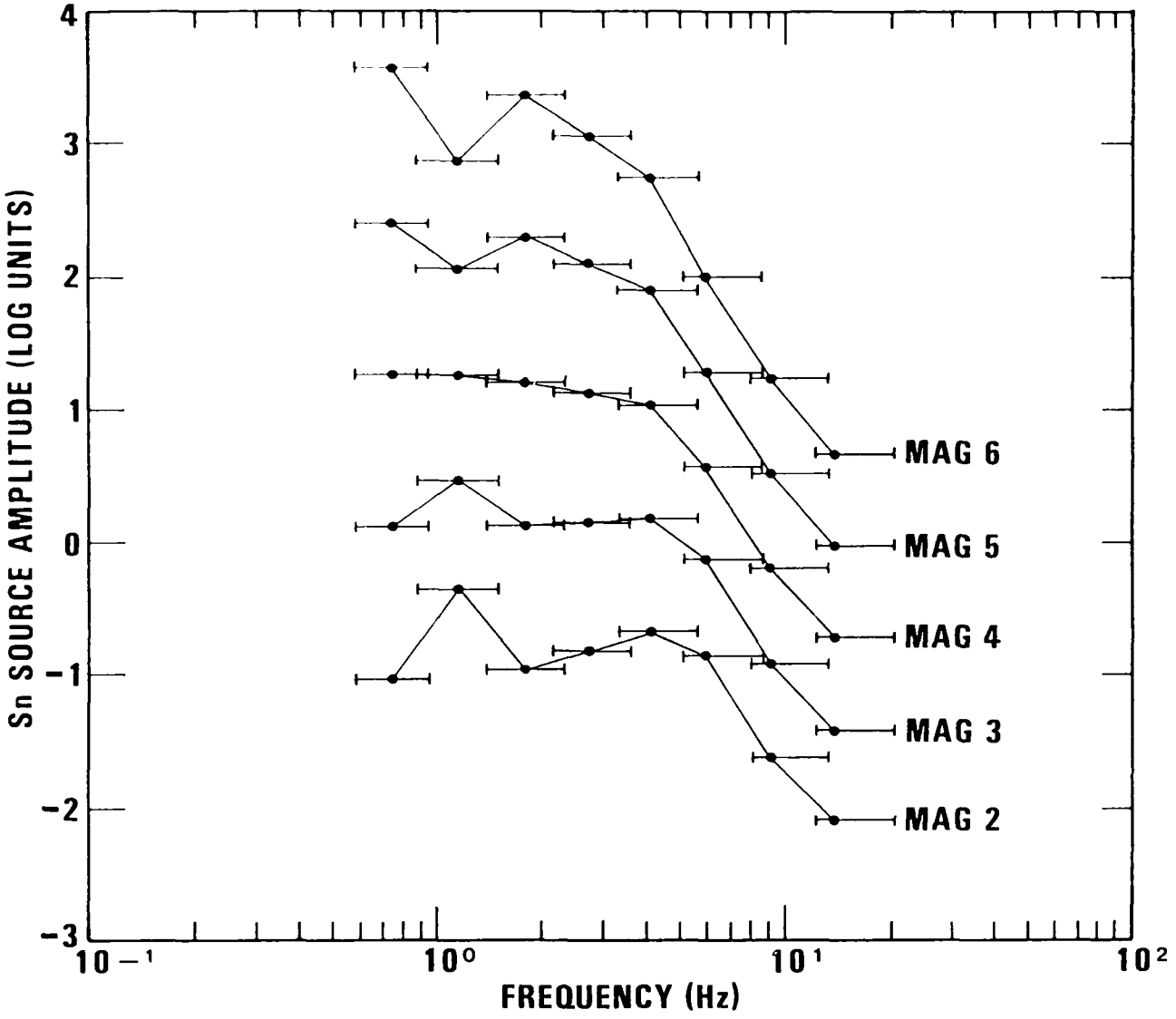


Figure 12. Source excitation functions estimated from *Sn* signals.

high frequency fall-off of $f^{-2}$ for a regionally recorded event in New York. To test this further, we computed ratios between *Pn* and *Sn* spectra for the same event, corrected for Q and instrument, recorded at regional distances at RSTN stations. Though we do not generally have enough good signal-to-noise above the corner frequency to make any strong statements, these ratios show no evidence that *P* has a faster fall-off rate than *S* above the corner frequency.

## Comparisons with Other Studies

The seismological literature is replete with formulas derived for the quality factors of regionals crustal arrivals, especially for Lg. Some of these are constant Q estimates, such as those of Evernden *et al* (1986) who did not want to be involved with details of frequency dependence. Nevertheless these authors also stated some limits to the frequency dependence of Q for short-period crustal P and S waves. A large number of the Q for regional arrivals given in the literature are frequency dependent. Some were derived by inverting multimode surface wave data (Mitchell 1981). Other set of numbers comes from coda Q studies (Singh and Herrmann 1983). Finally, a smaller set of results comes from the independent estimation of Q(f) from multistation data for each individual crustal phase (Campillo *et al* 1985, Mechler *et al* 1980, Chun *et al* 1987). Some results come from different geographical regions. Comparing these results gives us an idea of the reliability of the methods and the extent of world-wide regional variability of Q(f) for each phase as well.

The results of previous studies are summarized in Table 9 for tectonically stable "shield" areas and in Table 10 for regions with other tectonic regimes. The synopsis in Table 9 shows that $Q_{Lg}$ has been well studied in shield areas and that the results by various workers, including this report, are roughly comparable. Our results for *P–Pn* and *Sn* are, on the other hand, relatively new. Comparison of the shield results to those from other areas show that the Q(f) are lower overall, but some results, especially those of Mechler *et al* (1980) for France are

remarkably similar *in form* in that the Q(f) for *Sn* increases the most rapidly with frequency of all the regional arrivals, while that for Lg is the least frequency dependent. By exercising the computer program in Table 8 the reader can easily compare the various formulas for Q(f) using various $\Delta^{-n}$. It should be noted that $\Delta^{-5/6}$ is appropriate for the time domain *Lg* Airy phase spreading factor, but that spectra of *Lg* for constant group velocity windows have a geometrical spreading factor of $(sin\Delta)^{-1/2}$ (Shin 1985).

# TABLE 9

## Summary of Q Results from Studies for Shield Regions

### Pn

| Author | Q(f) | Geometrical Spreading + Dispersion | f (Hz) | Region | Method Distance Range |
|---|---|---|---|---|---|
| This report | $480f^{0.6}$ | $\Delta^{-1/2}$ | 1-9 | Central & ENA | time domain max amps Δ~500-3000 km |
| | $640\,f^{0.5}$ | $\Delta^{-5/6}$ | " | | |
| | $770\,f^{0.44}$ | $\Delta^{-1}$ | " | | |
| | $1840\,f^{0.1}$ | $\Delta^{-1.5}$ | " | | |
| Warren *et al* (1978) | ∞ | $\Delta^{-1.5}$ | ~1 | NENA,SENA | time domain max amps Δ~50-1700 km |
| Evernden *et al* (1986) | 9000 | $\Delta^{-2}$ | 5-50 | NENA | theoretical modeling of spectral shape Δ to at least 1000 km |

### Sn

| Author | Q(f) | Geometrical Spreading + Dispersion | f (Hz) | Region | Method Distance Range |
|---|---|---|---|---|---|
| This report | $610\,f^{0.85}$ | $\Delta^{-1/2}$ | 0.7-9 | Central & ENA | time domain max amps Δ~500-3000 km |
| | $825\,f^{0.8}$ | $\Delta^{-5/6}$ | " | | |
| | $1000\,f^{0.75}$ | $\Delta^{-1}$ | " | | |
| | $2660\,f^{0.5}$ | $\Delta^{-1.5}$ | " | | |
| Evernden *et al* (1986) | 4000 | $\Delta^{-2}$ | 5-50 | NENA | theoretical modeling of spectral shape Δ to at least 1000 km |

# Lg

| Author | Q(f) | Geometrical Spreading + Dispersion | f (Hz) | Region | Method Distance Range |
|---|---|---|---|---|---|
| This report | $1000\,f^{0.35}$ | $\Delta^{-5/6}$ | 0.5-13 | Central & ENA | time domain max amps $\Delta$~500-3000 km |
| Street (1976) | 900 | $\Delta^{-5/6}$ | 1 | US & Canada E of Rockies | time domain amplitudes $\Delta$~200-4500 km |
| Horner *et al* (1978) | 1500 | $\Delta^{-5/6}$ | 1 | Canadian shield | time domain amplitudes $\Delta$~300-7000 km |
| Mitchell (1981) | $\sim 900\,f^{0.2}$ | | 0.25-1 | ENA | theoretical modeling of spectral shape $\Delta$=500-2000 km |
| Nuttli (1981) | $800\,f^{0.5}$ | | ~1-5 | ENA | $\Delta \leq 1000$ km |
| | $1500\,f^{0.2}$ | | " | CUS | |
| Dwyer *et al* (1983) | $1280\,f^{0.4}$ | $\Delta^{-5/6}$ | 1-10 | Central US | time domain max amps from bandpass filtered data $\Delta$=200-2000 km |
| Singh & Herrmann (1983) | $900\,f^{0.35}$ | $\Delta^{-5/6}$ | 0.5-3.5 | NENA | Lg coda $\Delta$=300-800 km |
| | $1000\,f^{0.1}$ | " | " | S. Appalachians | " |
| | $1200\,f^{0.2}$ | " | " | Central US | " |
| | $900\,f^{0.25}$ | " | " | Central Central US | " |
| Pulli (1984) | $660\,f^{0.4}$ | | 0.75-10 | NENA | Lg coda amps $\Delta$~50-600 km |
| Hasegawa (1985) | $900\,f^{0.2}$ | $\Delta^{-1/2}$ | 0.6-20 | Canadian shield | spectra of ground acceleration $\Delta$~70-900 km |
| Shin (1985) | $(500\pm50)\,f^{(0.6-0.7)}$ | $\Delta^{-5/6}$ | 1-10 | Eastern Canada | time domain max amps |
| | $(500\pm50)\,f^{(0.6-0.7)}$ | $\Delta^{-1/2}$ | 1-10 | Eastern Canada | freq domain amp spectra $\Delta$~100-1000 km |
| Chun *et al* (1987) | $1100\,f^{0.19}$ | $\Delta^{-1/2}$ | 0.6-10 | Eastern Canada | spectral ratios $\Delta$=53-210 km |
| Gupta & McLaughlin (1987a) | $800\,f^{0.32}$ | $\Delta^{-5/6}$ | 0.5-7 | CUS & ENA | amplitudes from PSRV $\Delta$<1100 km |
| | 400 | " | 1 | CUS | |
| | 1100 | " | " | EENA | |
| | 1400 | " | " | Appalachians | |

TABLE 10

Summary of Q Results from Studies for Non-Shield Regions

Pn

| Author | Q(f) | Geometrical Spreading + Dispersion | f (Hz) | Region | Method Distance Range |
|---|---|---|---|---|---|
| Mechler *et al* (1980) | $810\,f^{0.1}$ | $\Delta^{-5/6}$ | 2-8 | France | time domain max amps from bandpass filtered data Δ=350-1100 km |
| Evernden *et al* (1986) | ~1000-2000 | | 5-50 | tectonic regions | theoretical modeling of spectral shape Δ to at least 1000 km |

Pg

| Author | Q(f) | Geometrical Spreading + Dispersion | f (Hz) | Region | Method Distance Range |
|---|---|---|---|---|---|
| Mechler *et al* (1980) | $200\,f^{0.64}$ | $\Delta^{-5/6}$ | 0.5-8 | France | time domain max amps from bandpass filtered data Δ=350-1100 km |

Sn

| Author | Q(f) | Geometrical Spreading + Dispersion | f (Hz) | Region | Method Distance Range |
|---|---|---|---|---|---|
| Mechler *et al* (1980) | $490\,f^{0.73}$ | $\Delta^{-5/6}$ | 1-8 | France | time domain max amps from bandpass filtered data Δ=350-1100 km |

Lg

| Author | Q(f) | Geometrical Spreading + Dispersion | f (Hz) | Region | Method Distance Range |
|---|---|---|---|---|---|
| Mechler *et al* (1980) | $400\ f^{0.44}$ | $\Delta^{-5/6}$ | 0.5-8 | France | time domain max amps from bandpass filtered data $\Delta$=350-1100 km |
| Nuttli (1981) | $200\ f^{0.7}$ | | ~1-5 | S. Calif. | $\Delta \leq 1000$ km |
| Campillo *et al* (1985) | $290\ f^{0.52}$ | $\Delta^{-5/6}$ | 0.5-10 | France | time domain max amps & theoretical modeling $\Delta$=150-2000 km |
| Chavez & Priestly (1986) | $206\ f^{0.68}$ | $\Delta^{-1/2}$ | 0.3-10 | US Great Basin explosion | frequency domain amplitudes $\Delta$=200-500 km |
| | $214(\pm 50)\ f^{0.54\pm 0.09}$ | " | 0.3-5 | US Great Basin earthquakes | " |

## Noise Spectra at RSTN Stations

Noise spectral estimates are important in estimating the detection thresholds of different sites. We have calculated noise spectral estimates for the five RSTN sites corrected for instrument response from a suite of noise samples recorded on the short period vertical instruments. The noise samples were chosen just prior to the onset of signals from 57 of the 114 earthquakes used in our regression analysis. The suite represents a random sampling occurring at all times of day and night and during all seasons of the year.

Figures 13 through 22 show the day time and night time log-averaged noise spectra for each of the five RSTN sites along with curves at $\pm 1$ standard deviation, $\sigma$, from the mean. For each data set, the mean and the standard deviation were computed separately at each frequency to produce the mean spectra shown in the figures. The RSCP noise spectra are only valid to around 8 Hz since RSCP has a sharp high frequency cutoff filter which takes effect at 8 Hz. Beyond that frequency, the spectra exhibit only roundoff errors in the digitizer, not true ground

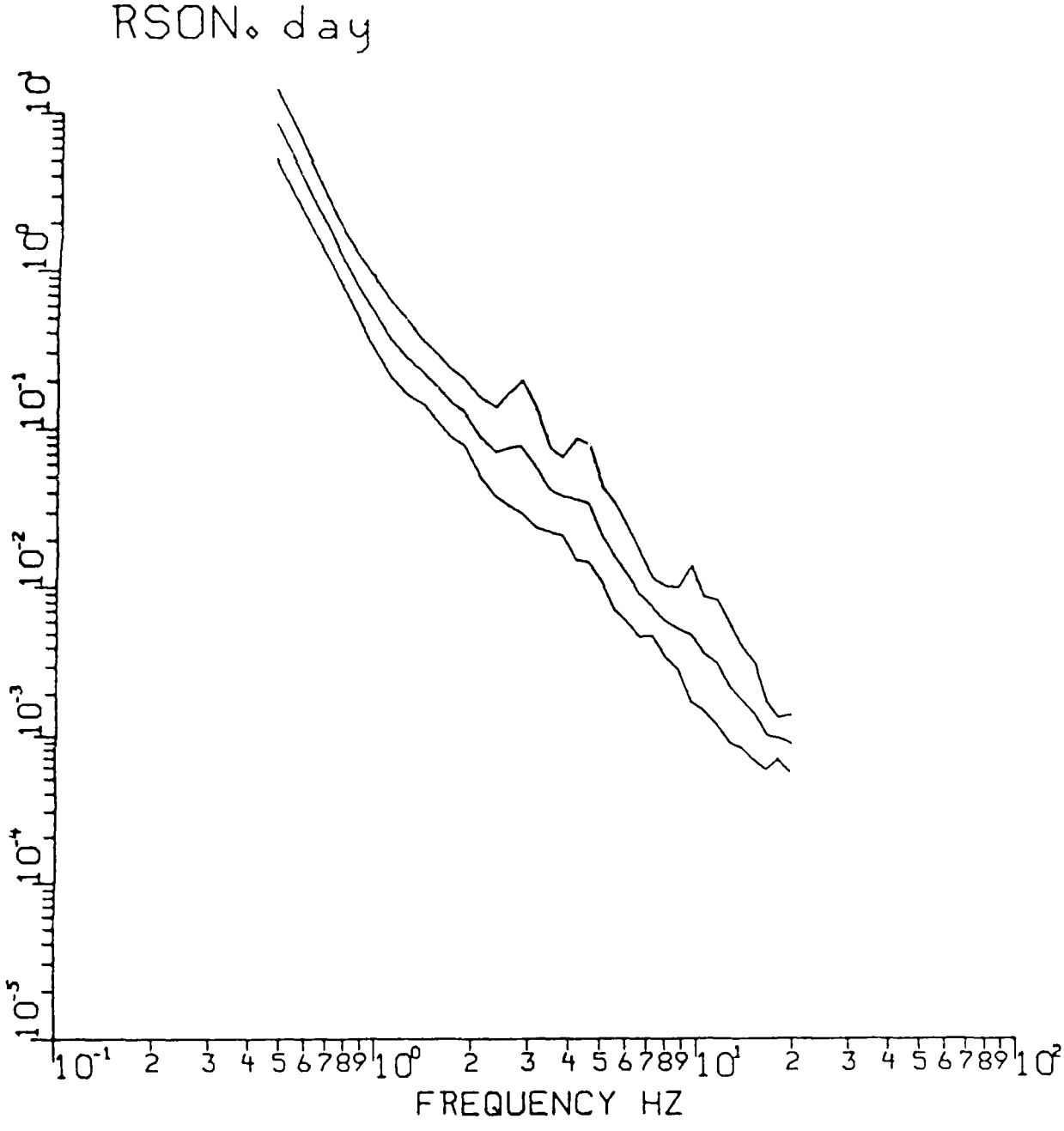


**Figure 13.** Average daytime noise spectra at RSON. Mean and one standard deviation limits indicated.

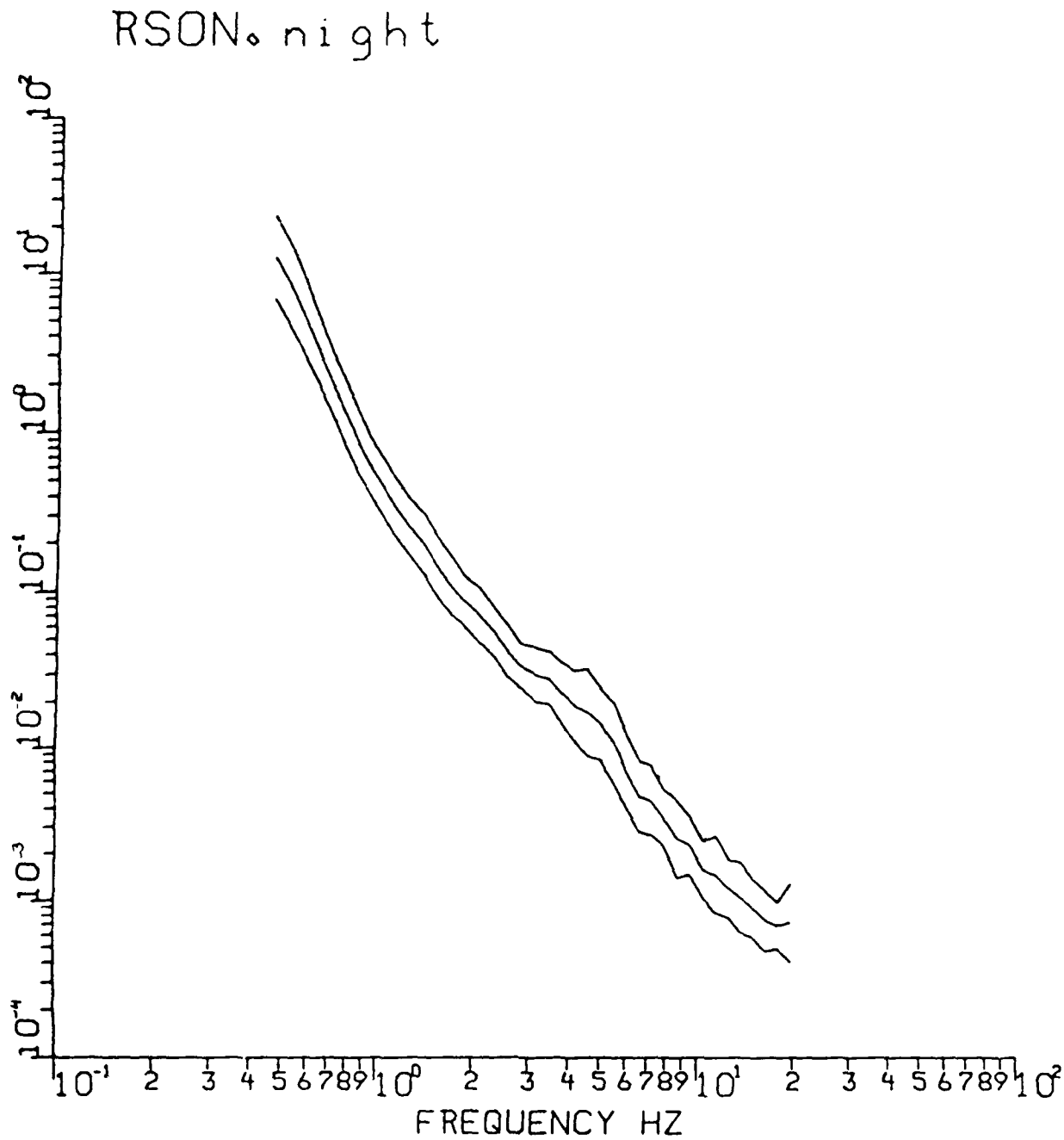


**Figure 14.** Average nighttime noise spectra at RSON. Mean and one standard deviation limits indicated.

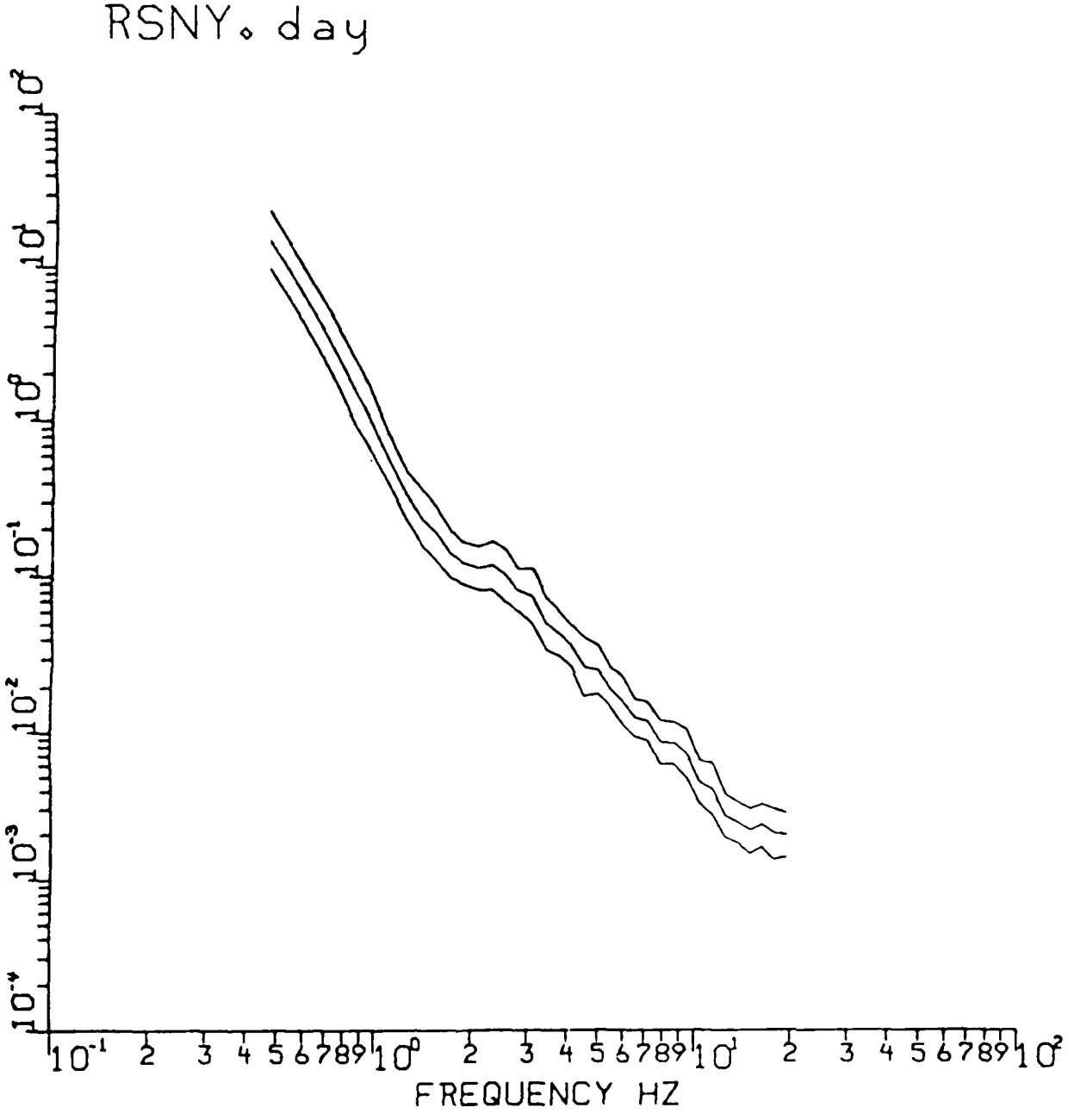


**Figure 15.** Average daytime noise spectra at RSNY. Mean and one standard deviation limits indicated.

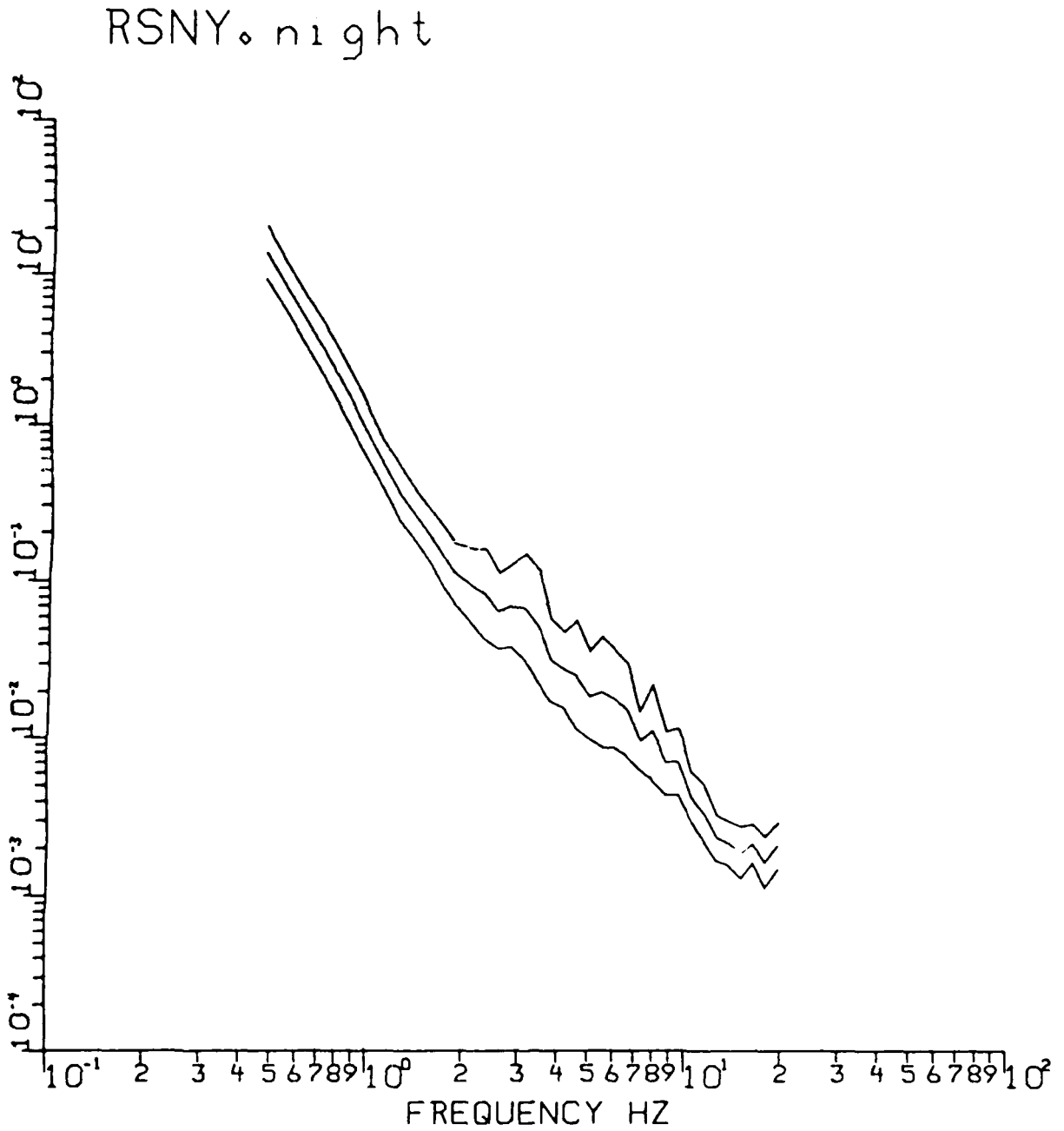


**Figure 16.** Average nighttime noise spectra at RSNY. Mean and one standard deviation limits indicated.

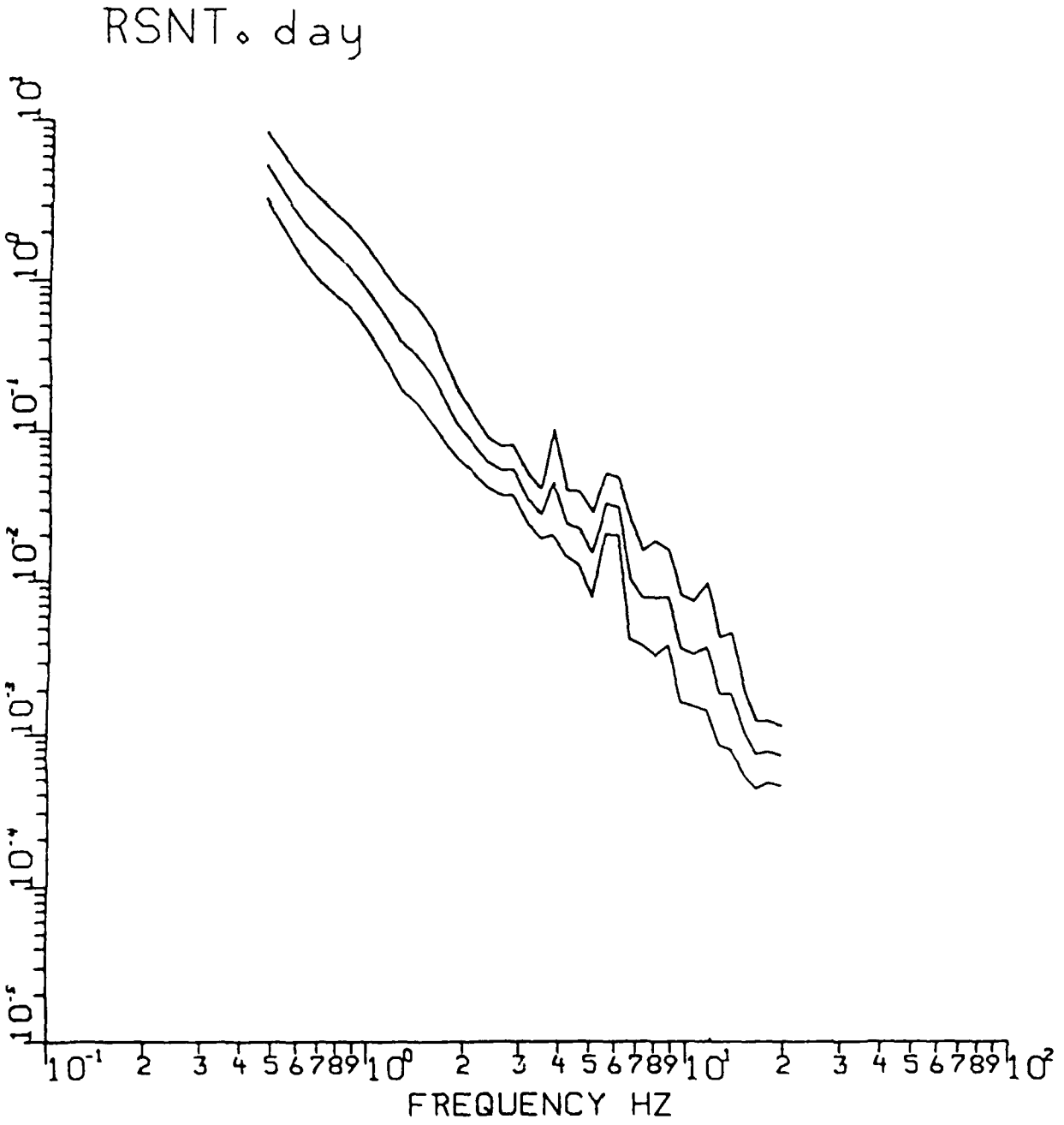


**Figure 17.** Average daytime noise spectra at RSNT. Mean and one standard deviation limits indicated.

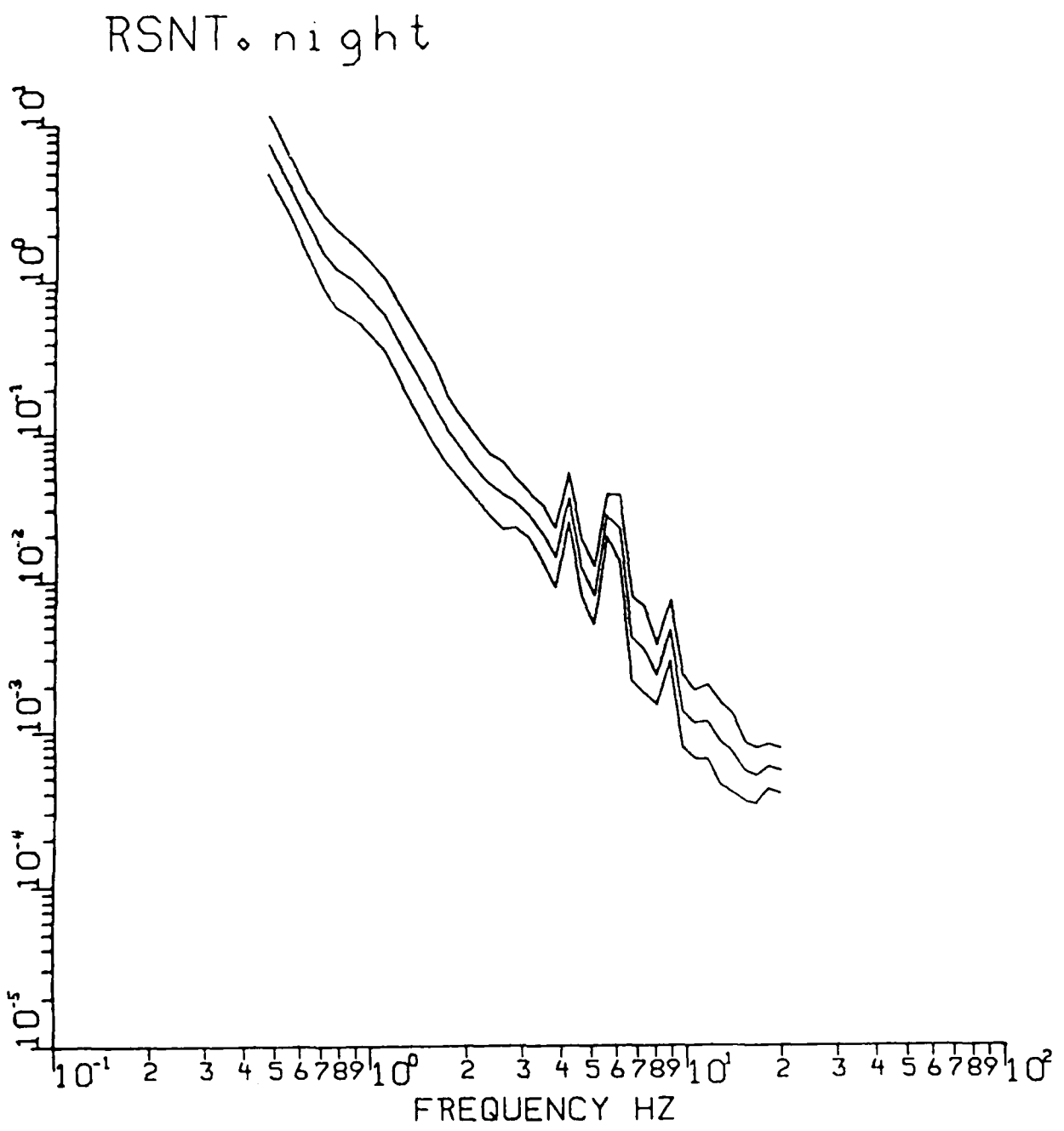


**Figure 18.** Average nighttime noise spectra at RSNT. Mean and one standard deviation limits indicated.

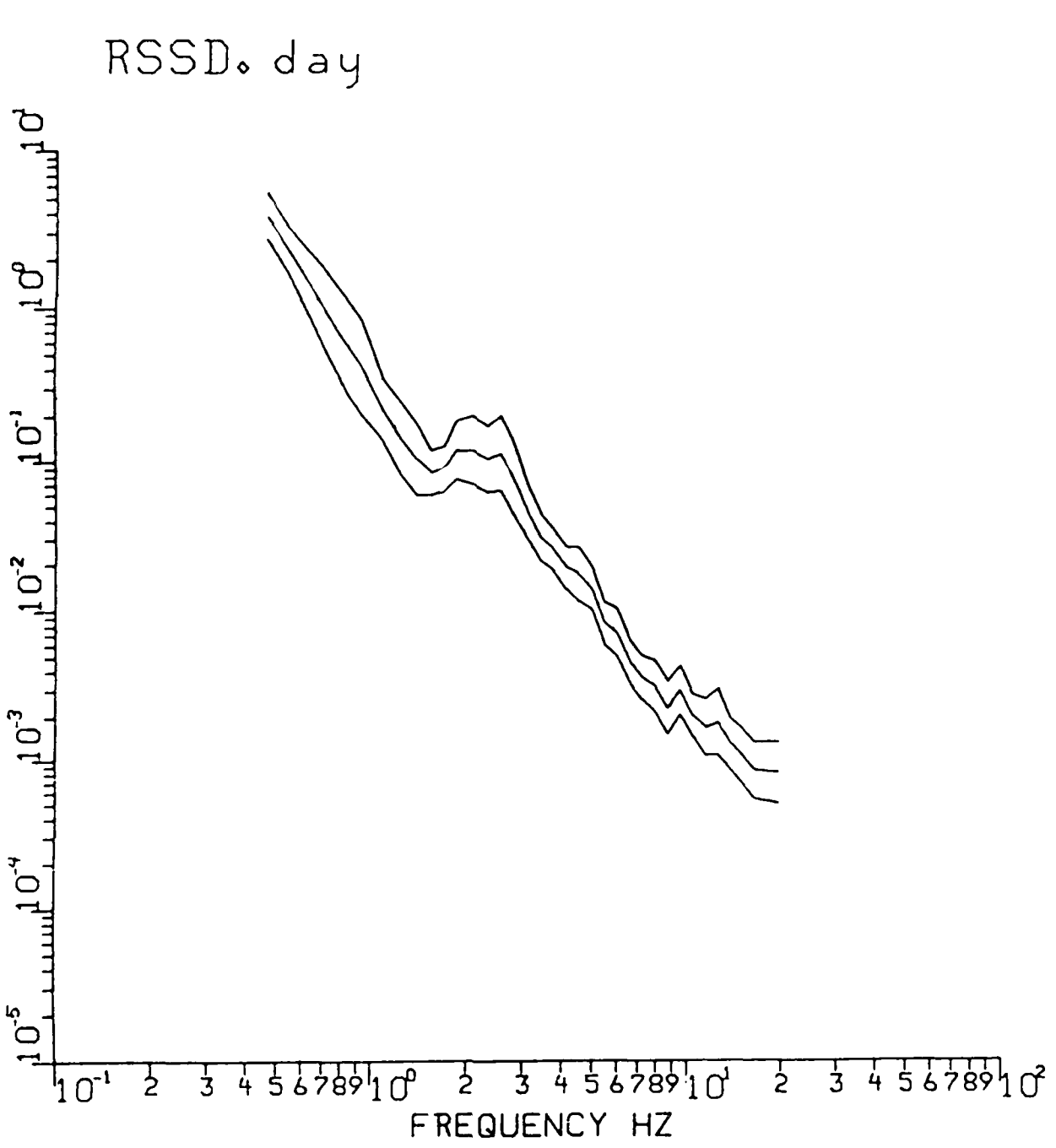


**Figure 19.** Average daytime noise spectra at RSSD. Mean and one standard deviation limits indicated.

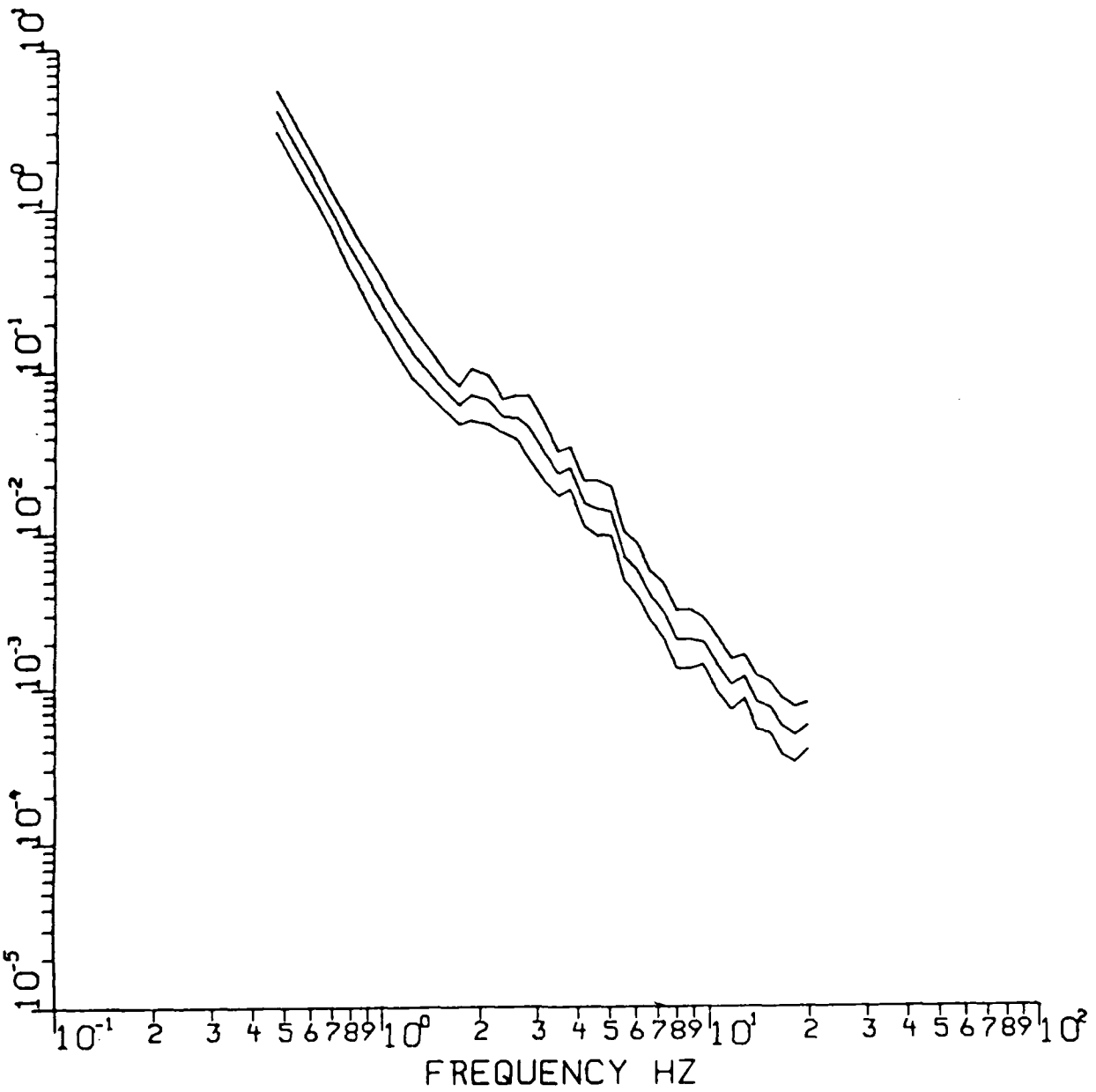


**Figure 20.** Average nighttime noise spectra at RSSD. Mean and one standard deviation limits indicated.

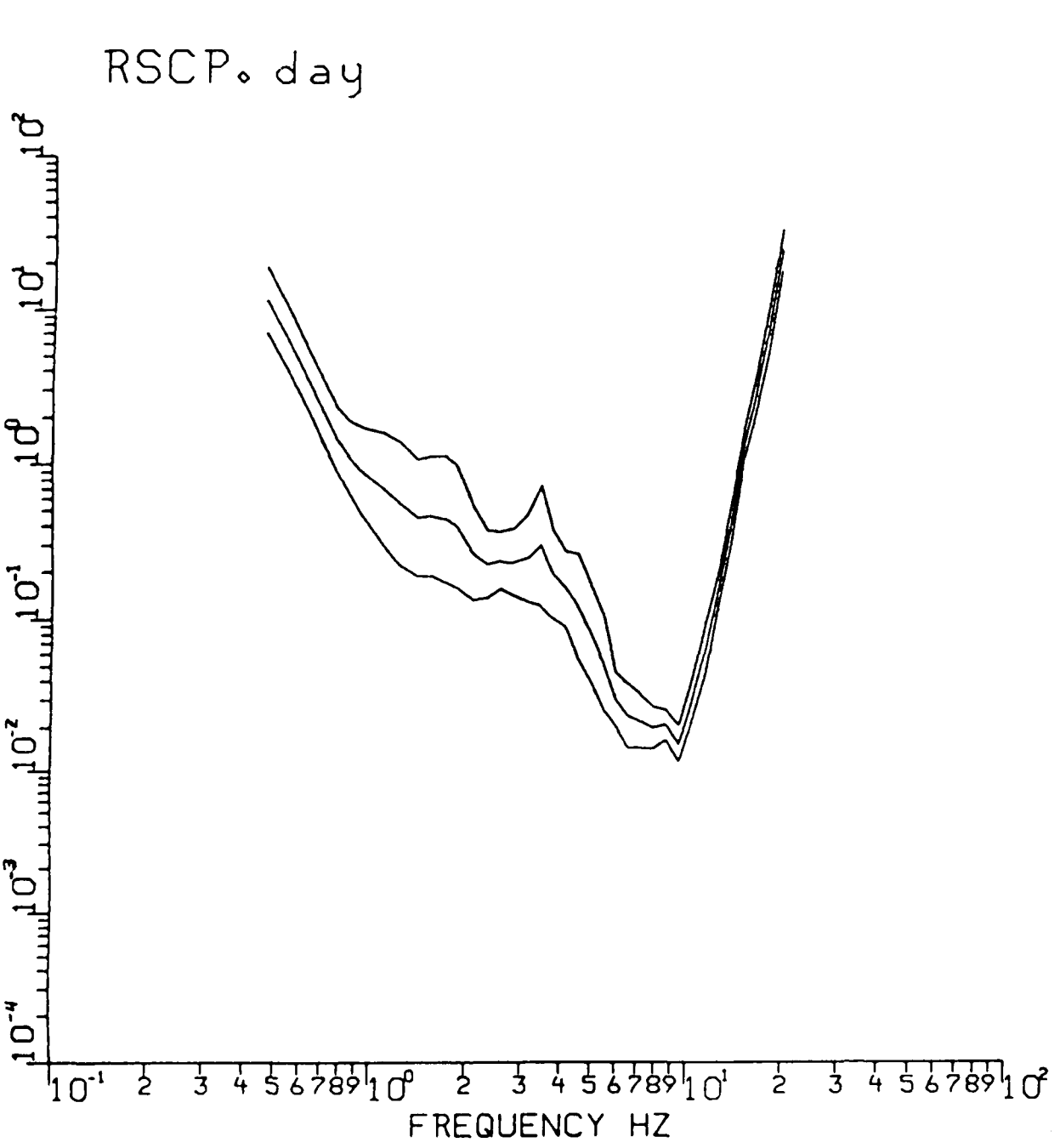


**Figure 21.** Average daytime noise spectra at RSCP. Mean and one standard deviation limits indicated.

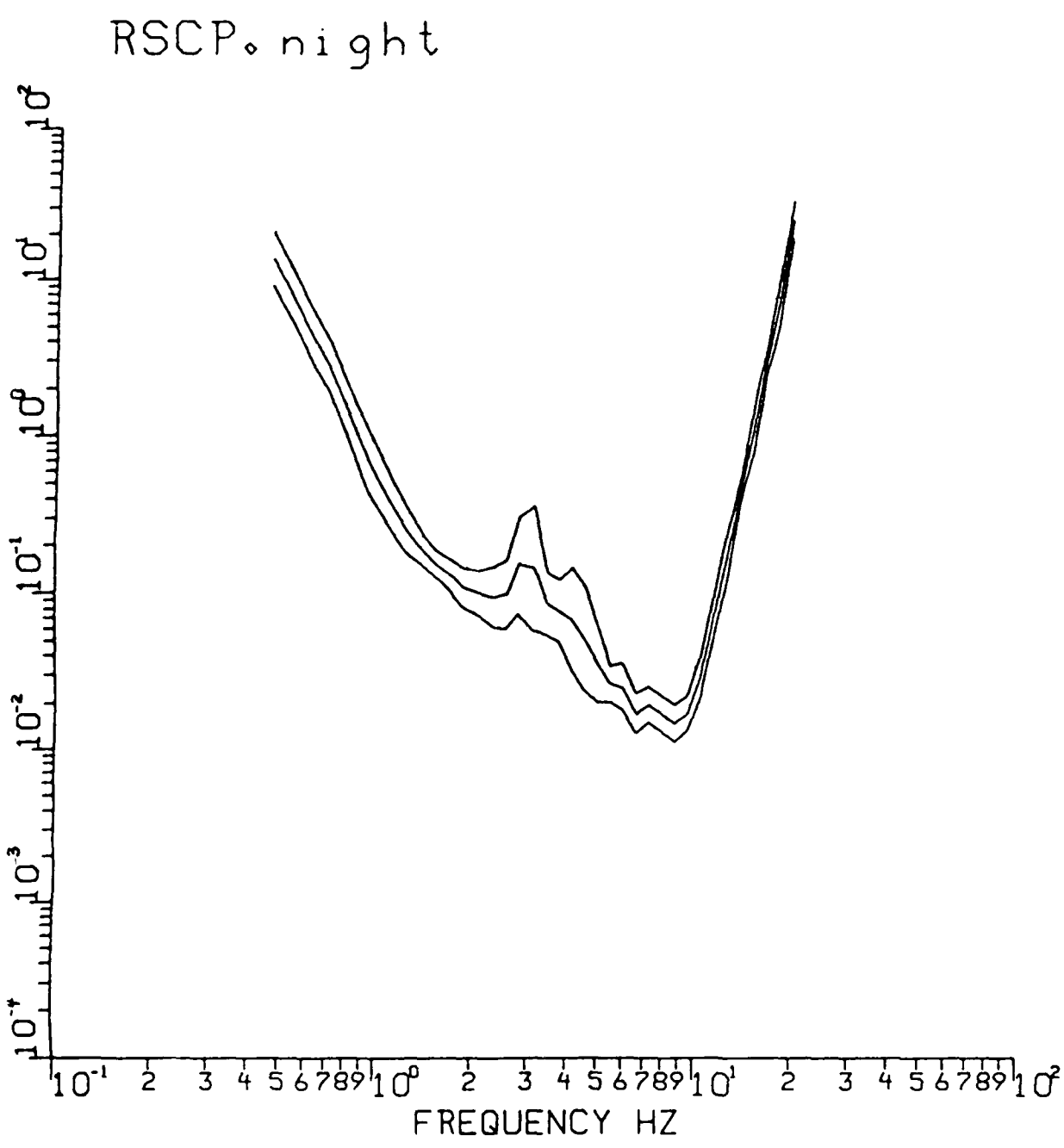


Figure 22. Average nighttime noise spectra at RSCP. Mean and one standard deviation limits indicated.

motion. Consequently, when the instrument correction is applied, this A-to-D roundoff error, which is in fact a flat spectrum, increases with frequency at the inverse of the filter falloff rate.

For comparison, the noise spectral level was also calculated from the peak readings of the envelope time traces. For RSSD, the spectral estimate which most closely approximates the one calculated from peak readings of the envelope time traces is the upper bound estimate. Table 11 shows the log-average noise level and the normalized standard deviation of the noise estimate at five frequencies (1, 2, 4, 8 and 18 Hertz) for each of the RSTN sites.

TABLE 11

Noise Displacement Amplitude at the RSTN Stations in $nm/\sqrt{Hz}$

| Freq | 1 Hz | | 2 Hz | | 4 Hz | | 8 Hz | | 18 Hz | |
|---|---|---|---|---|---|---|---|---|---|---|
| Station | $\bar{m}$ | $\sigma_n$ | $\bar{m}$ | $\sigma_n$ | $\bar{m}$ | $\sigma_n$ | $\bar{m}$ | $\sigma_n$ | $\bar{m}$ | $\sigma_n$ |
| RSSD | 0.27 | 67% | 0.093 | 65% | 0.021 | 43% | 0.0025 | 52% | 0.00064 | 61% |
| RSON | 0.48 | 60 | 0.098 | 62 | 0.029 | 100 | 0.0046 | 76 | 0.00084 | 50 |
| RSNT | 0.76 | 79 | 0.087 | 63 | 0.038 | 95 | 0.0045 | 151 | 0.00067 | 54 |
| RSNY | 0.80 | 49 | 0.108 | 44 | 0.036 | 56 | 0.0096 | 74 | 0.00192 | 44 |
| RSCP | 0.66 | 102 | 0.227 | 151 | 0.118 | 95 | 0.0186 | 33 | | |

A diurnal variation in the noise levels is observed at all of the RSTN sites, with the daytime noise averaging 1.5 times higher than the nighttime noise at RSSD and up to 3 time higher at some frequencies at RSCP and RSON. The site with the largest seasonal variation is RSNT which is quietest in the winter when the Great Slave Lake is frozen. For frequencies above 2 or 3 Hz, the noise amplitude spectra fall off as $f^{-2.2}$ to $f^{-2.6}$. RSSD is the quietest station while RSNY and RSCP are the noisiest. These results, including the general details of the spectral peaks and nulls, agree very closely with spectral noise estimates made for the RSTN stations by LLNL (Rodgers *et al* 1987). The noise levels at the RSTN stations are similar to the noise levels in southeastern Norway (Bungum *et al* 1985), and are not quite as low as the quiet noise levels at Lajitas.

## DETECTION THRESHOLDS FOR REGIONAL SIGNALS

One of the most important reasons for this study is to determine the detection thresholds for the various crustal arrivals as functions of epicentral distance and frequency. The results are of prime importance for predicting the performance of any CTBT monitoring network installed in or around the USSR.

The detection thresholds for all regional phases were estimated following the approach used by Blandford *et al* (1983). We have plotted the quantity of $m_b$ - log(A/N) for each frequency band against distance for each phase, where A is the signal envelope amplitude and N is the preceding noise envelope amplitude measured off the bandpass filtered outputs. This quantity is an estimate of the magnitude at which the signal amplitude equals that of the noise, which may be assumed to be the 50% detection threshold. Due to the spectral differences associated with source scaling this approach tends to give conservative (too high) threshold estimates.

These 50% thresholds, of course, cannot be applied in practice since the associated numbers of false alarms would be unacceptably high (Israelson 1986a,b). In order to achieve, say, 84% detection efficiency we must raise the 50% detection thresholds by one standard deviation of the $m_b$-$\log_{10}$(S/N) population. Our data set has typically 0.3-0.4 m.u. standard deviations and this is the amount by which the thresholds shown below must be increased to achieve 84% efficiency. 98% detection thresholds require the increase of an additional standard deviation.

Figures 23 to 26 show our 50% detection threshold estimates for *Pn*, *Pg*, *Sn*, and *Lg*, respectively, as functions of frequency for various epicentral distance ranges. As expected, the *Lg* detection thresholds are the lowest at low frequencies but approach those of the *Sn* at high frequencies and small distances. This is understandable since at small distances *Lg* is very

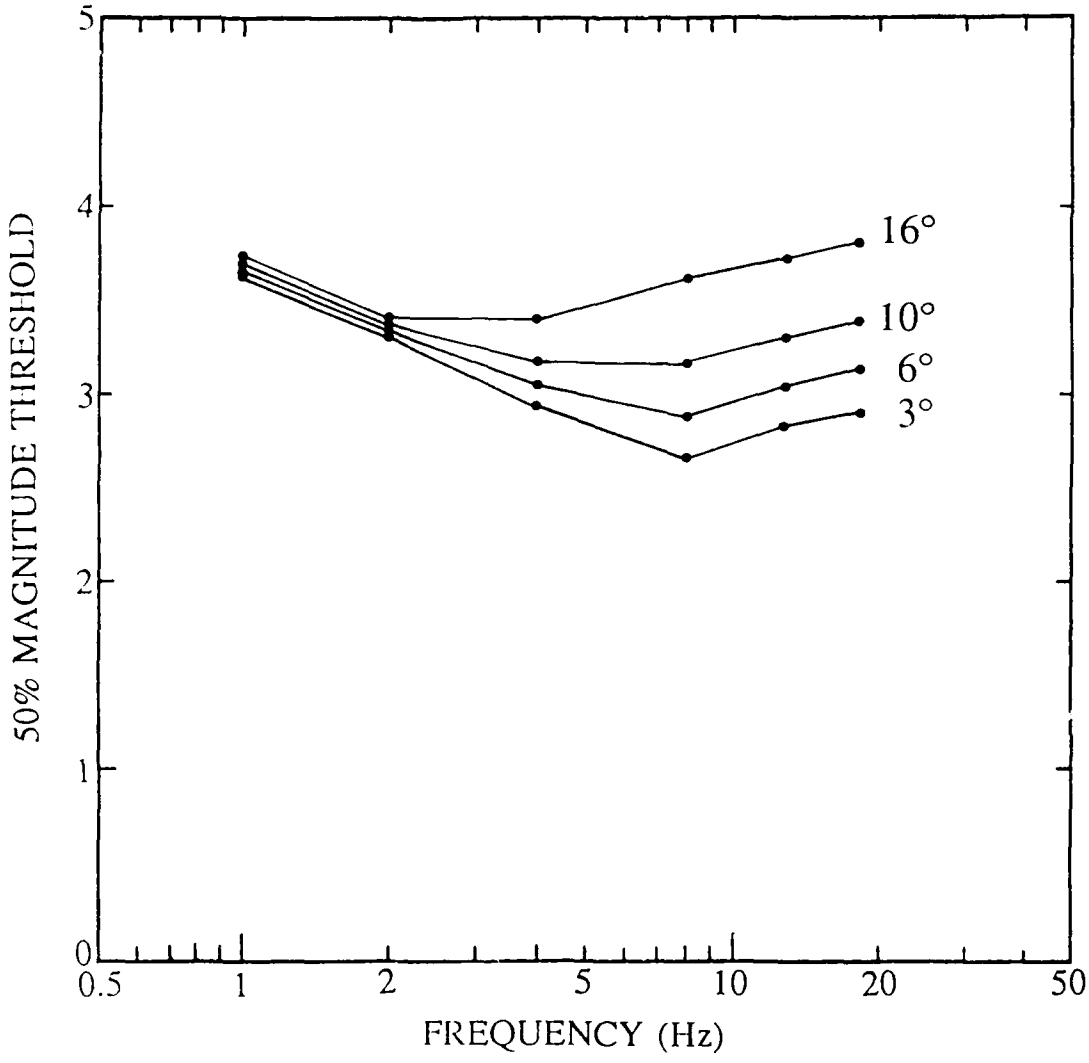


**Figure 23.** Average RSTN 50% detection threshold curves as a function of frequency for *Pn* for distances from 3 to 16°.

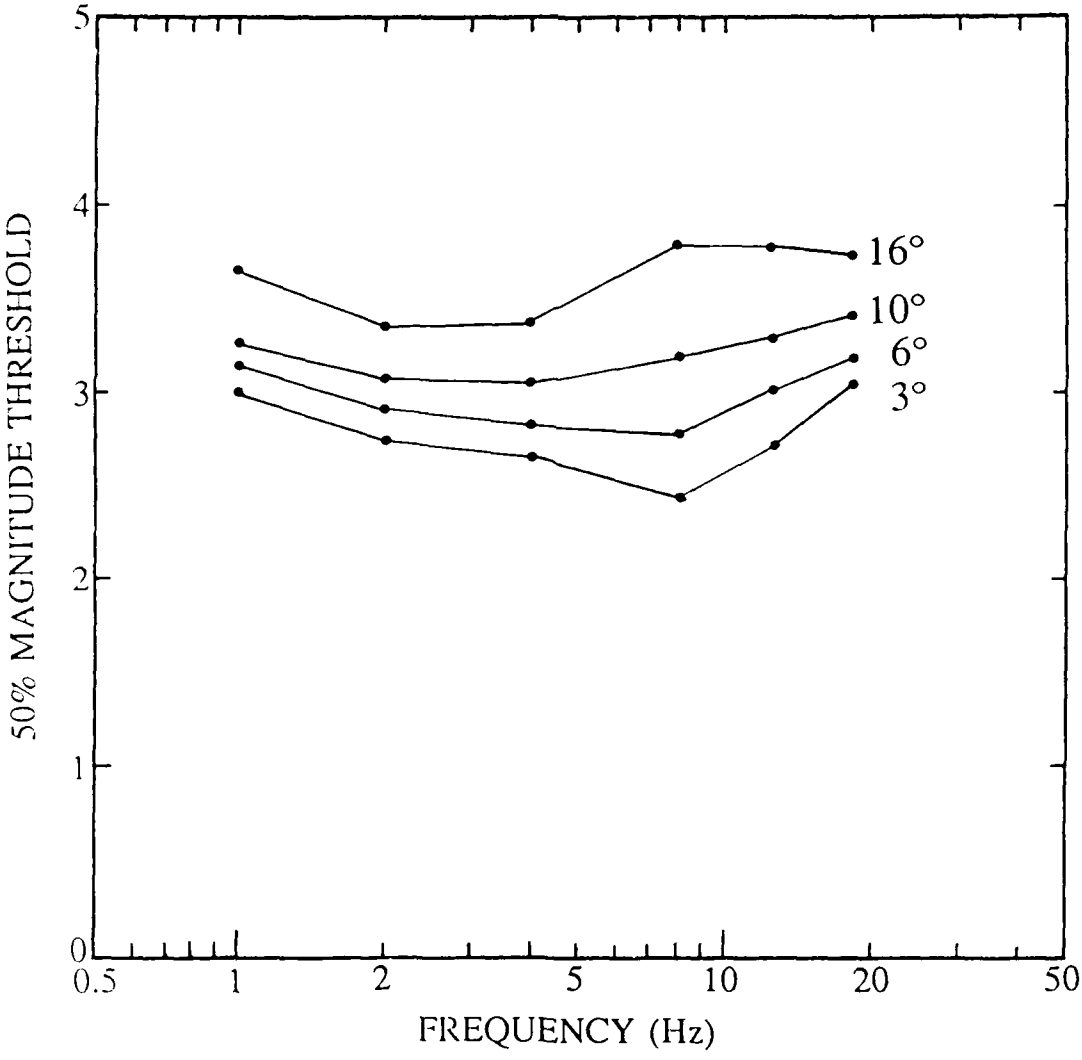


**Figure 24.** Average RSTN 50% detection threshold curves as a function of frequency for *Pg* for distances from 3 to 16°.

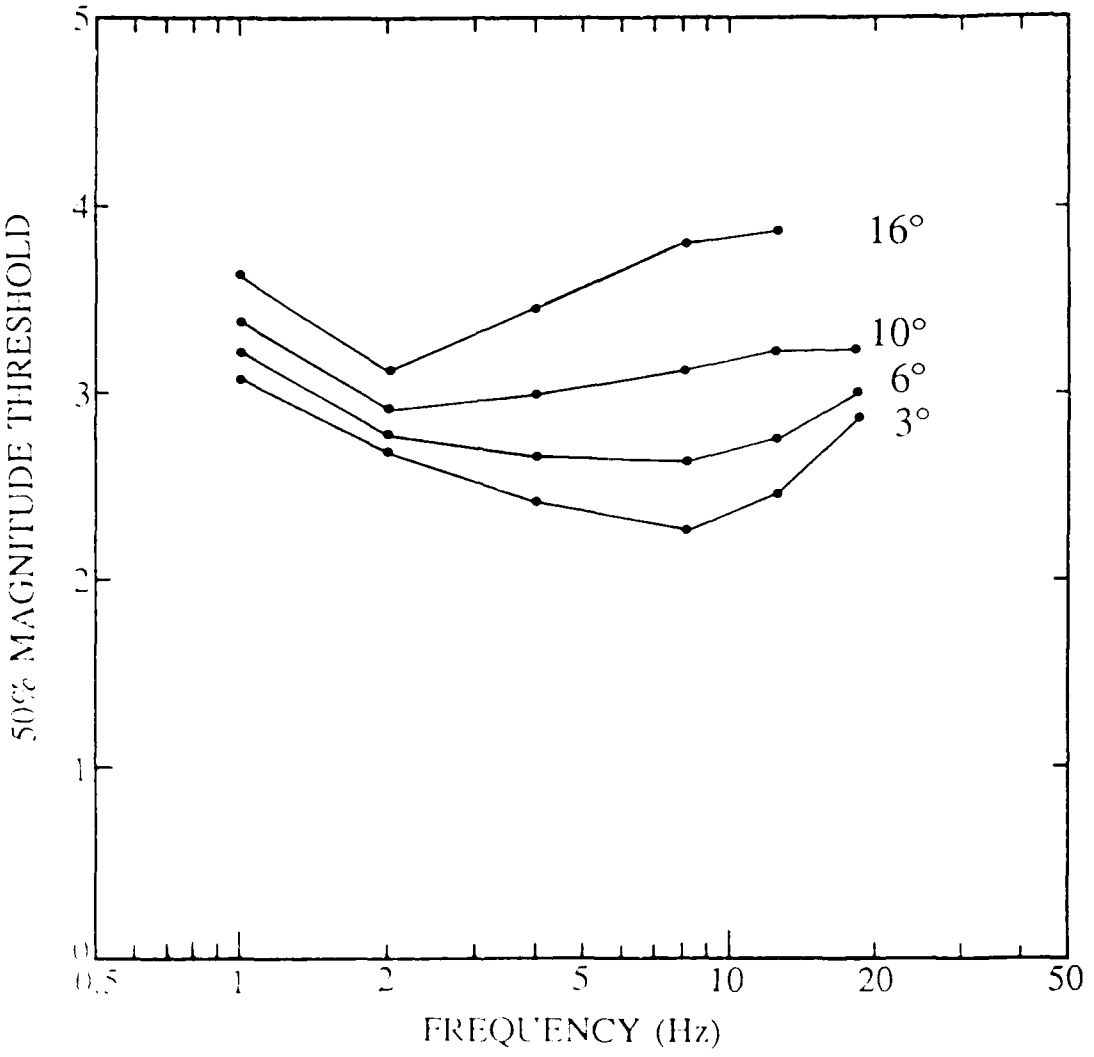


**Figure 25.** Average RSTN 50% detection threshold curves as a function of frequency for *Sn* for distances from 3 to 16°.

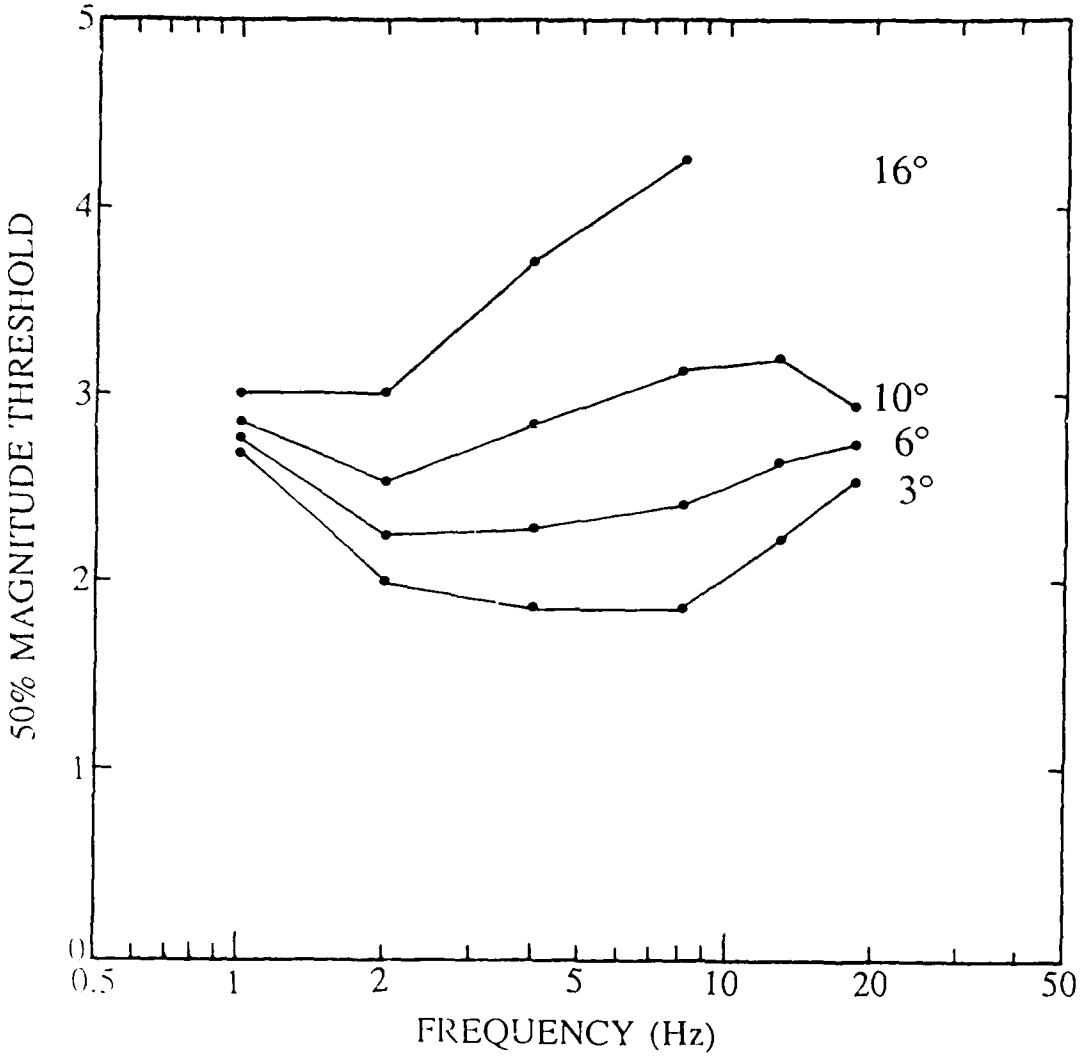


Figure 26a. Average RSTN 50% detection threshold curves as a function of frequency for *Lg* for distances from 3 to 16°. Curves for averages of threshold estimates.

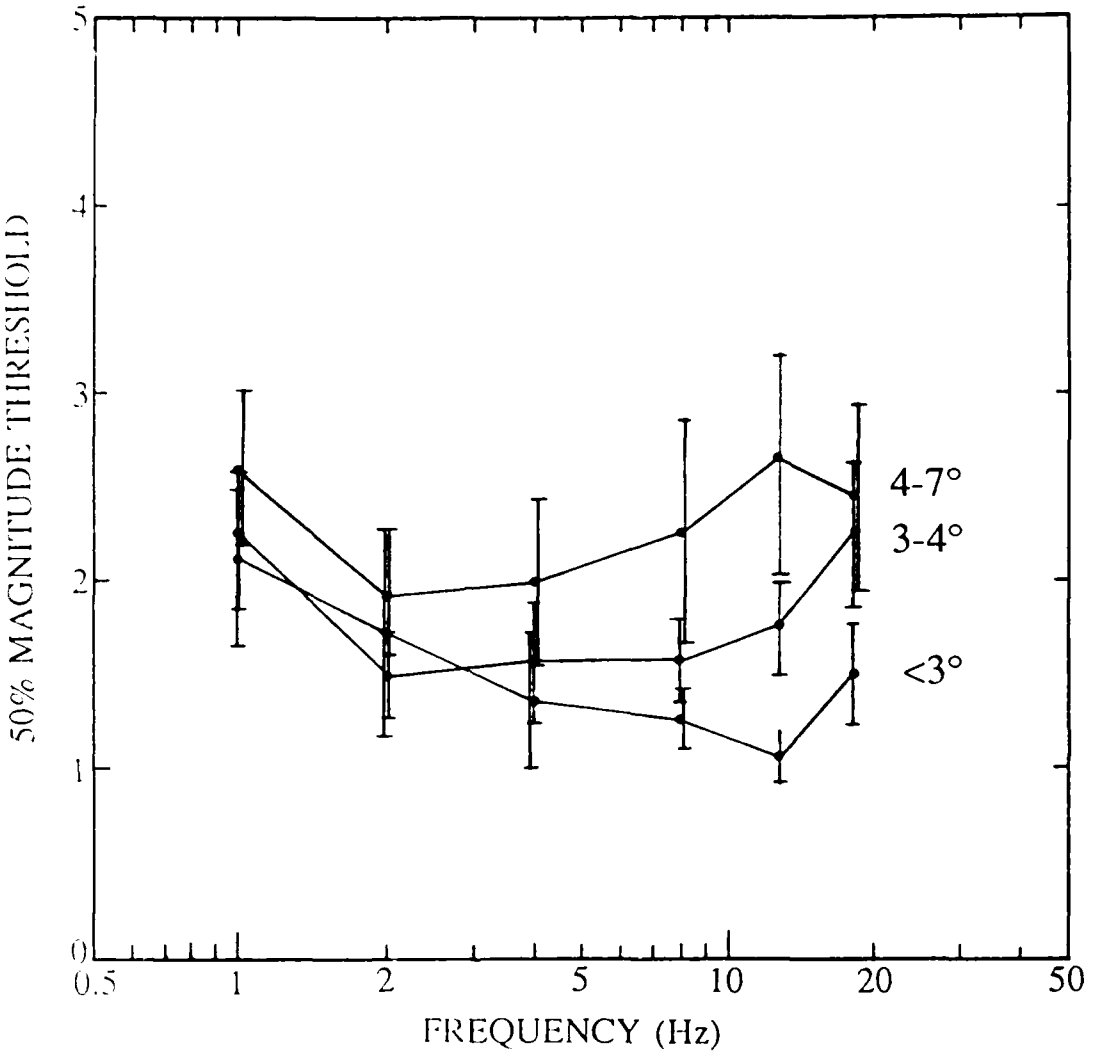


**Figure 26b.** Average RSTN 50% detection threshold curves as a function of frequency for *Lg* for distances from <3 to 4°. Curves for maximum likelihood threshold estimates. At the higher frequencies, there appears to be some separation between thresholds for events at distances of <3° and 3-4°. Even with the large error bars, it is clear that the minimum threshold shifts to higher frequencies for shorter distances.

close and sometimes indistinguishable from *Sn*. At high frequencies and large distances the *Lg* thresholds are higher than those of the *Pn* and *Sn* because *Lg* contains little high frequency energy and most of the high frequency energy observed is probably in the coda of *Sn*. At small distances and high frequencies the *Pn* and *Sn* thresholds are very close because the two phases have similar amplitudes, at lower frequencies the *Sn* thresholds are lower than for *Pn*. Because *Pg* is seen infrequently along paths contained entirely in the tectonically stable parts of North America, our thresholds for this phase probably have larger errors than those for the other phases. In agreement with the predictions of Evernden et al (1986), the lowest absolute values of detection thresholds are associated with the high frequency *Pn* and *Sn-Lg* phases at distances less than 8°.

Comparing the thresholds estimated for individual stations to those for the whole RSTN network reveals some differences. The detection capability of RSCP is somewhat lower than that of the "average" RSTN station. RSNY and RSON have about the same thresholds as the RSTN average station.

We have also looked at the same quantities for the individual RSTN stations RSCP, RSNY and RSSD. Two stations RSON and RSNT did not cover enough events over a large enough range of distances to sketch out the detection thresholds similarly to the others. The estimates agree generally with the results by Blandford et al (1983) and the predictions of Evernden *et al* (1986) that very small events can be detected the most efficiently at high frequencies in tectonically stable regions. The examples of envelope seismograms further illustrate this point

Our results are also in general agreement with the detection thresholds estimated by LLNL (Heusinkveld 1986). At regional distances, both studies agree that *Lg* is the best detector from among the regional phases in the 1-3 Hz band. *Sn* is the next best detector, and then

*Pn*. At higher frequencies and larger distances (>15°), *Pn* is a better detector than is *Lg*. Generally, for a given distance, at the 50% detection threshold level, our results predict detection of slightly lower $m_b$s than do LLNL's results. The two studies agree fairly closely with respect to *Lg* detectability. The differences in the results between the two studies may be due to a number of factors. About a third of LLNL's data set consisted of events occurring in the WNA while our data set contains mostly events in the ENA and CNA; due to the greater attenuation of the WNA crust and mantle relative to the ENA, this would bias our detection thresholds to be lower than LLNL's. Because we are concentrating on ENA events, our data set doesn't include data from RSNT. Our data set is somewhat biased in that it was culled initially to only include events with an *Lg* observable on the raw unfiltered trace. Thus, our thresholds are extrapolated from the signal to noise ratios of larger events following Blandford *et al* (1983). In this study we have used more and narrower bandpasses than were used in the LLNL study; for marginal cases this may allow a detection in some narrow frequency band while a detection would not be made on a trace filtered with a wider frequency band.

The detection thresholds for regional phases at RSTN stations can also be estimated from the previously obtained estimates of attenuation, source, and noise spectra. The family of source spectral estimates, modified by the geometrical spreading and dispersion factor, the instrument response, and the expected attenuation as a function of frequency, estimates the expected signal spectra at any given distance from the epicenter. By combining the expected signal spectra for a phase and the noise spectra for the RSTN sites, the signal-to-noise ratio for the given phase can be estimated at each frequency for each RSTN site at the given distance. In this way we can estimate the detection thresholds for regional signals at any given distance and also determine over what frequency band the given signal will be seen. These detection threshold estimates are 50% detection threshold estimates because we are again estimating the magnitude at which the signal amplitude equals that of the noise.

Figure 27 shows the expected *Lg* spectra for the family of eastern US earthquakes (mb = 2, 3, 4, ...) at a distance of 5 degrees from RSSD. The mean noise spectra at RSSD is also drawn to scale on this plot. These curves show that an event of magnitude 2.0 could be detected at RSSD over the frequency band of 2 to 12 Hz. Figure 28 shows envelope time traces for a 2.5 magnitude event at 6.3 degrees from RSCP where the *Lg* phase is easily seen in the middle frequencies but not at the low frequencies.

Another example is shown on Figures 29 and 30. Here the distance is 12.6 degrees. The same average RSSD noise spectra is plotted on the expected signal spectra. From the spectral plot we would expect to be able to detect a magnitude 3 event over the middle frequency range (1.1 to 4.1 Hz). The time series plots for a magnitude 3 event at 12.6 degrees from RSSD show no signal on the first filtered trace (0.5 Hz), some evidence of the *Lg* on the next three traces (0.7 through 1.8 Hz) and none at higher frequencies.

A third example at 20 degrees shows that a magnitude 3.5 event might be detectable over the 2nd, 3rd and 4th frequency bands (Figure 31). The accompanying time trace plot (Figure 32) shows that a magnitude 3.5 event 19.7 degrees from RSSD shows some evidence of the *Lg* phase on the 2nd, 3rd and 4th filtered envelopes.

Finally, the expected *Lg* spectra at 30 degrees shows that RSSD can not detect a magnitude 4 or smaller event at that distance (Figure 33).

The results in Figures 29, 31, and 33 are consistent with the thresholds determined above from relative signal and noise amplitude levels and those determined by LLNL (Heusinkveld 1986). The *Lg* threshold for 5° in Figure 27 is up to a magnitude unit lower at some frequencies than the previously determined thresholds and the LLNL thresholds. Our source estimate at 5° may not be as good as at the larger distances because 5° is near one end of the distance range used in the combined inversions for source, site, and attenuation, and thus extrapolations

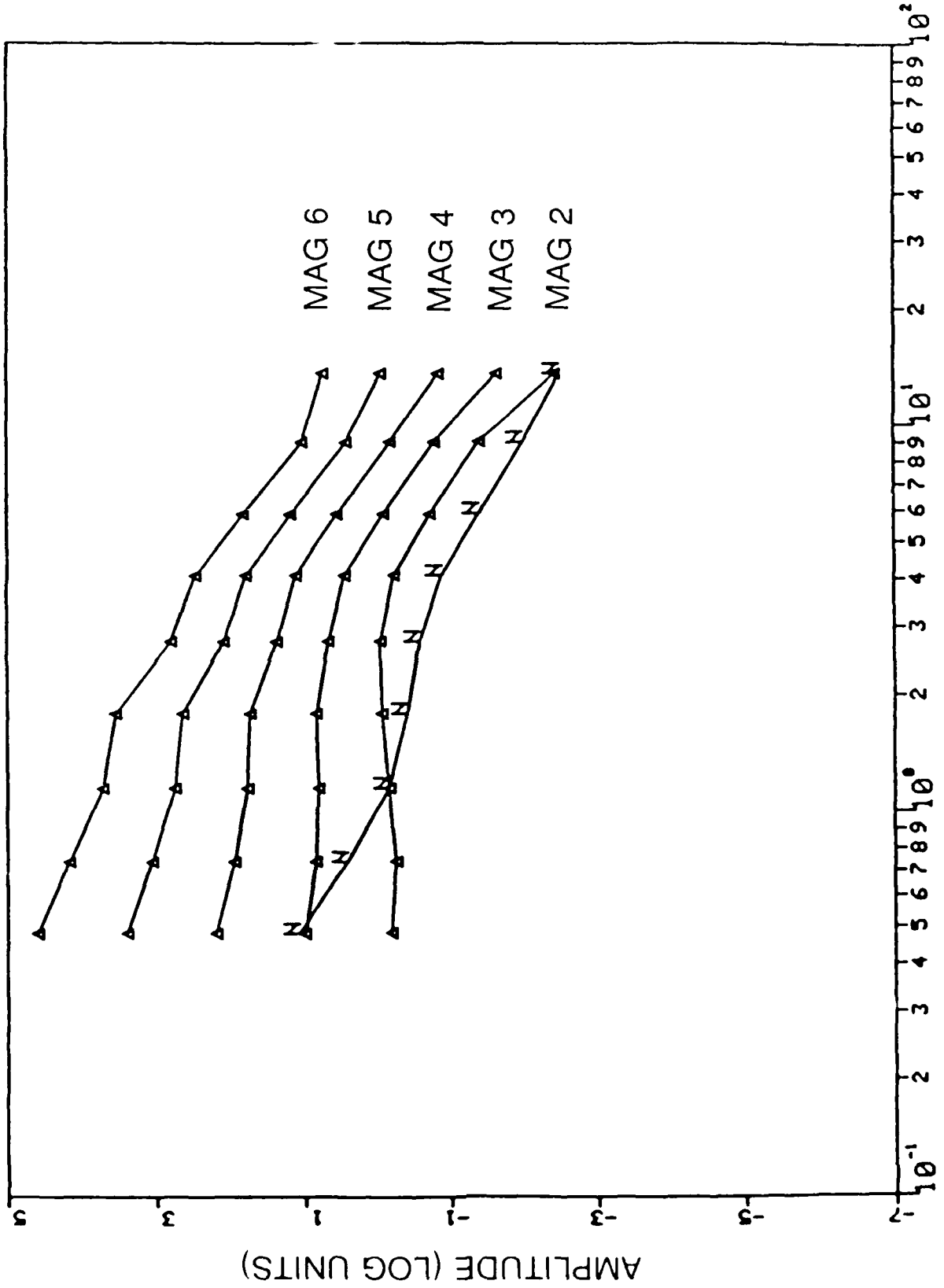


*Figure 27.* Expected $L_g$ signal amplitude at RSSD from eastern US earthquakes 5 degrees distant. Triangles represent the predicted maximum peak to peak signal amplitude for a suite of magnitudes while N's represent the noise rms amplitude.

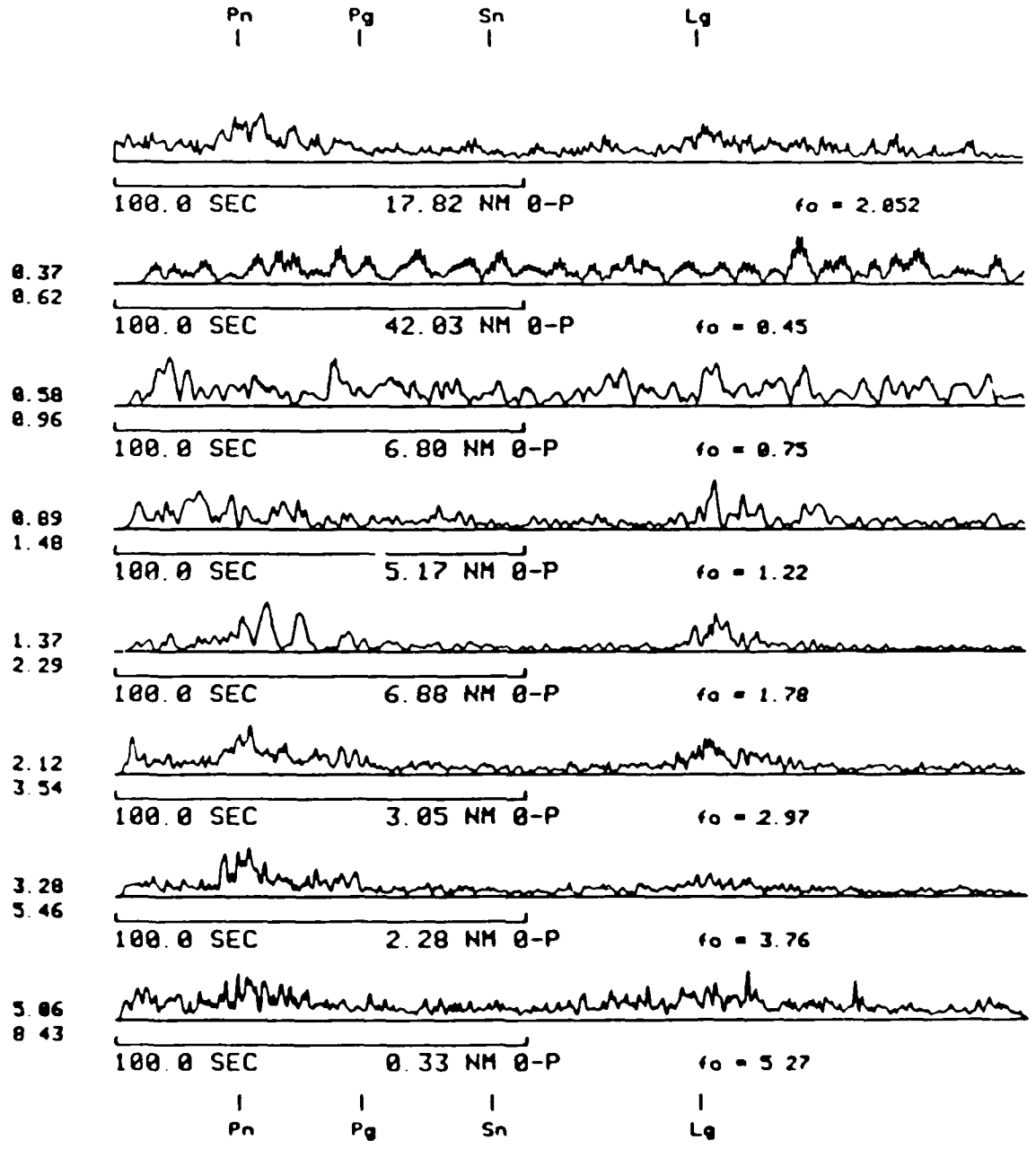


Figure 28. Envelope seismograms at RSCP from an $m_b$ 2.5 earthquake, event 4P014b, 6.3 degrees distant

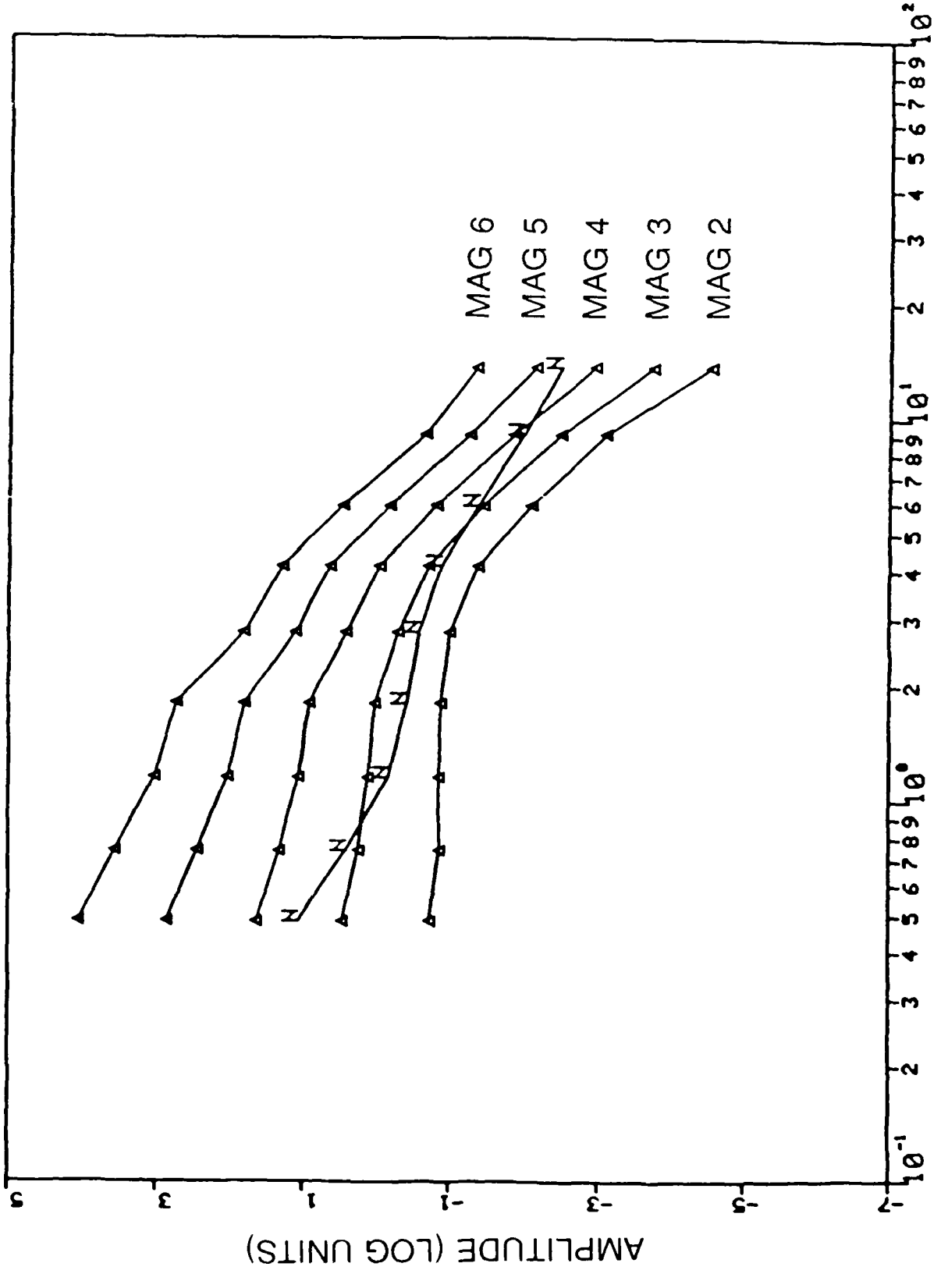


Figure 29. Same as Figure 27 for earthquakes 12.6 degrees distant.

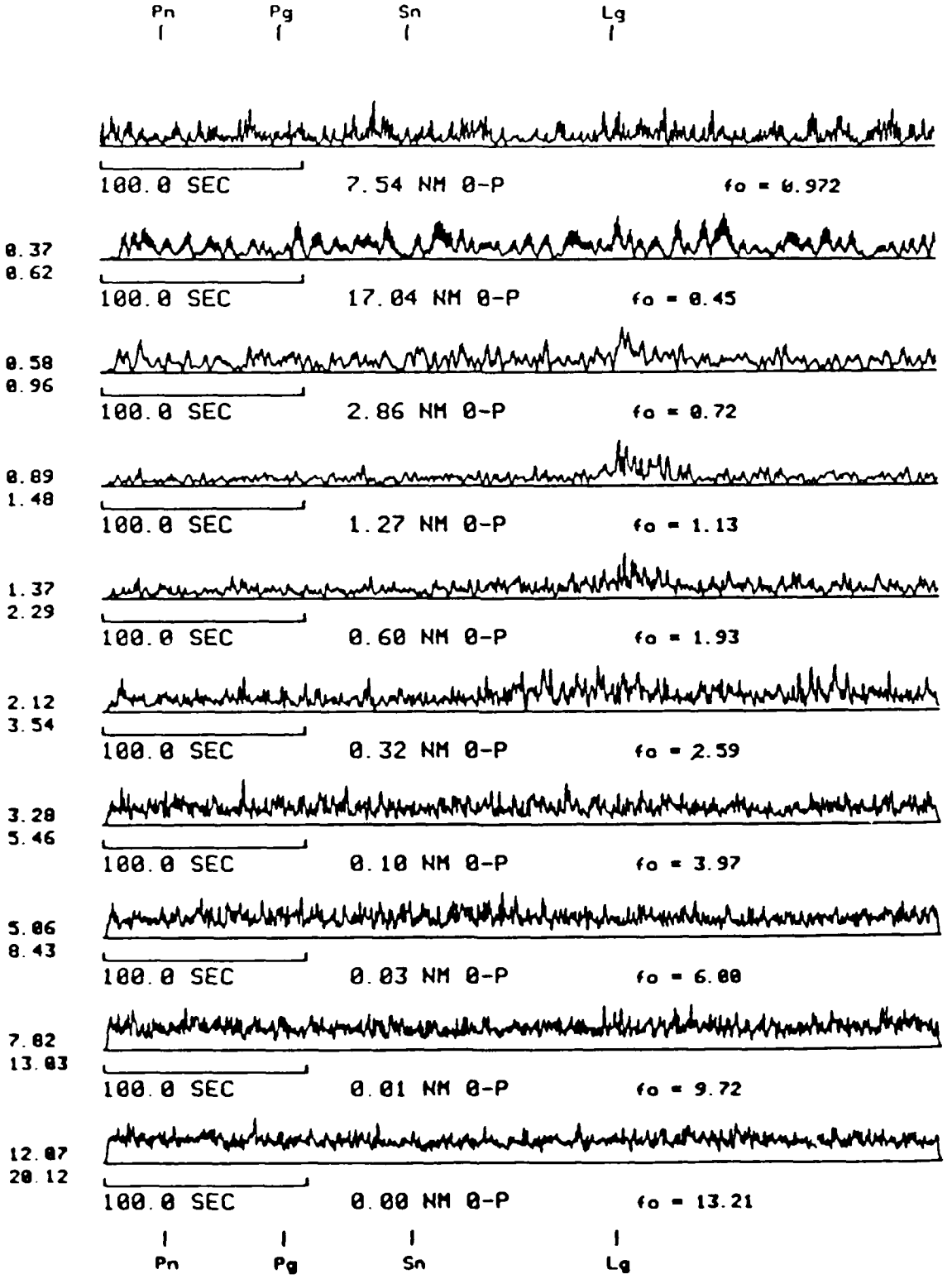


Figure 30. Envelope seismograms at RSSD from an $m_b$ 3.0 earthquake, 4P012, 12.6 degrees distant.

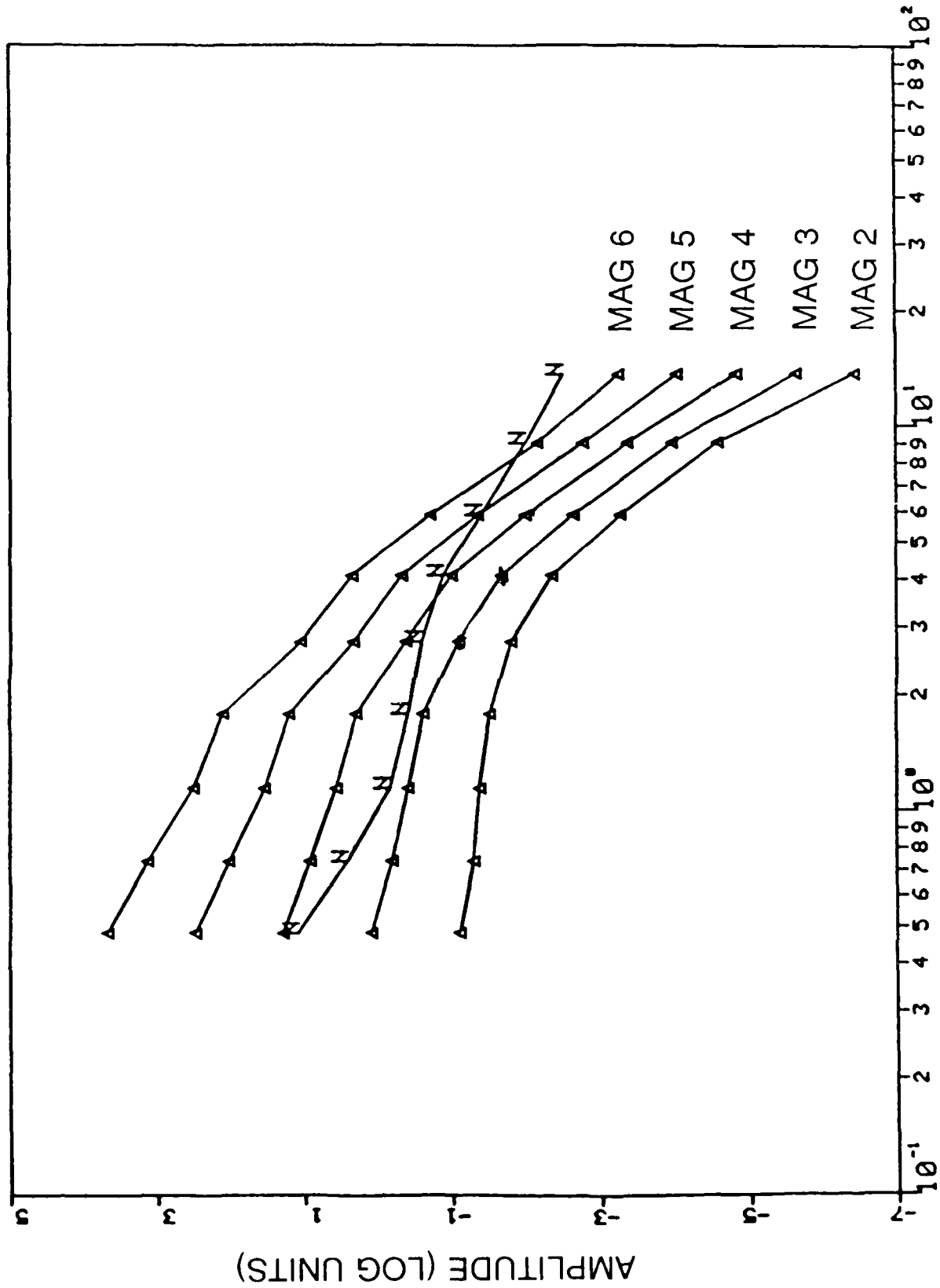


Figure 31. Same as Figure 27 for earthquakes 20 degrees distant.

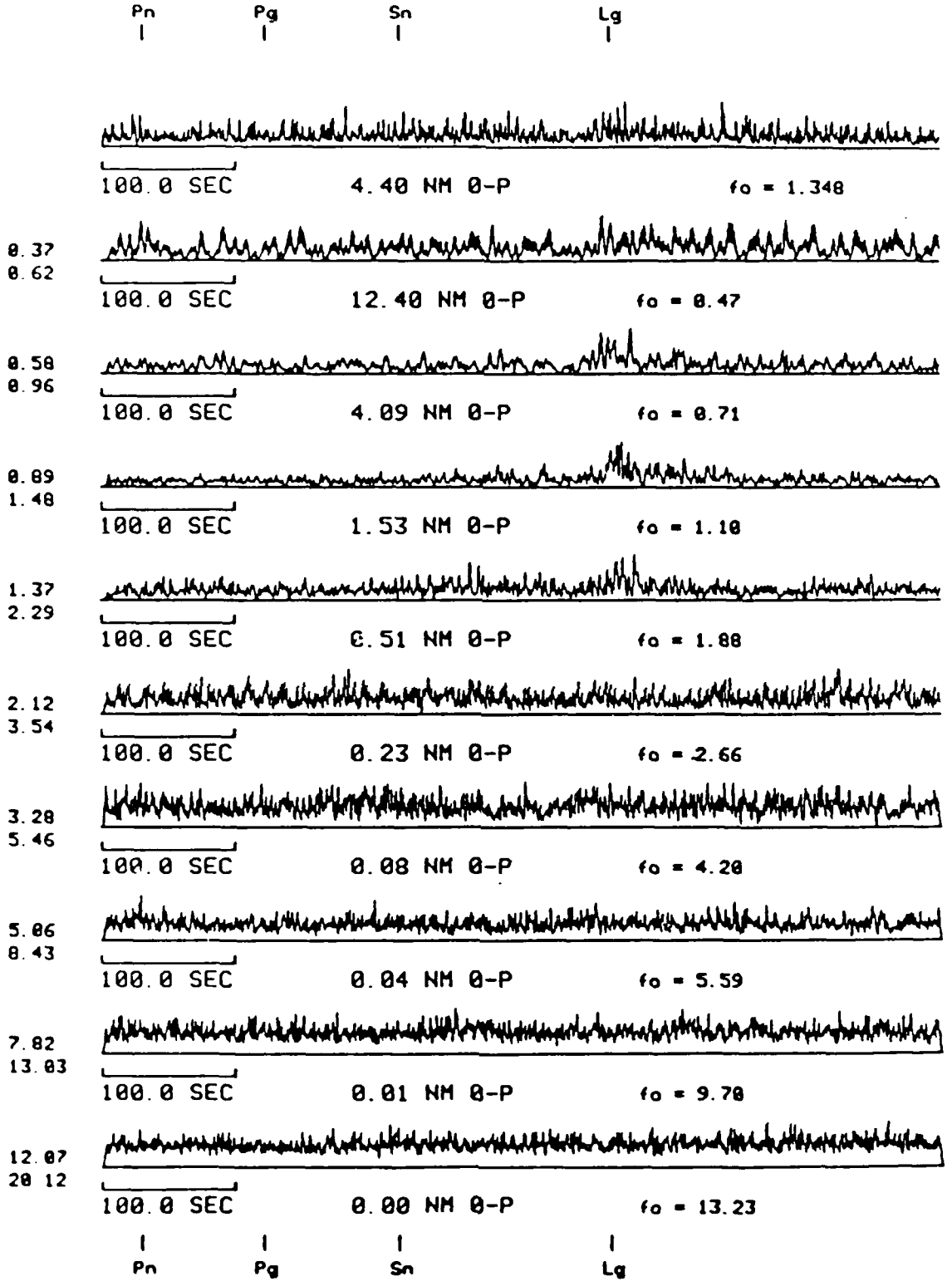


Figure 32. Envelope seismograms at RSSD from an $m_b$ 3.5 earthquake, event 3V026b, 19.7 degrees distant.

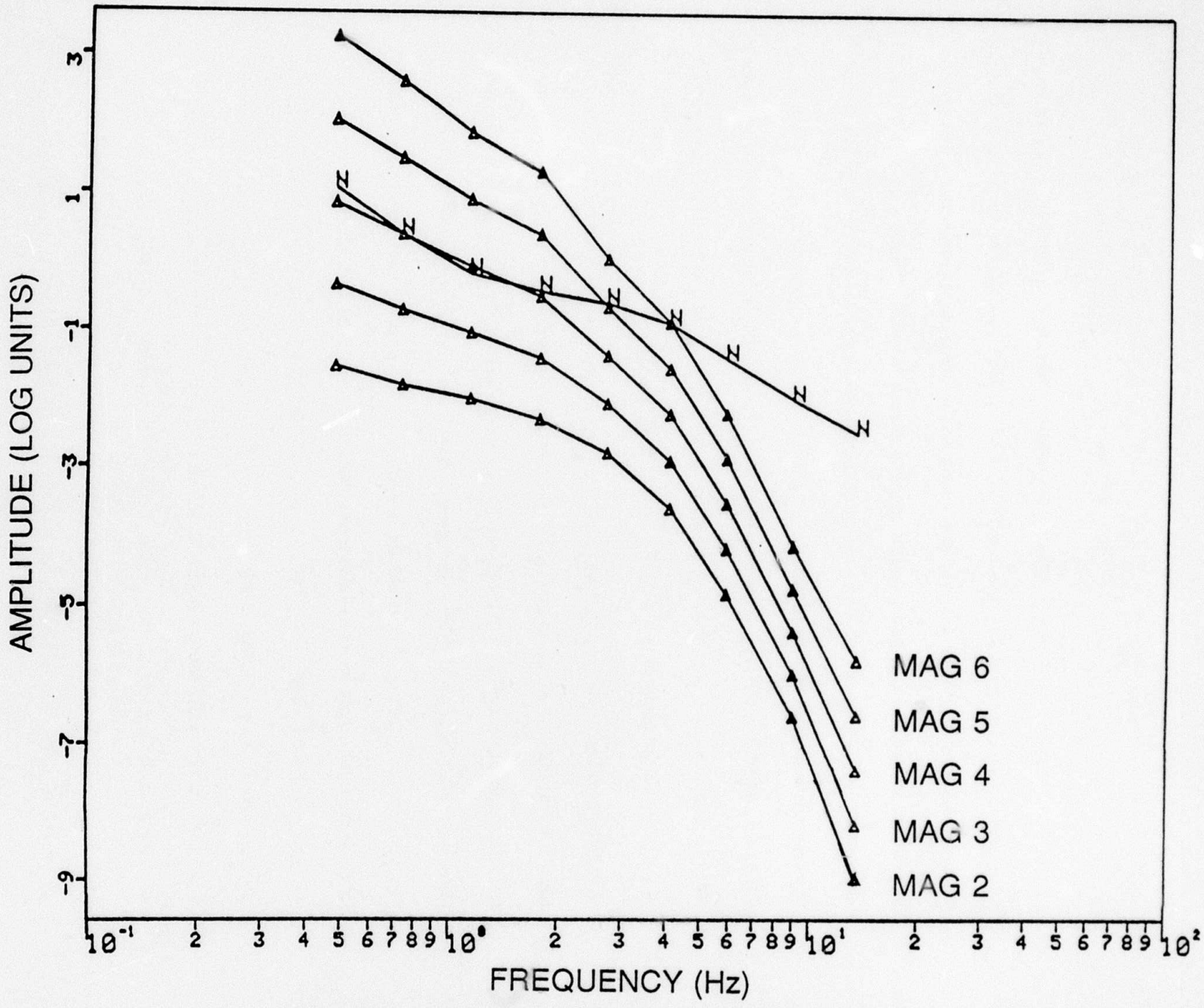


**Figure 33.** Same as Figure 27 for earthquakes 30 degrees distant.

may give additional inaccuracies.

## CONCLUSIONS

This study provides results of apparent attenuation and detection threshold estimates for the regional phases *Pn*, *Pg*, *Sn*, and *Lg* recorded at RSTN stations from events in Eastern North America (ENA). Knowledge of attenuation and its frequency dependence is important in yield estimation and the attenuation of regional phases is quite different than that of the more often studied teleseismic direct phases. Detection thresholds for regions with wave propagation characteristics similar to those in the Soviet Union are important with regards to designing a seismic monitoring network should a CTBT or TTBT be signed. ENA is a good place for such a study since most of ENA is relatively shield-like in character, similar to many of the major Soviet nuclear test sites.

For the attenuation part of the study, rectified seismograms that had been bandpass filtered by a suite of filters were used to provide measurements of the amplitudes of the different regional phases as a function of frequency for each event. The bandpass filtered traces were used instead of taking the spectral amplitudes because they provide a complete time and frequency picture of the behavior of each phase. For paths which propagate in ENA, *Lg* is the most prominent phase at lower frequencies to about 10 Hz, after which *Pn* and *Sn* are the most prominent phases. Often *Pg* is not observed at all. For paths that are predominantly in western North America (WNA), *Pg* and *Lg* are the dominant phases at all frequencies, and *Pn* and *Sn* are very weak arrivals if seen at all. Similar regional wave propagation characteristics have been for waves traveling across France (i.e. Mechler *et al* 1980) which is also a region that has undergone recent tectonic activity. The difference in propagation characteristics between ENA and WNA is probably due to the very different crustal structures in the two

regions. However, a better understanding of regional crustal structures and of the physics of the propagation of regional phases is needed to explain these results. Some attempts have been made at modeling regional phases: *Pn* and *Sn* have been modeled as whispering gallery phases (Menke and Richards 1980) or, for oceanic *Pn* and *Sn*, as leaky modes (Sereno and Orcutt 1987), while *Pg* and *Lg* have been modeled as the sum of many modes trapped in the upper crust (Harvey 1981, Bouchon 1982, Campillo *et al* 1984, 1985). All of these modes of wave propagation are particularly sensitive to the details of the crustal and lithospheric velocity structure and the differences in crustal structure between shield and tectonic regions may explain why different regional phases propagate more efficiently in different regions.

Through a regression analysis, $Q$(f) was determined for *Pn*, *Sn*, and *Lg* (since most of the paths were in ENA, not enough data was available to estimate a $Q$ for *Pg*). The $Q$ measurements are of apparent attenuation which include both intrinsic and scattering contributions to the attenuation. The results are presented below, assuming a geometrical spreading factor of $(\sin \Delta)^{-1/2}$ and a dispersion term of $\Delta^{-1/3}$, suitable for an Airy phase. These terms are correct for time domain analysis of *Lg*, though it is not clear what the correct geometrical spreading term should be for *Pn* and *Sn*. $Q$(f) for these phases assuming different geometrical spreading terms was presented in Table 7.

| Phase | $Q$ | Frequency Range (Hz) |
|---|---|---|
| *Pn* | $640\, f^{0.5}$ | 1.0-9 |
| *Sn* | $825\, f^{0.8}$ | 0.7-9 |
| *Lg* | $1000\, f^{0.35}$ | 0.5-13 |

$Q_{Sn}$ has the strongest frequency dependence, and $Q_{Lg}$ the weakest. $Q_{Sn}$ is greater than $Q_{Pn}$ for all frequencies in this study and greater than $Q_{Lg}$ for frequencies above 2 Hz. Even if other reasonable values of the combined geometrical spreading and dispersion coefficient are used,

$Q_{Sn} > Q_{Pn}$ for all frequencies above about 2 Hz. These frequency dependent $Q$ values imply that the *Sn* to *Pn* amplitude ratio will increase with frequency, and this is what is observed, for example see Figures 4b and 4c.

These results are similar in trend to those of Mechler *et al* (1980) (Figure 34), though higher in absolute $Q$'s since this study contains mostly shield paths while Mechler *et al*'s paths are across central (and more recently tectonic) France. Both studies cover roughly the 1 to 10 Hz frequency band and find that $Q_{Sn}$ has the strongest frequency dependence, and that *Sn* has the highest $Q$ values. Mechler *et al* find that the frequency dependence of $Q_{Pg}$ is very similar to that of $Q_{Sn}$, although the absolute $Q$s are lower for *Pg*. Both studies also find the same frequency dependence for $Q_{Lg}$, though we find a significantly higher frequency dependence for $Q_{Pn}$ than do Mechler *et al*. This may be because *Pn* propagates much more efficiently across shield regions than tectonic regions, at least in North America (see Figure 4).

Butler *et al* (1987) and Sereno and Orcutt (1987), studying oceanic *Pn* and *Sn* (or *Po* and *So*) also find $Q_{Sn} > Q_{Pn}$. Butler *et al* suggest that either there is a significant amount of bulk attenuation in the lithosphere or that oceanic *P* propagates as a leaky mode while the oceanic *S* is more effectively trapped in the lithosphere.

The curves for $Q_{Pn}$ and $Q_{Sn}$ along with those for $Q_P$ and $Q_S$ from Evernden *et al* (1986) are plotted in Figure 35. The $Q_{Sn}$ curve crosses the Evernden *et al* $Q_S$ curve around 7 Hz, while, if extrapolated, the $Q_{Pn}$ curve would cross the Evernden *et al* $Q_P$ curve around 200 Hz. In estimating $Q_P$ and $Q_S$, Evernden *et al* used the relation $Q_P/Q_S = 2.25$, which is generally consistent with observations of mantle $Q$ values. However, the physics of wave propagation must be very different in the crust than in the mantle, at least in the 1 to 10 Hz range, since $Q_{Pn}/Q_{Sn} < 1$, and decreases with increasing frequency.

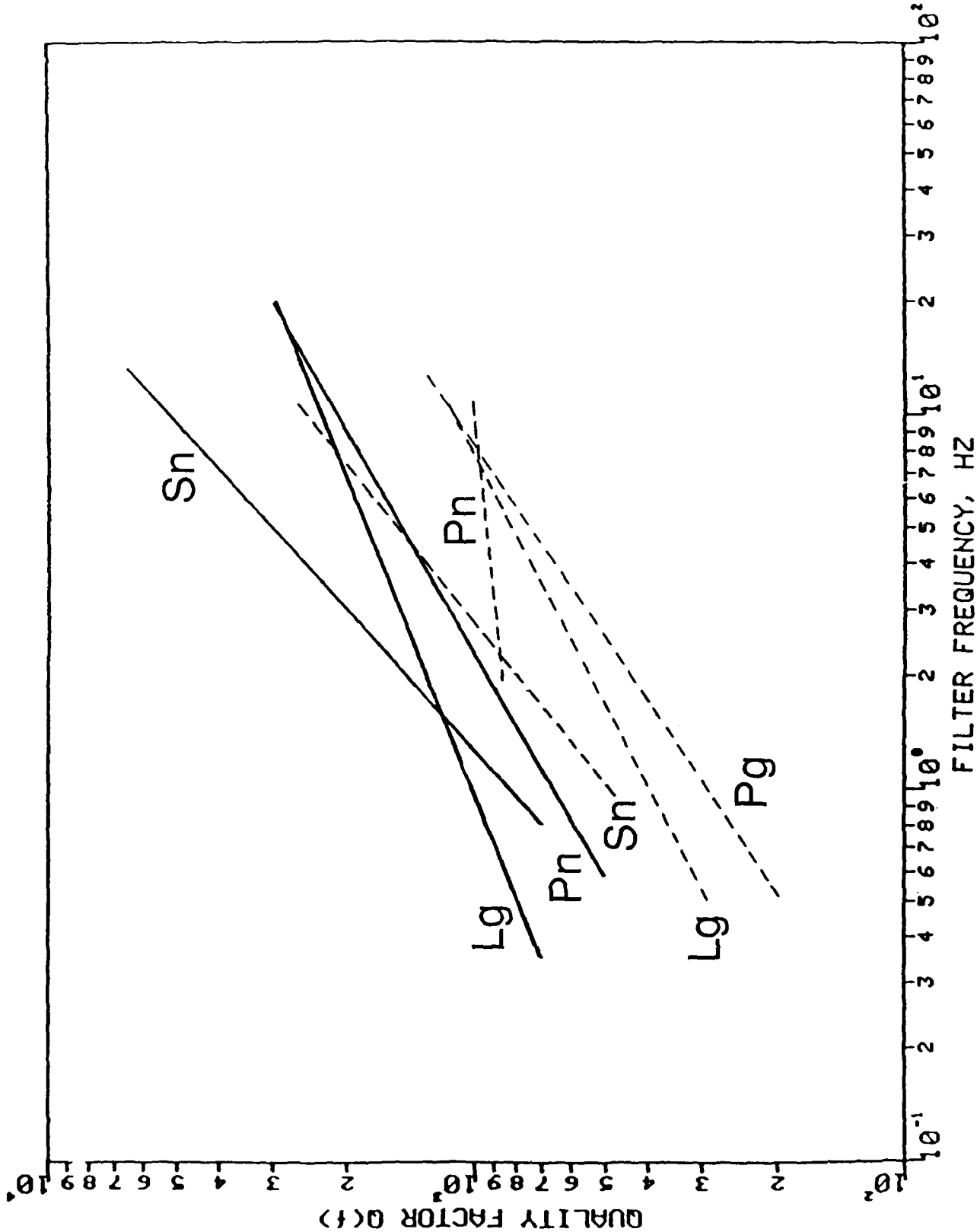


**Figure 34.** *Q* versus frequency for regional phases from this study (solid lines) and Mechler *et al* (1980) (dashed lines).

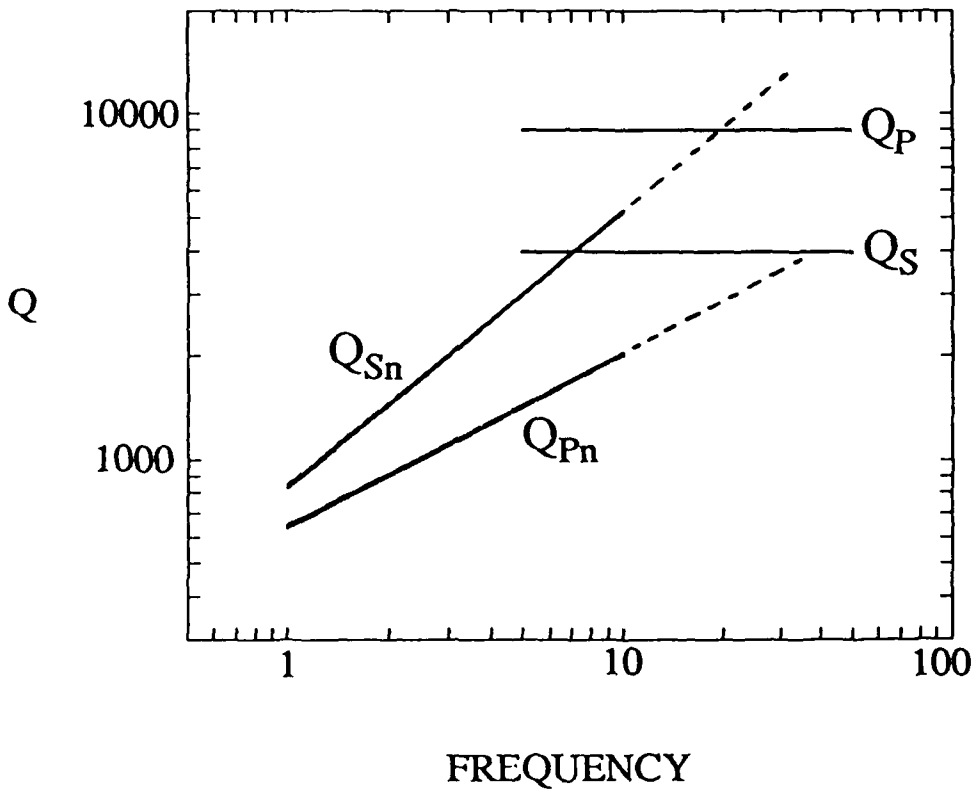


Figure 35. $Q$(f) for $P$ and $S$ from Evernden *et al* (1986) and $Pn$ and $Sn$ from this study (labeled $Q_P$, $Q_S$, $Q_{Pn}$, and $Q_{Sn}$, respectively). The dotted lines are extrapolations of our results beyond the frequency range from which data was used.

One obvious mechanism to explain the $Q$ differences between $P$ and $S$ is bulk attenuation in the crust and lithosphere (Butler *et al* 1987, Sereno and Orcutt 1987). However, a number of hypotheses about the mode of regional wave propagation have also been put forth which are consistent with the observations of $Q_{Pn}/Q_{Sn} < 1$, $Q_{Pg}/Q_{Lg} < 1$ (tectonic France), and $Q_{Pd}/Q_{So} < 1$ at high frequencies, above 1-2 Hz. The general idea is that regional phases tend to propagate as modes or rays trapped in the crust or lithosphere. Although both $P$ and $S$ have post-critical reflections in the medium which has trapped them, at each reflection the $P$ transmits some $S$ and thus dissipates as a "leaky" phase or by tunneling while this mechanism is not available to $S$ (Haskell 1966, Pomeroy and Chen 1980, Menke and Richards 1983, Butler *et al* 1987, Sereno and Orcutt 1987).

However, the most important observation for threshold estimation is the total amplitude attenuation due to the effects of both $Q$ and the combined geometrical spreading-dispersion. As we mentioned above, there appears to be a strong tradeoff between the apparent frequency dependences of Q and the assumed geometrical spreading-dispersion rates for the various phases since the amplitude goes as

$$A \sim A_0 \Delta^{-n} e^{-\gamma \Delta}, \quad \text{where } \gamma = \frac{\pi f}{UQ} \quad \text{and } Q = Q_0 f^{\xi} .$$

If one assumes a low value for the exponent of the distance (-n) then the Q will be strongly frequency dependent. The exponent of frequency ($\xi$) will decrease if we attribute a higher portion of the amplitude decrease to geometrical spreading-dispersion effects and the frequency dependence will be less strong. It is near impossible to differentiate the various models because of the scatter in amplitude data.

In Figure 35, it is clear that $Q_{Pn}$(f) and $Q_{Sn}$(f) as found in this report are very different from $Q_P$(f) and $Q_S$(f) as estimated by Evernden et al (1986). Much of the difference is due to the fact, however, that the combined geometrical spreading/dispersion terms used in the two

studies are $\Delta^{-5/6}$ and $\Delta^{-2}$, respectively. Figures 36 and 37 show the relative attenuation predicted at several frequencies for *Pn* and *Sn*, respectively, by Evernden et al (1986) (labeled EAC on the Figures) for combined geometrical spreading and dispersion of $\Delta^{-2}$ (solid line) and by this study for $\Delta^{-5/6}$, $\Delta^{-1.5}$, and $\Delta^{-1.75}$ (dashed lines). The difference between the dashed lines is a measure of the variations due to the application of the program in Table 8 and for a suite of frequencies and subsequent fitting of $Q(f)=e^{-\gamma\Delta}$ to the data. The curves are all normalized to unit amplitude at a distance of 500 km. Generally, there is a surprisingly good agreement in the amplitude decay predicted by the different formulations. For *Pn* at low frequency, Evernden et al predict a slightly steeper slope than this study, and at high frequency and larger distance, they overpredict the amplitude by more than a factor of two relative to the results of this study. For *Sn*, Evernden et al (1986) predict a steeper slope than does this study at all frequencies, and they significantly overestimate the total attenuation at larger distances.

It is also important that the total attenuation due to anelastic absorption and the combined geometrical spreading-dispersion be consistent with the observed fall-off of amplitude with distance for regional phases. For ~1 Hz *Pn* propagating in shield regions, Warren et al (1978) found total attenuation around $\Delta^{-1.5}$ for the eastern United States and Der et al (1982) found $\Delta^{-1.3}$ for the shield region of southern Africa. For *Sn* around 1 Hz, Der et al found $\Delta^{-1.9}$ for southern Africa. For *Lg* around 1 Hz in the eastern United States, Nuttli (1973) found $\Delta^{-0.9}$ for $0.5 \leq \Delta \leq 4°$ and $\Delta^{-1.66}$ for $4 \leq \Delta \leq 30°$. From Figures 36, 37, and 38, our attenuation models at 1 Hz, assuming a combined geometrical spreading-dispersion of $\Delta^{-5/6}$, give total attenuation at 1 Hz of $\Delta^{-1}$ to $\Delta^{-1.5}$ for *Pn*, $\Delta^{-1}$ to $\Delta^{-1.5}$ for *Sn*, and $\Delta^{-1}$ to $\Delta^{-2}$ for *Lg*. These are in general agreement with the observations quoted above, and as discussed in the introduction, not enough is known about the physics to be sure exactly what the geometrical spreading term should be for *Pn* and *Sn*. The total attenuation fall-offs of $\Delta^{-2}$ used by Evernden et al (1986) for *P* and *S* seem a little high, though their models were developed for frequencies

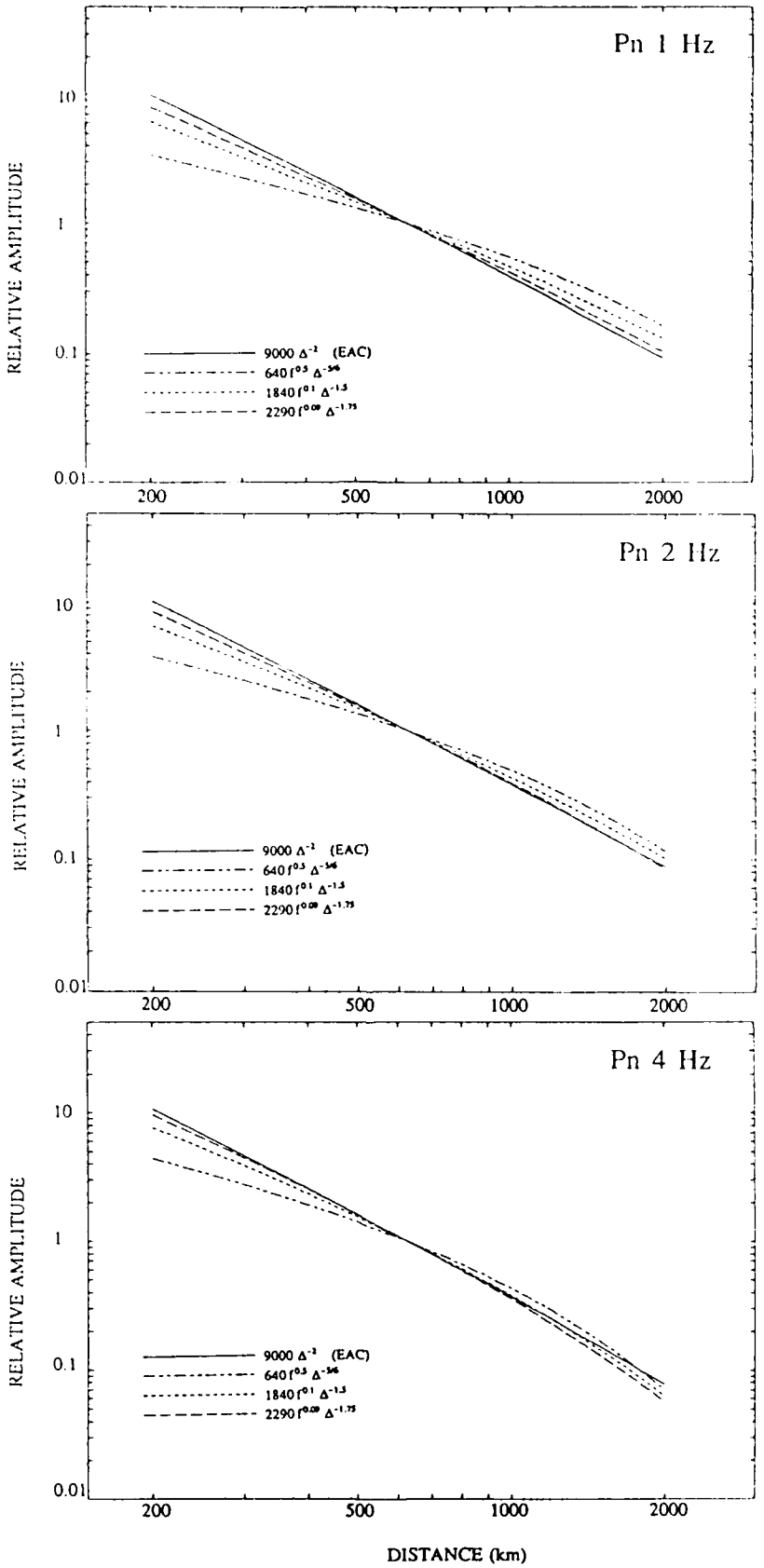


**Figure 36.** Relative amplitude versus distance for *Pn* at frequencies of 1, 2, 4, 8, and 16 Hz for several $Q(f)$ models and their corresponding combined geometrical spreading/dispersion terms ($\Delta^{-n}$). The solid line corresponds to the model of Evernden et al (1986) and the dashed lines correspond to the models developed in this report (see Table 9). The curves are all normalized to unit amplitude at a distance of 500 km.

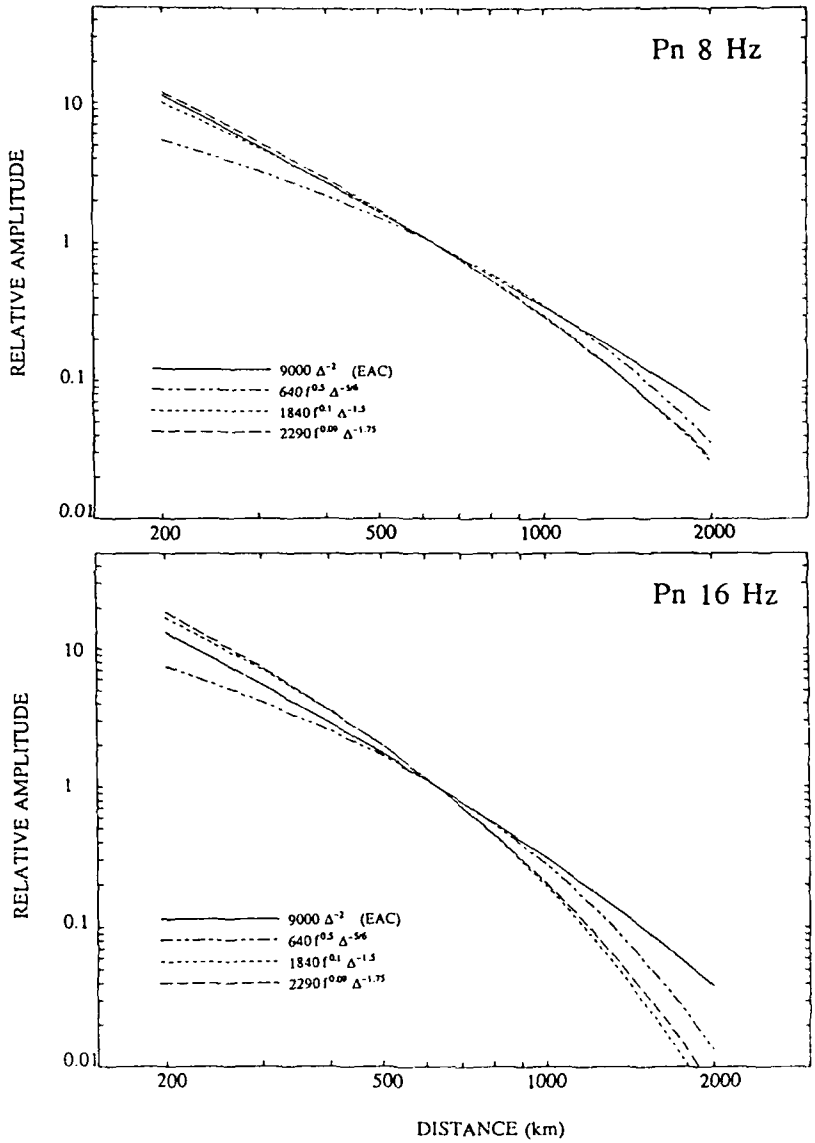


*Figure 36* (continued).

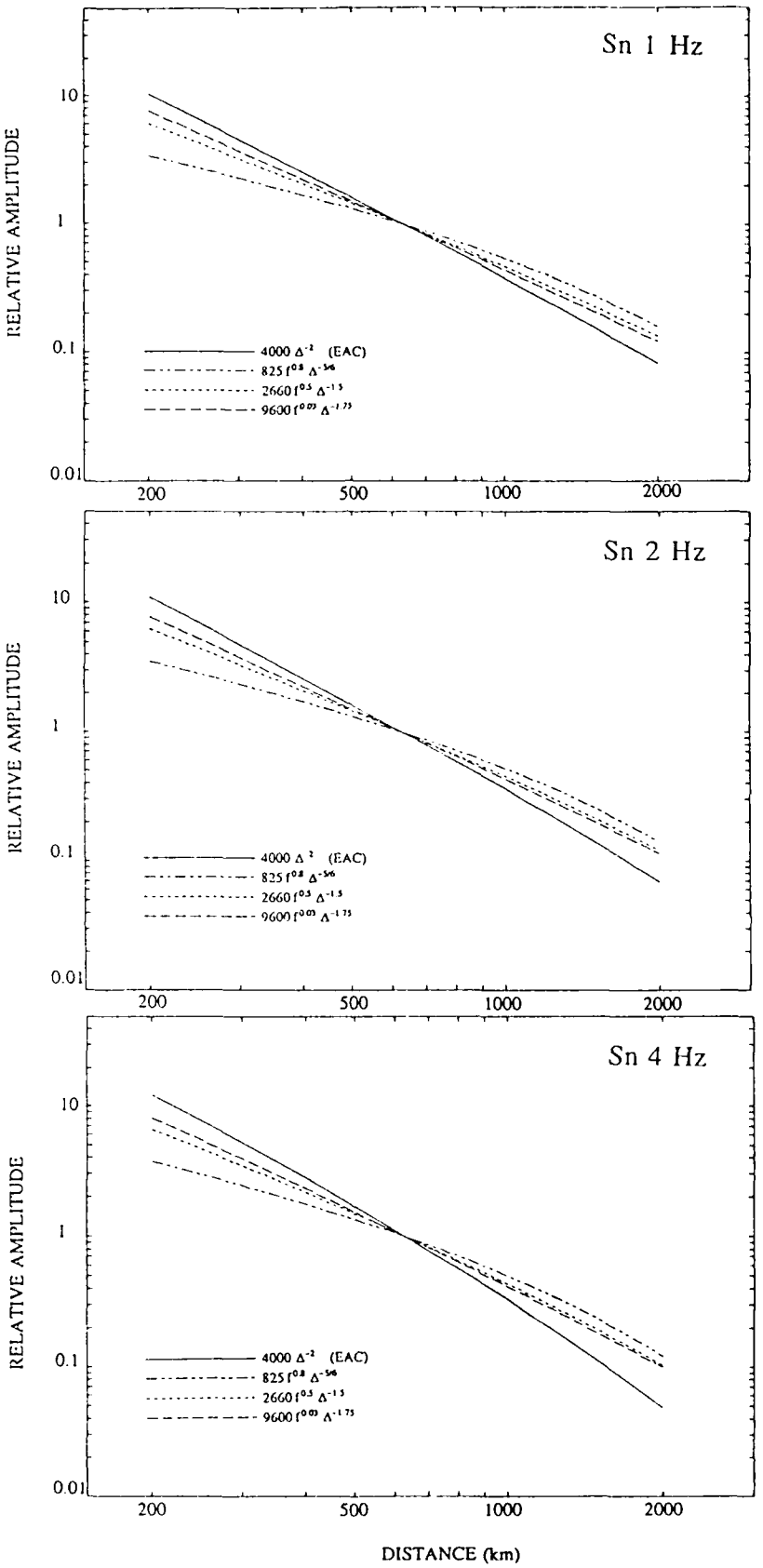


**Figure 37.** Relative amplitude versus distance for *Sn* at frequencies of 1, 2, 4, 8, and 16 Hz for several $Q(f)$ models and their corresponding combined geometrical spreading/dispersion terms ($\Delta^{-\gamma}$). The solid line corresponds to the model of Evernden et al (1986) and the dashed lines correspond to the models developed in this report (see Table 9). The curves are all normalized to unit amplitude at a distance of 500 km.

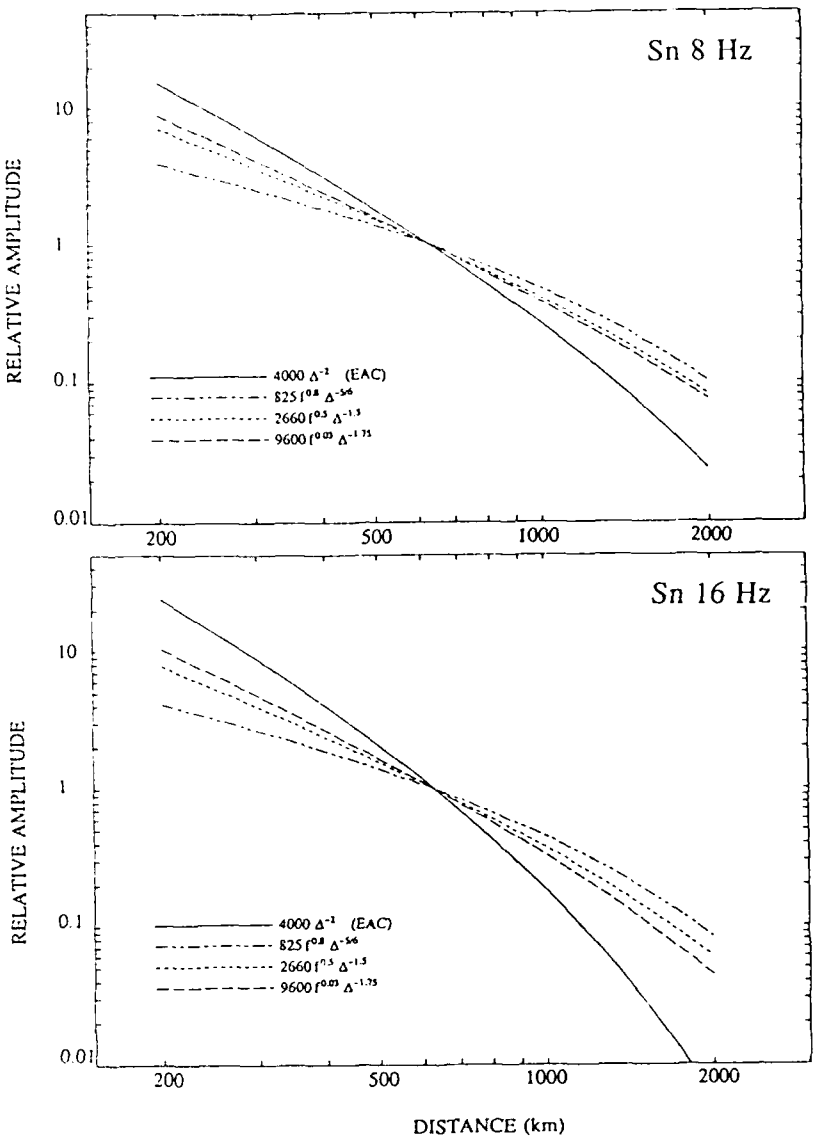


Figure 37 (continued).

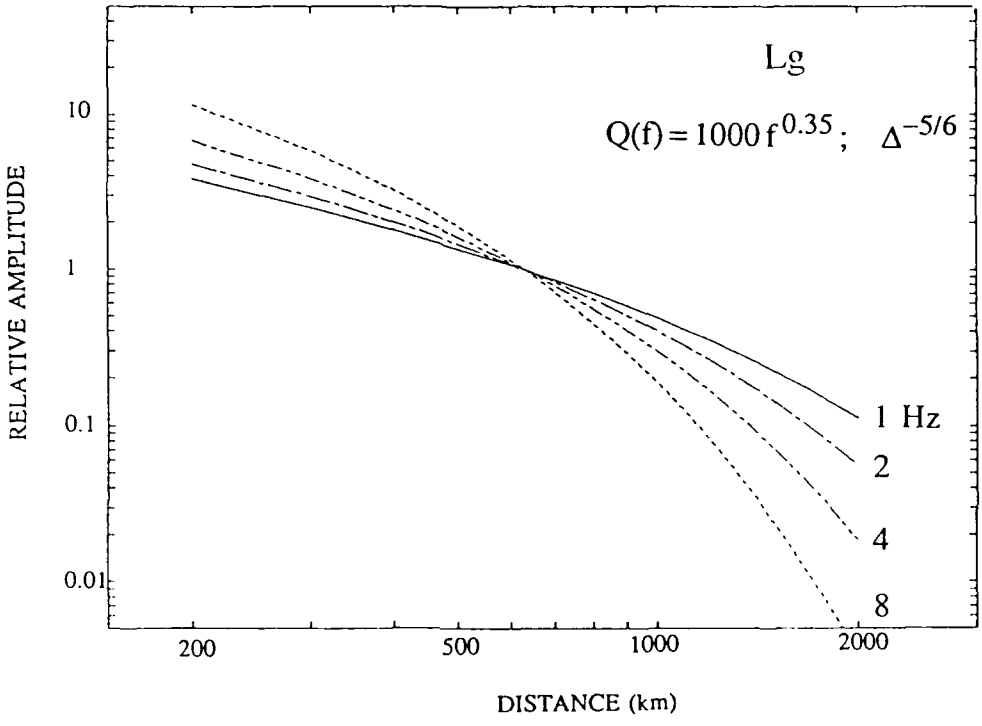


**Figure 38.** Relative amplitude versus distance for *Lg* at frequencies of 1, 2, 4, and 8 Hz for the $Q(f)$ model developed in this report and a combined geometrical spreading/dispersion term of $\Delta^{-5/6}$.

above 5 Hz.

The regression analysis also results in estimates of the source spectra and the relative site terms. The source spectra show ill-defined corner frequencies which shift to lower frequencies with increasing magnitude as most proposed scaling laws predict. Part of the lack of resolution of the corner frequencies is because the source spectra are averages of the source spectra for many events in ENA and central North America (CNA). The decay of the source spectral estimates above the corner frequency goes as $f^{-2}$ to $f^{-3}$ for all three phases. Thus, we found no evidence to support the hypothesis that the $P$ and $S$ wave amplitude spectra fall off at different rates. It seems premature to conclude that $P$ waves from explosions and earthquakes can be discriminated reliably on the basis of spectral content. Although we believe that explosion $P$ wave spectra fall off as the square of frequency, after correcting for attenuation effects, earthquake $P$ waves may fall off at various rates. Therefore the discrimination of numerous, small detected events may still be a major problem in monitoring.

The relative site terms (the sum of which is constrained to be 0 at each frequency) are relatively flat for frequencies up to 3 Hz. Above about 5 Hz, RSCP and RSNT are not included in the calculations because of a low pass filter and minimal data, respectively. Of the remaining site terms, RSON and RSNY increase positively with frequency, offset by a decrease with frequency by the RSSD site term.

Noise spectra for the four RSTN sites out to 20 Hz show that the system noise for these RSTN's is less than the seismic background at least to 20 Hz. The response of RSCP prior to April 1985 had a filter which cutoff sharply at 8 Hz so that the RSCP output exhibited nothing but A-to-D round off (i.e. system) noise above that frequency. After day 102 in 1985 the seismometer at RSCP matched the other four. Since then RSCP could also reproduce the earth noise background to 20 Hz without system noise distortion. In addition, our noise spectra

matched those measured by Sandia and other groups for the RSTN stations.

The seismic noise displacement amplitude (in nm/sqrt Hz) falls off inversely as the square of frequency from 1 Hz to 20 Hz, the Nyquist frequency limit for the RSTN's. We estimated the diurnal variation at all of the RSTN sites however; the daytime noise averaging 1.5 times higher than the nighttime noise at RSSD, the quietest site, and up to 3 times higher, day over night, at RSCP and RSON. The site with the largest seasonal variation is RSTN, which is quietest in winter when the Great Slave Lake is frozen. The statements in Evernden *et al* (1986) concerning the low seasonal variation and the falloff rates of noise spectra with increasing frequency are supported by our findings.

The final part of this study involved estimation of regional phase detection thresholds at the RSTN stations. We find for distances less than 16° *Lg* has the lowest detection threshold, followed by *Sn*, *Pg*, and *Pn*. The results for *Pg* are marginal because *Pg* is not often a prominent arrival on our mostly eastern US paths. The frequency at which each phase has its minimum threshold decreases rapidly with distance, most dramatically for *Lg*. At 3°, all four phases have their lowest thresholds in the 4-8 Hz range; this shifts to 1-4 Hz by 16°. These results are consistent with the observations of the behavior of regional phases from the bandpassed filtered seismograms. Minimum 50% detection thresholds for *Lg* range from magnitude 1.9 at 3° to magnitude 3 at 16°. The standard deviation of these estimates is 0.3 to 0.4 m.u., and the addition of 2 m.u. is required to bring the detection thresholds to the 98% level.

## REFERENCES

Blandford, R.R., Goncz, J., Baumstark, R. and K.L. McLaughlin (1983). Evaluation of the RSTN network and further improvement to automatic association, *TGAL-TR-83-5*, Teledyne-Geotech, Alexandria, VA.

Bollinger, G.A. (1979). Attenuation of the Lg phase and the determination of $m_b$ in the southeastern United States, *Bull. Seism. Soc. Am., 71*, 959-971.

Bouchon, M. (1982), The complete synthesis of seismic crustal phases at regional distances. *J. Geophys. Res., 87*, 1735-1741.

Bungum, H., S. Mykkeltveit, and T. Kvaerna (1985). Seismic noise in Fennoscandia, with emphasis on high frequencies, *Bull. Seism. Soc. Am., 75*, 1489-1513.

Butler, R., C.S. McCreery, L.N. Frazer, and D.A. Walker (1987). High-frequency seismic attenuation of oceanic *P* and *S* waves in the western Pacific, *J. Geophys. Res., 92*, 1383-1396.

Campillo, M., M. Bouchon, and B. Massinon (1984). Theoretical study of the excitation, spectral characteristics, and geometrical attenuation of regional seismic phases, *Bull. Seism. Soc. Am., 74*, 79-90.

Campillo, M., J. Plantet, M. Bouchon (1985). Frequency dependent attenuation in the crust beneath central France from Lg waves: data analysis and numerical modeling. *Bull. Seism. Soc. Am., 75*, 1395-1411.

Chavez, D.E. and K.F. Priestly (1986). Measurement of frequency dependent *Lg* attenuation in the Great Basin, *Geophys. Res. Let., 13*, 551-554.

Chun, K-Y, West, G.F., Kokoski, R.J. and C. Samson (1987). A novel technique for measuring Lg attenuation - results from eastern Canada between 1-10 Hz, *Bull. Seism. Soc. Am., 77*, 398-419.

Der, Z.A., A. O'Donnell, T.W. McElfresh, R. Jutila, J.A. Burnetti, M. Marshall, M. Silk, and E. Gordon (1982).A study of seismic wave propagation at regional distances in five areas of the world, *VSC-TR-82-14*, Teledyne Geotech, Alexandria, Virginia.

Dwyer, J.J., R.B. Herrmann, and O.W. Nuttli (1983). Spatial attenuation of the *Lg* wave in the central United States. *Bull. Seism. Soc. Am. 73*, 781-796.

Evernden, J.F. (1967), Magnitude determination at regional and near-regional distances in the United States. *Bull. Seism. Soc. Am. 57*, 591-639.

Evernden, J.F., C. Archambeau, E. Cranswick (1986). An evaluation of seismic decoupling and underground nuclear test monitoring using high frequency seismic data. *Reviews of Geophysics, 24*, 143-215.

Ewing, W.M., W. S. Jardetzky, F. Press (1957). Elastic waves in layered media. McGraw-Hill Book Co., NY/Tor/Lon, pg 358.

Gupta, I.N. and J.A. Burnetti (1980). Amplitude-distance relationships for regional phases in shield regions, *SDAC-TR-80-7a*, Teledyne-Geotech, Alexandria, VA.

Gupta, I.N. and K.L. McLaughlin (1987a). Attenuation of ground motion in the eastern United States, *Bull. Seism. Soc. Am., 77*, 366-383.

Gupta, I.N. and K.L. McLaughlin (1987b). Regional crustal frequency dependent Q and site effects estimated from LRSN and RSTN data, Draft Paper for EPRI Workshop on Earthquake Ground-Motion Estimation in Eastern North America, March 31 to April 2 1987.

Harvey, D.J. (1981). Seismogram synthesis using normal mode superposition, the locked mode approximation, *Geophys. J. Roy. astr. Soc., 66.*, 37-70.

Hasegawa, H.S. (1985). Attenuation of Lg waves in the Canadian shield, *Bull. Seism. Soc. Am., 75*, 1569-1582.

Haskell, N.A. (1966). The leakage attenuation of continental crustal P waves, *J. Geophys. Res., 71*, 3955-3967.

Heusinkveld, M., editor (1986). Seismic monitoring research program, annual report, *UCID-20628-86*, Lawrence Livermore National Laboratory, Livermore, California.

Horner, R.B., A.E. Stevens, H.S. Hasegawa, and G. LeBlanc (1978). Focal parameters of the July 12, 1975, Maniwaki, Quebec, earthquake - an example of intraplate seismicity in eastern Canada, *Bull. Seism. Soc. Am., 68*, 619-640.

Israelson, H. (1986a), Detection of underground explosions by the GSETT seismological station network. In Technical Report C86-05 (quarterly), Center for Seismic Studies, Science Applications Inc., Arlington, VA.

Israelson, H. (1986b), Noise levels and detection thresholds of RSTN stations during GSETT. In "Regional Seismic Test Network Research Symposium Proceedings" Sandia Report SAND85-1243, Sandia National Laboratories, Albuquerque NM.

Kennett, B.L.N. and T.J. Clarke (1983a). Rapid calculation of surface wave dispersion, *Geophys. J. Roy. astr. Soc., 72*, 619-632.

Kennett, B.L.N. and T.J. Clarke (1983b). Seismic waves in a stratified half space - IV: P-SV wave decoupling and surface wave dispersion, *Geophys. J. Roy. astr. Soc., 72*, 633-646.

Kennett, B.L.N. and S. Mykkeltveit (1984). Guided wave propagation in laterally varying media - II. *Lg* waves in north-western Europe, *Geophys. J. Roy. astr. Soc., 79*, 257-267.

Kennett, B.L.N., S. Gregersen, S. Mykkeltveit, and R. Newmark (1985). Mapping of crustal heterogeneity in the North Sea basin via the propagation of *Lg*-waves, *Geophys. J. Roy. astr. Soc., 83*, 299-306.

Kim, W-Y, Kulhanek, O., van Eck, T. and R. Wahlstrom (1985) The Solberg, Sweden, earthquake of September 29, 1983. Seismological Department, Uppsala University, Uppsala, Sweden.

Kvaerna, T. and F. Ringdal (1986). Stability of various f-k estimation techniques, in Semiannual Technical Summary, NORSAR Scientific Report no. 1-86/87, L.B. Loughran ed.

Mechler, P., Nicolas, M. and A. Chaouch (1980). Seismic crustal and subcrustal phase propagation, Final report for the AFOSR, Laboratoire de Geophysique Appliquee, Universite Pierre et Marie Curie, Paris, France.

Menke, W.H. and P.G. Richards (1980). Crust-mantle whispering gallery phases: a deterministic model of teleseismic *Pn* wave propagation, *J. Geophys. Res., 85,* 5416-5422.

Mitchell, B.J. (1975). Regional Rayleigh wave attenuation in North America. *J. Geophys. Res. 80,* 4904,4916.

Mitchell, B.J. (1981), Regional variations and frequency dependence of $Q_\beta$ in the crust of the North America, *Bull. Seism. Soc. Am., 71,* 1531-1538.

Mykkeltveit, S. and T. Kvaerna (1986). Propagation characteristics of regional phases and NORESS real time processing performance, Proceedings of the DARPA/AFGL Seismic Research Symposium, 6-8 May 1986, US Air Force Academy, Colorado Springs, CO, pp. 117-124.

Nicolas, M., B. Massinon, P. Mechler, M. Bouchon (1982). Attenuation of regional phases in western Europe. *Bull. Seism. Soc. Am., 72,* 2089-2106.

Noponen, I. and J. Burnetti (1980). Alaskan regional data analysis, In "Studies of Seismic Wave Characteristics at Regional Distances" *AL-80-1,* Teledyne-Geotech, Alexandria, VA 22314.

Nuttli, O.W. (1973). Seismic wave attenuation and magnitude relations for eastern North America, *J. Geophys. Res. 78,* 876-885.

Nuttli, O.W. (1980). The excitation and attenuation of seismic crustal phases in Iran. *Bull. Seism. Soc. Am., 70,* 469-485.

Nuttli, O.W. (1981). Similarities and differences between western and eastern United States earthquakes, and their consequences for earthquake engineering, in *Earthquakes and Earthquake Engineering: the eastern United States,* J.E. Beavers, Editor, Ann Arbor Science Publishers, Ann Arbor, Michigan, 25-51.

Pomeroy, P.W. and T.C. Chen (1980). Regional seismic wave propagation, *03-80-3,* Final Technical Report, Rondout Associates, Inc., Stone Ridge, N.Y.

Pulli, J. (1984). Attenuation of coda waves in New England, *Bull. Seism. Soc. Am., 74,* 1149-1166.

Rodgers, P.W., S.R. Taylor, and K.K. Nakanishi (1987). System and site noise in the regional seismic test network from 0.1 to 20 Hz, *Bull. Seism. Soc. Am., 77,* 663-678.

Sereno, T.J. and J.A. Orcutt (1987). Synthetic *Pn* and *Sn* phases and the frequency dependence of *Q* of oceanic lithosphere, *J. Geophys. Res., 92,* 3541-3566.

Shin, T.-C. (1985). *Lg* and coda wave studies of eastern Canada, *Ph.D. Dissertation,* Saint Louis University, Saint Louis, Missouri, 185 pp.

Shin, T.-C. and R.B. Herrmann (1987). Lg attenuation and source studies using 1982 Miramichi data, *Bull. Seism. Soc. Am., 77,* 384-397.

Singh, S. and R.B. Herrmann (1983). Regionalization of crustal coda Q in the continental United States, *J. Geophys. Res., 88,* 527-538.

Street, R.L. (1976). Scaling northeastern United States / southeastern Canadian earthquakes by their *Lg* waves, *Bull. Seism. Soc. Am., 66,* 1525-1537.

Warren, D.H., Healy, J.H., Hoffman, J.C., Kempe, R., Rauula, S. and D.J. Stuart (1978), Project Early Rise: travel times and amplitudes. United States Geological Survey, Open File Report #1024.

(THIS PAGE INTENTIONALLY LEFT BLANK)

# SEISMIC ATTENUATION STUDIES AT U.K. ARRAYS

by

D. Wilmer Rivers

(THIS PAGE INTENTIONALLY LEFT BLANK)

## SUMMARY

Work on this task was performed while the principal investigator was a Visiting Scientist at the Blacknest seismological facility of the United Kingdom Atomic Weapons Research Establishment (AWRE) in Aldermaston, England. The data archive at Blacknest is an important one for seismic research, particularly for research in the seismic monitoring of nuclear explosions, since it consists of a lengthy historical database of events recorded at an invariantly configured network which was designed especially for monitoring purposes. With attention in the seismic community once more being directed towards the use of arrays for signal processing, it is important that this data resource be made readily available to investigators who can use it in a wide range of research projects. Unfortunately, it has been awkward to carry out data retrieval and analysis at Blacknest on account of the hardware and software involved. The database management tasks are all performed on a PDP11/34 computer, using jobs which are written in undocumented assembly language code. These jobs require occasional revision (obviously, a difficult assignment on account of their coding), and the computer and its peripheral devices suffer frequent malfunction due to their age. The analysis of the data is performed using a powerful mainframe computer at the main site of AWRE, but this must be done in a batch mode using punched cards for programs and alphanumeric input. In addition to the limitation of receiving output only twice a day from the batch jobs, the researcher must cope with the problem of dealing with the enormous programs [physically, they consist of multiple trays of cards] which have been developed, over a period of years, for handling the seismic array data. These programs are poorly documented, and they are written in FORTRAN IV using constructions (*e.g.*, a host of "computed GOTO" statements) which make the logic difficult to follow and to modify. The principal program for analyzing Blacknest data, a massive example of awkwardly written and poorly documented code called BAPPL, presents

more of an obstacle than a pathway for research. Without the support of a staff of analysts and/or programmers, a scientist will thus find it difficult to retrieve and process the volume of data which is typically used in a research project. In light of the potential value to research of the Blacknest data base, a more effective procedure needs to be devised for the data to be retrieved and processed (in at least a preliminary investigation) so that they can be made available to seismologists working at Blacknest and to those in the US. Under this contract we have explored means by which the data can be made available more easily, using the Sun-2 workstation at Blacknest.

It was decided that the productivity both of any future U.S. researchers using Blacknest data and of the Blacknest staff themselves would be significantly enhanced if the interactive graphics capability of the Sun workstation were used for the analysis of seismic array data. The Sun had been installed at Blacknest in the autumn of 1984 for use in the Group of Scientific Experts Technical Test (GSETT). Unfortunately, the staff at Blacknest (which has become small in recent years) does not possess the necessary expertise in the UNIX operating system, the SunCore graphics language, the SunWindows window management system, nor in data base management systems to utilize the Sun as an alternative to the existing batch data processing. It was therefore decided that the principal investigator would work on devising data base display and analysis software that could be used on the Sun workstation at Blacknest. In particular, software would be installed that would make the Blacknest data accessible by programs already written to handle data archived at the Center for Seismic Studies in Arlington, Virginia. This would make the U.K. data readily available to future U.S. researchers, and it would lay the necessary groundwork for any international data exchange experiment that, unlike the GSETT, would involve the exchange of waveforms as well as of parameter data. Also, the principal investigator would instruct the Blacknest staff in the use of the new software, so that they could add to it and, over a period of time, adapt their data analysis from

the batch mode processing on the mainframe computer to interactive processing on the Sun workstation. This plan of action was approved by administrators at both Blacknest and DARPA as being beneficial to research in the U.S. and in the U.K., and especially as being needed for the exchange of data and software between Blacknest and the Center for Seismic Studies. With the approval of both the sponsor and the host, this task thus evolved from one of performing a particular research project at Blacknest (involving using BAPPL to generate a suite of spectra) to one of performing a general software development project there, which would be useful for other research projects (including the computation of spectra).

Although the software development project involved performing a variety of tasks such as writing and maintaining utility programs and copying selected software from the Center, there were two programs that were developed which are the most important for researchers who wish to process U.K. seismic array data on the Sun workstation. The first of these programs is RDBNST, which de-archives the array data that are stored in a dozen different formats in the Blacknest tape library and converts them to the ".w" format used at the Center. The original version of this program was written by M. Tiberio at the Center prior to this contract, but many new features were added to it, and it was extensively re-written for use at Blacknest. The new version is much more "user friendly", and this is a necessary feature for the program to be used by Blacknest personnel who are inexperienced with UNIX and who are unfamiliar with the Center's data base structure. When coupled with the seismogram display capabilities that were developed for the Sun, the RDBNST program should make it easy for the staff at Blacknest to satisfy requests from the U.S. for data from specific events. This was tested successfully when data were provided to the Center for 2 specific spans of 2 hours duration, for each one of the 4 U.K. seismic arrays, in response to a request from DARPA.

The only seismogram display program that existed on the Sun at Blacknest was the Graphical Parameter Measurement (GPM) program that had been developed at the Center for use during the GSETT. The GPM program permits measurements to be made on individual waveforms, so only one trace at a time is displayed on the graphics screen. Although this procedure is suitable for examining RSTN data, it is less than ideal for examining data from a seismic array, where the output of many data channels ought to be displayed simultaneously. Another problem with using GPM is that the code, like that of the large Blacknest data processing jobs, contains at best scanty documentation, so it is difficult to modify to do anything other than the specific set of operations which it was designed to perform. This problem is particularly accute since GPM is 9200 lines long and is written in C, a language with which the staff at Blacknest is unfamiliar. All of the graphics displays and interactions use the "SunWindows" system, a complicated C-language software package for managing windows and for manipulating pixels on the bit-mapped screen, and the use of this system further adds to the difficulty of modifying GPM. It was therefore decided not to attempt to introduce modifications to this program but instead to write new software particularly for the purpose of examining seismic array data such as those which are archived at Blacknest. In order that this software be easily modified by Blacknest staff, most of the code was written in FORTRAN 77. On the Sun, old FORTRAN IV library routines copied off the AWRE mainframe can be recompiled and used along with the new FORTRAN 77 code, so the programs that were written under this contract will continue to be developed by the Blacknest staff by the addition of their own code (both old routines and new ones). Although it was necessary to write some routines in C, they can easily be loaded along with the FORTRAN routines. The C routines can be called from the FORTRAN code in such a way that the FORTRAN programmer does not need to understand how they operate, so the inclusion of these routines does not present a hindrance to the staff at Blacknest.

In addition to writing new FORTRAN code to be used as an alternative to GPM, the principal investigator installed on the Sun at Blacknest the extensive "SPEX" and "DISPLAY" software packages written by J. Wang at S-Cubed and by J. Carter at Rondout Associates, respectively. Both of these packages are written in C and use SunWindows graphics, however, so they are not so suitable for modification by programmers at Blacknest as are the new programs that were written in FORTRAN. Seminars were given to the Blacknest staff in the use of these programs for analyzing seismic data and in the use of the Center's data base management programs.

In addition to being written in FORTRAN rather than in C, another major difference between the code that was developed under this contract and the GPM, SPEX, and DISPLAY packages is that our program is based on the "SunCore" graphics system rather than on "SunWindows" (although it does make some use of "SunWindows", again in such a way that programmers at Blacknest need not be concerned with it). The "SunCore" graphics system operates at a higher level than does the "SunWindows" system, so it is much easier to program. (The difference between the two systems is in some ways similar to the difference between FORTRAN and assembly language, since "SunCore" actually operates by making repeated calls to the primitive drawing functions of "SunWindows".) Another advantage of using "SunCore" is that it is an implementation of the ACM Core graphics standard. Since this standard is widely used throughout the computing industry, it should (at least in theory) be considerably easier to transfer our software to another type of computer (such as a VAX) than it would be to transfer GPM, which is so strongly tied to the particular functions used for drawing on the Sun's bit-mapped screen. Of course, a price must be paid in terms of performance for using a graphics system which operates at a high level close to the programmer rather than at a lower level close to the operating system. Nevertheless, we have found that the code which we have developed so far operates satisfactorily fast for its intended purpose to

permit U.K. array data to be retrieved and displayed. The speed could be improved further with the addition of a floating-point accelerator board to the hardware configuration, and it would certainly be enhanced if the code were transferred from the Sun-2 to a Sun-3 workstation equipped with a floating-point accelerator, so we do not feel that much has been sacrificed by our decision to use the higher level graphics.

The program that was developed at Blacknest for displaying and making measurements on multi-channel data is known as the Interactive Display of Array Seismograms (IDAS) program. It has been ported from the Sun workstation at Blacknest to workstations at the Center, so researchers there can examine the U.K. array data also. Copies of IDAS have been provided to other contractors in the U.S., namely Science Applications International, ENSCO, and Science Horizons. Copies have also been sent to the Australian National University and to the Ruhr - Universitat Bochum Institut fur Geophysik in Germany. Documentation of the program has furthermore been provided to other international participants in the GSETT. IDAS has been used for the analysis of data not only from the 4 arrays operated by the U.K. but also for the analysis of data recorded at NORESS and at Grafenberg. There follows an excerpt from the documentation that was distributed with the program code.

## OVERVIEW OF THE IDAS PROGRAM

The Interactive Display of Array Seismograms [IDAS] program permits a user of the Sun-2 or Sun-3 workstation to display on the screen simultaneously the same time window in the records of every data channel of a seismic array. This display of the entire array's seismograms permits the analyst to make a visual inspection of the data, identifying those data channels which will be most useful for further analysis and those which should be deleted from the waveform processing, and it allows him to see how the waveforms vary across the array and to make comparisons among the vertical and horizontal channels and among the short-, intermediate-, and long-period channels. When the analyst has identified those channels which are suitable for the purpose, he can then use IDAS to combine them into a sum-and-delay beam, which will be displayed on the screen along with the individual data channels.

The analyst can choose a single channel (including the newly-formed "beam" channel) from out of the display for a more detailed examination. The screen will be cleared, and the chosen seismogram will be re-drawn on a larger scale. The analyst can next select a shorter segment (shorter in time and/or amplitude) from out of this waveform to expand still further in a new plot on the screen known as the "analysis window". The operator can choose the size, shape, and location on the screen of the "analysis window" (so long as it is confined to that region of the screen which lies beneath the plot of the entire seismogram). He can then perform certain manipulations on the graph of the waveform segment which appears in this window, using the Sun workstation's "mouse" input device to control the movement of cursors on the screen. These waveform manipulations include de-spiking, measuring the amplitude and period of individual peaks, and picking the signal arrival time (which will be transmitted back to the main grid on which all the waveforms are displayed simultaneously, where markers are then drawn indicating both the predicted and picked arrival times on every waveform). The

results of all operations are saved in an ASCII output file.

The operator can next proceed to display a number of graphs related to spectral processing of those time intervals on this waveform which were marked as the "signal" and "noise" windows. (The position of these windows will have moved if the operator chose to make a pick of the signal arrival time that was different from the predicted signal arrival time.) He can display graphs of the tapered waveform segments within the signal and/or noise windows (as they enter into the Fourier transform routine and as they would be reconstructed by inverting the transform), of the displacement or power spectra for both the signal and noise, of the signal phase spectrum, and of the seismograph's amplitude and phase response (for this particular data channel) which are removed from the signal and noise spectra. As was the case for the "analysis window", the operator has control over the size, shape, and location of each of these plots; in particular, he can overlay them. Finally, the operator can choose whether to add the signal and noise spectra to a stack (for the short-period vertical data channels only), thereby building up a frequency-domain counterpart to the time-domain sum-and-delay beam which was created earlier. He can then return to the initial display of all the channels together and select another one on which to repeat this detailed analysis.

Input to IDAS consists of the digital waveforms for every data channel of the seismic array, each in its own ".w" waveform file with a common ".wfdisc" seismogram header file, in conformance with the database structure used at the Center for Seismic Studies. Hypocentral information about the particular event under study, which is used by the program to make the predictions about signal arrival time, azimuth, and slowness, is specified by the operator along with information about how long he wishes the signal and noise windows to be and where he wishes them to be placed with respect to the signal arrival. This information can be typed in at the keyboard or read in from an ASCII file which the analyst has edited in advance. All

other interaction between the analyst and the program is performed using the mouse, except for a few possible interactions in which the analyst will respond to queries from the program by typing responses at the keyboard. Most of the interaction performed by the operator consists of choosing items from "menus" of possible actions that the program can perform next; these menus appear in a corner of the screen (usually in response to the operator's requesting them, although some appear automatically when a new phase of the analysis, such as the spectral processing, is begun), and the operator picks the "menu item" to be performed next by moving the mouse in such a way as to place a cursor on top of the selected item. The operator will also move the mouse, and hence move cursors on the screen, in order to select which waveform to display by itself, to choose a segment of that waveform to display in the "analysis window", to position the analysis window and the various spectral graphs on the screen, to pick the signal arrival time, and to make period and amplitude measurements.

(THIS PAGE INTENTIONALLY LEFT BLANK)

DISTRIBUTION LIST
FOR UNCLASSIFIED REPORTS
DARPA-FUNDED PROJECTS
(Last Revised: 5 Jan 1987)

| RECIPIENT | NO. OF COPIES |
|---|---|
| **DEPARTMENT OF DEFENSE** | |
| DARPA/GSD<br>ATTN: Dr. R. Alewine and Dr. R. Blandford<br>1400 Wilson Boulevard<br>Arlington, VA 22209-2308 | 2 |
| DARPA/PM<br>1400 Wilson Boulevard<br>Arlington, VA 22209-2308 | 1 |
| Defense Intelligence Agency<br>Directorate for Scientific and<br>Technical Intelligence<br>Washington, D.C. 20301 | 1 |
| Defense Nuclear Agency<br>Shock Physics<br>Washington, D.C. 20305-1000 | 1 |
| Defense Technical Information Center<br>Cameron Station<br>Alexandria, VA 22314 | 12 |
| **DEPARTMENT OF THE AIR FORCE** | |
| AFGL/LWH<br>ATTN: Dr. J. Cipar and Mr. J. Lewkowicz<br>Terrestrial Sciences Division<br>Hanscom AFB, MA 01731-5000 | 2 |
| AFOSR/NPG<br>ATTN: Director<br>Bldg. 410, Room C222<br>Bolling AFB, Washington, D.C. 20332 | 1 |

AFTAC/CA 1
ATTN: STINFO Officer
Patrick AFB, FL 32925-6001

AFTAC/TG 3
Patrick AFB, FL 32925-6001

AFWL/NTESG 1
Kirtland AFB, NM 87171-6008

DEPARTMENT OF THE NAVY

NORDA 1
ATTN: Dr. J.A. Ballard
Code 543
NSTL Station, MS 39529

DEPARTMENT OF ENERGY

Department of Energy 1
ATTN: Mr. Max A. Koontz (DP-52)
International Security Affairs
*1000 Independence Avenue*
Washington, D.C. 20545

Lawrence Livermore National Laboratory 2
ATTN: Dr. J. Hannon and Dr. M. Nordyke
University of California
P.O. Box 808
Livermore, CA 94550

Los Alamos Scientific Laboratory 2
ATTN: Dr. K. Olsen and Dr. T. Weaver
P.O. Box 1663
Los Alamos, NM 87544

Sandia Laboratories 1
ATTN: Mr. P. Stokes
Geosciences Department 1255
Albuquerque, NM 87185

OTHER GOVERNMENT AGENCIES

*Central Intelligence Agency* 1
ATTN: Dr. L. Turnbull
OSI/NED, Room 5G48
Washington, D.C. 20505

U.S. Arms Control and Disarmament Agency 1
ATTN: Dr. M. Eimer
Verification and Intelligence Bureau, Rm 4953
Washington, D.C. 20451

U.S. Arms Control and Disarmament Agency 1
ATTN: Mrs. M. Hoinkes
Multilateral Affairs Bureau, Rm 5499
Washington, D.C. 20451

U.S. Geological Survey 1
ATTN: Dr. T. Hanks
National Earthquake Research Center
345 Middlefield Road
Menlo Park, CA 94025

U.S. Geological Survey 1
ATTN: Dr. R. Masse
Global Seismology Branch
Box 25046, Stop 967
Denver Federal Center
Denver, CO 80225

UNIVERSITIES

Boston College 1
ATTN: Dr. A. Kafka
Western Observatory
381 Concord Road
Weston, MA 02193

California Institute of Technology 1
ATTN: Dr. D. Harkrider
Seismological Laboratory
Pasadena, CA 91125

Columbia University 1
ATTN: Dr. L. Sykes
Lamont-Doherty Geological Observatory
Palisades, NY 10964

Cornell University 1
ATTN: Dr. M. Barazangi
INSTOC
Snee Hall
Ithaca, NY 14853

Harvard University 1
ATTN: Dr. J. Woodhouse
Hoffman Laboratory
20 Oxford Street
Cambridge, MA 02138

Massachusetts Institute of Technology 3
ATTN: Dr. S. Soloman, Dr. N. Toksoz, and Dr. T. Jordan
Department of Earth and Planetary Sciences
Cambridge, MA 02139

Southern Methodist University 1
ATTN: Dr. E. Herrin
Geophysical Laboratory
Dallas, TX 75275

State University of New York at Binghamton 1
ATTN: Dr. F. Wu
Department of Geological Sciences
Vestal, NY 13901

St. Louis University 2
ATTN: Dr. O. Nuttli and Dr. R. Herrmann
Department of Earth and Atmospheric Sciences
3507 Laclede
*St. Louis, MO 63156*

The Pennsylvania State University 1
ATTN: Dr. S. Alexander
Geosciences Department
403 Deike Building
University Park, PA 16802

University of Arizona 1
ATTN: Dr. T. Wallace
Department of Geosciences
Tucson, AZ 85721

University of California, Berkeley 1
ATTN: Dr. T. McEvilly
Department of Geology and Geophysics
Berkeley, CA 94720

University of California Los Angeles 1
ATTN: Dr. L. Knopoff
405 Hilgard Avenue
Los Angeles, CA 90024

University of California, San Diego 1
ATTN: Dr. J. Orcutt
Scripps Institute of Oceanography
La Jolla, CA 92093

University of Colorado 1
ATTN: Dr. C. Archambeau
CIRES
Boulder, CO 80309

University of Illinois 1
ATTN: Dr. S. Grand
Department of Geology
1301 West Green Street
Urbana, IL 61801

University of Michigan 1
ATTN: Dr. T. Lay
Department of Geological Sciences
Ann Arbor, MI 48109-1063

University of Nevada 1
ATTN: Dr. K. Priestley
Mackay School of Mines
Reno, NV 89557

University of Southern California 1
ATTN: Dr. K. Aki
Center for Earth Sciences
University Park
Los Angeles, CA 90089-0741

## DEPARTMENT OF DEFENSE CONTRACTORS

Applied Theory, Inc. 1
ATTN: Dr. J. Trulio
930 South La Brea Avenue
Suite 2
Los Angeles, CA 90036

Center for Seismic Studies 2
ATTN: Dr. C. Romney and Mr. R. Perez
1300 N. 17th Street, Suite 1450
Arlington, VA 22209

ENSCO, Inc.
ATTN: Mr. G. Young 1
5400 Port Royal Road
Springfield, VA 22151

ENSCO, Inc. 1
ATTN: Dr. R. Kemerait
445 Pineda Court
Melbourne, FL 32940

Gould Inc. 1
ATTN: Mr. R. J. Woodard
Chesapeake Instrument Division
6711 Baymeado Drive
Glen Burnie, MD 21061

Pacific Sierra Research Corp. 1
ATTN: Mr. F. Thomas
12340 Santa Monica Boulevard
Los Angeles, CA 90025

Rockwell International 1
ATTN: B. Tittmann
1049 Camino Dos Rios
Thousand Oaks, CA 91360

Rondout Associates, Inc. 1
ATTN: Dr. P. Pomeroy
P.O. Box 224
Stone Ridge, NY 12484

Science Applications, Inc. 1
ATTN: Dr. T. Bache, Jr.
P.O. Box 2351
La Jolla, CA 92038

Science Horizons 2
ATTN: Dr. T. Cherry and Dr. J. Minster
710 Encinitas Blvd.
Suite 101
Encinitas, CA 92024

Sierra Geophysics, Inc. 2
ATTN: Dr. R. Hart and Dr. G. Mellman
11255 Kirkland Way
Kirkland, WA 98124

SRI International 1
ATTN: Dr. A. Florence
333 Ravensworth Avenue
Menlo Park, CA 94025

S-Cubed, A Division of 1
Maxwell Laboratories Inc.
ATTN: Dr. S. Day
P.O. Box 1620
La Jolla, CA 92038-1620

S-Cubed, A Division of
Maxwell Laboratories Inc.
ATTN: Mr. J. Murphy
11800 Sunrise Valley Drive
Suite 1212
Reston, VA 22091 — 1

Teledyne Geotech
ATTN: Dr. Z. Der and Mr. W. Rivers
314 Montgomery Street
Alexandria, VA 22314 — 2

Woodward-Clyde Consultants
ATTN: Dr. L. Burdick and Dr. J. Barker
556 El Dorado St.
Pasadena, CA 91105 — 2

NON-U.S. RECIPIENTS

National Defense Research Institute
ATTN: Dr. O. Dahlman
Stockholm 80, Sweden — 1

Blacknest Seismological Center
ATTN: Mr. P. Marshall
Atomic Weapons Research Establishment
UK Ministry of Defence
Brimpton, Reading RG7-4RS
United Kingdom — 1

NTNF NORSAR
ATTN: Dr. F. Ringdal
P.O. Box 51
N-2007 Kjeller
Norway — 1

OTHER DISTRIBUTION

To be determined by the project office — 9